Max-Planck-Institut für Kolloid- und Grenzflächenforschung Abteilung für Kolloidchemie

POLY(IONIC LIQUID) STABILIZERS AND NEW SYNTHETIC APPROACHES

Dissertation
zur Erlangung des akademischen Grades
„doctor rerum naturalium"
(Dr. rer. nat.)

in der Wissenschaftsdisziplin „Polymer- und Kolloidchemie"

eingereicht an der
Mathematisch-Naturwissenschaftlichen Fakultät
der Universität Potsdam

von
Konrad Grygiel
geboren am 27.07.1988 in Kielce, Polen

Potsdam, März 2015

"You will hold this book in your hands, and learn all the things I learned, right along with me:

There is no immortality that is not built on friendship and work done with care. All the secrets in the world worth knowing are hiding in plain sight. (...) It's not easy to imagine the year 3012, but that doesn't mean you shouldn't try. We have new capabilities now–strange powers we're still getting used to. (...) Your life must be an open city, with all sorts of ways to wander in.

After that, the book will fade, the way all books fade in your mind. But I hope you will remember this (...)"

— Robin Sloan, *Mr. Penumbra's 24-hour bookstore*

To my family,

who supported me for all these years,

and will never read it.

ABSTRACT

The main focus of the present thesis was to investigate the stabilization ability of poly(ionic liquid)s (PILs) in several examples as well as develop novel chemical structures and synthetic routes of PILs. The performed research can be specifically divided into three parts that include synthesis and application of hybrid material composed of PIL and cellulose nanofibers (CNFs), thiazolium-containing PILs, and main-chain imidazolium-type PILs.

In the first chapter, a vinylimidazolium-type IL was polymerized in water in the presence of CNFs resulting in the *in situ* electrostatic grafting of polymeric chains onto the surface of CNFs. The synthesized hybrid material merged advantages of its two components, that is, superior mechanical strength of CNFs and anion dependent solution properties of PILs. In contrast to unmodified CNFs, the hybrid could be stabilized and processed in organic solvents enabling its application as reinforcing agent for porous polyelectrolyte membranes.

In the second part, PILs and ionic polymers containing two types of thiazolium repeating units were synthesized. Such polymers displayed counterion dependent thermal stability and solubility in organic solvents of various dielectric constants. This new class of PILs was tested as stabilizers and phase transfer agents for carbon nanotubes in aqueous and organic media, and as binder materials to disperse electroactive powders and carbon additives in solid electrode in lithium-ion batteries. The incorporation of S and N atoms into the polymeric structures makes such PILs also potential precursors for S, N - co-doped carbons.

In the last chapter, reactants originating from biomass were successfully harnessed to synthesize main-chain imidazolium-type PILs. An imidazolium-type diester IL obtained *via* a modified Debus-Radziszewski reaction underwent transesterification with diol in a polycondensation reaction. This yielded a polyester-type PIL which CO_2 sorption properties were investigated. In the next step, the modified Debus-Radziszewski reaction was further applied to synthesize main-chain PILs according to a convenient, one-step protocol, using water

as a green solvent and simple organic molecules as reagents. Depending on the structure of the employed diamine, the synthesized PILs after anion exchange showed superior thermal stability with unusually high carbonization yields.

Overall, the outcome of these studies will actively contribute to the current research on PILs by introducing novel PIL chemical structures, improved synthetic routes, and new examples of stabilized materials. The synthesis of main-chain imidazolium-type PILs by a modified Debus-Radziszewski reaction is of a special interest for the future work on porous ionic liquid networks as well as colloidal PIL nanoparticles.

TABLE OF CONTENTS

1. INTRODUCTION

Poly(ionic liquid)s (or alternatively polymerized ionic liquids, PILs) are macromolecules derived from polymerizable ionic liquid compounds, called ionic liquid monomers (ILMs). The studies on PILs date back to the early 1970s when the pioneering research on the free radical polymerization of ionic vinyl monomers was performed by Salamone and others.[1] Initially, the interest on such polymers was mainly focused on the synthesis and physical properties of polycations bearing tetraalkylammonium or aromatic charged groups (e.g. imidazolium, pyridinium). It is worth noting that they had not attracted much attention nor had they been specifically classified as PILs until they were rediscovered in the late 1990s. Then, such structures were categorized as "polymerized ionic liquids" and investigated as potential materials for solid state electrolytes by Ohno *et al.*[2-5] Ohno's work coincided in time with the technological progress which triggered the growing need to develop more efficient and safer materials for energy storage and ion transport. The effects of several structural parameters [such as the type of counterions, polymer structure, glass transition temperature (T_g), and mesophase morphology] on the ion conductivity of PILs have been systematically and intensively studied.[2, 3, 5-12] Even though we presently know that due to unsatisfactory intrinsic ion conductivity of un-doped PILs, they failed to bring a breath of wind to the field of solid state electrolytes, PILs have ever since been utilized as a multifunctional platform for many noteworthy materials applications giving rudiments to the present work.

PILs bear IL moieties in the repeating units of their polymeric chains, therefore by definition they are a subclass of polyelectrolytes. Their fundamental building blocks, ILMs, are polymerizable organic salts which due to efficiently suppressed crystallization are liquids

below 100 °C. Their amorphous character originates from several factors: asymmetric chemical structure (introducing steric hindrance), weak Coulombic interactions between ions, charge delocalization, and lack of intermolecular interactions, just to name a few. The structure of PILs, which merges the polymeric nature with the charged IL moiety covalently immobilized in each repeating unit, results in their unique physicochemical properties. As PILs retain some features of ILs, they are recognized as versatile and remarkably tunable materials. It is worth noting that PILs inherit from their low molar mass IL precursors the highly charged character and the counterion-dependent solubility in aqueous and organic media. Due to the presence of charges among polymer chains, bulk PILs possess a certain ion conductivity (usually below 10^{-6} S/cm) which initiated studies on PILs as potential materials for solid state electrolytes. The tunable solubility substantially broadens the application spectrum of PILs in the fields where processing in organic media of a wide range of polarity is unavoidable.[13-15] It is important to denote that by this property PILs outmatch traditional polyelectrolytes which are typically soluble only in water and high polarity organic media, such as dimethyl sulfoxide (DMSO) or dimethyl formamide (DMF). Additionally, PILs possess often superior thermal stability. In regard to their polymeric nature, PILs are mechanically more robust and can be more easily processed into spatially controlled shapes than ILs.[16-18] Among the disadvantages of PILs, the high affinity of even hydrophobic PILs towards water molecules emerges as a substantial drawback.[19] Nevertheless, several methods like the introduction of large, fluorinated counterions in order to decrease hydrophilicity and the scrupulous purification (drying at high temperatures and high vacuum, the repeated precipitation from water miscible organic solvents, and lyophilization) were applicable to minimize the water content in PILs.

1.1 The chemical structure and physical properties of PILs

Recently the growing interest on PILs yielded the abundance of novel materials possessing a variety of chemical structures and polymeric architectures. The wide choice of polymerizable cations and anions as well as a multitude of available counterions supplies the scientists with countless number of accessible PILs. In addition, the properties of PILs have been effectively altered by common methods in polymer chemistry, for instance modification of their polymeric architecture or synthesis of PIL copolymers.

The family of PILs can be categorized according to the type of charges which are attached to the polymer backbones. Thereupon, it is generally accepted to divide PILs into three main subgroups: polycations, polyanions and polyzwitterions. Among them, the cationic PILs, especially those which contain imidazolium moieties, are extensively studied.[4, 20-27] Since poly(1-vinyl-3-alkyl imidazolium) polymers reflect the most representative properties of the whole PIL family, they are a good example to describe diverse features of this group of polyelectrolytes. When reacted with strong bases, the imidazolium-type PILs undergo deprotonation at C2 position to yield highly reactive carbenes. In other distinctive reactions of PILs, the counterion exchange is recognized as a straightforward and efficient method for tuning their properties. PILs possessing hydrophilic counterions like iodide, bromide, or chloride dissociate in water towards polysalts. They are typically well soluble in polar organic solvents, like methanol (MeOH, Table 1). When hydrophilic counterions are exchanged into fluorinated and non-solvating species, the solution properties of PILs are significantly altered. PILs become then insoluble in water, but soluble in various organic solvents, for instance tetrahydrofuran (THF), ethyl acetate (EtAc), and acetone (Table 1). This feature is often associated with the reduced Coulombic interactions between charged groups attached to the polymeric backbone and hydrophobic counterions like tetrafluoroborate (BF_4^-),

hexafluorophosphate (PF$_6^-$) and bis(trifluoromethane sulfonate)imide (TFSI$^-$). Thus, the solubility properties of PILs can be easily shifted from water to organic solvents without the necessity of changing the chemical structure of their main-chains. In addition, it is worth noting that the choice of counterion has a strong effect on other physicochemical properties of PILs, for instance thermal stability and T_g. Besides the effect of counterion, also the structure of alkyl substituents attached to the imidazolium ring affects the physical features and solution properties of ILs and their polymers. For example, in the case of imidazolium-type ILs, the length of the alkyl side-chain influences the hydrophobicity (and consequently solubility) as well as melting points of ILs.

Table 1. The solubility of poly(1-vinyl-3-ethyl imidazolium) [P(ViEtIm$^+$X$^-$)] polymers as the example of the dependence of PILs solution properties on the type of counterion (X$^-$ - counterion defined in the first column of the table).[15]

P(ViEtIm$^+$X$^-$)	H$_2$O	MeOH	Acetone	THF	EtAc
Br$^-$	+	+	-	-	-
PF$_6^-$	-	-	+	-	-
BF$_4^-$	-	-	-	-	-
CF$_3$SO$_3^-$	-	+	+	-	-
(CF$_3$SO$_2$)$_2$N$^-$	-	-	+	+	-
(CF$_3$CF$_2$SO$_2$)$_2$N$^-$	-	+	+	+	+

Apart from the imidazolium species, the library of cationic PILs encloses the abundance of other functional groups, including tetraalkyl ammonium,[28, 29] pyridinium,[30, 31] piperidinium,[32] pyrrolidinium,[33] pyrrolium[32] and triazolium[34, 35] moieties (Figure 1). Such a diversity of implemented cationic moieties not only originates from the scientific curiosity to explore unknown structural models, but substantially affects properties of PILs and widens their application scope (discussed in the latter section of this chapter).

PILs bearing anionic functionalities in their polymeric chains have attracted by far less attention than polycations. Hence, the list of reported anionic PILs is relatively short, which can be associated mainly with the complicated synthesis of the corresponding ILMs. Nevertheless, examples of sulfonate, carboxylate, trifluoromethanesulfonamide, phosphoric, or amide-type anionic PILs combined with alkyl-imidazolium, pyridinium, or tetralkylamonium mobile counterions have been reported (Figure 1).[36]
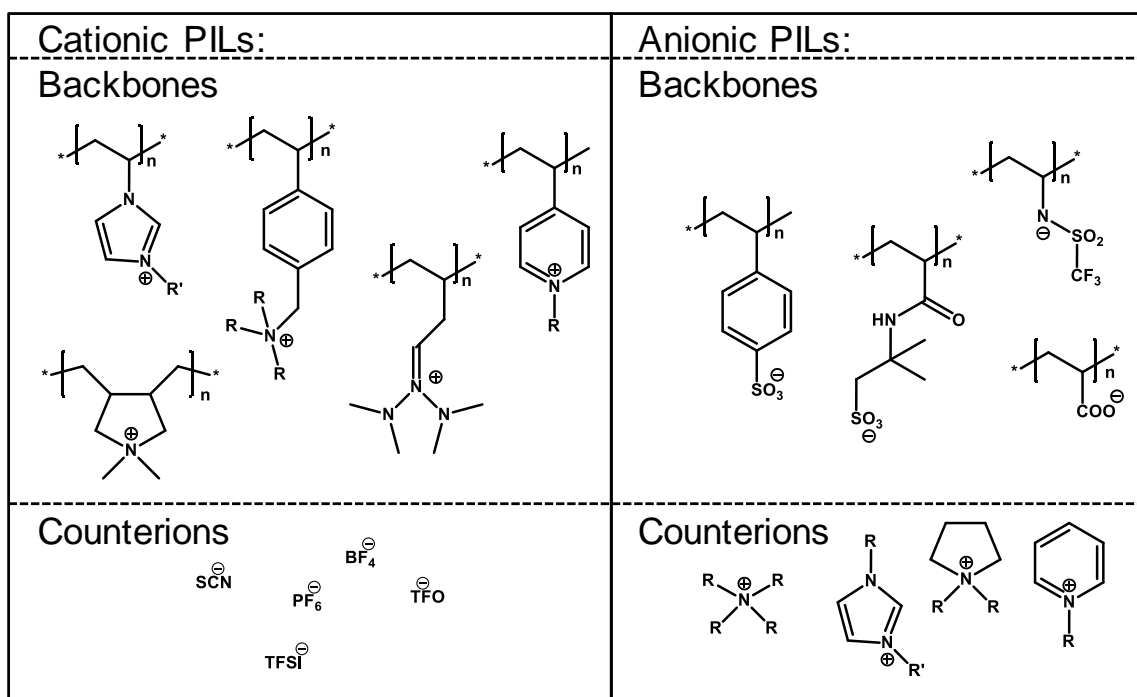
Figure 1. Examples of most common anions and cations incorporated in the structures of PILs.[36]

Finally, several studies reporting zwitterionic PILs are also available in the literature. Zwitterionic PILs bear both, cationic and anionic species chemically bounded to the polymeric chains. Usually monomeric precursors of these polymers do not achieve liquid state below 100 °C, so by definition they cannot be included into the scope of ILMs. However, due to the structural similarity and interesting properties, they are often enclosed into studies discussing PIL research. For example, imidazolium and tetraalkylammonium cations have been

incorporated into the structure of polymers together with anions like sulfonate, trifluoromethanesulfonamide, or alkoxydicyanoethenolate anions.[36]

1.2 Synthesis of PILs

The majority of the reported synthetic methods towards PILs involve the direct polymerization of ILMs. In order to obtain PILs with diverse properties, an anion exchange reaction must be performed at the stage of ILM synthesis or after its polymerization (Figure 2). The first pathway requires the replacement of counterions in ILMs followed by polymerization of each ion-exchanged ILM. Such PILs are typically of high purity, being free of contamination of undesired anions or cations. In addition, this method is often utilized in order to access copolymers of PILs with various charged or neutral polymers. Nevertheless, it is synthetically complicated since the polymerization conditions must be optimized independently for each monomer. In addition, the polymerization of ILMs with large counterions may proceed slowly and in some cases end up unfavorably with oligomers due to steric hindrance. The latter method involves the synthetically facile counterion exchange of existent PILs. Nevertheless, non-quantitative anion exchange is reckoned as a common obstacle, which in some fields may limit the application scope of such polymers.[36] However, it is worth noting that the amount of residual non-exchanged counterion can be minimized by repeating the ion-exchange procedure.
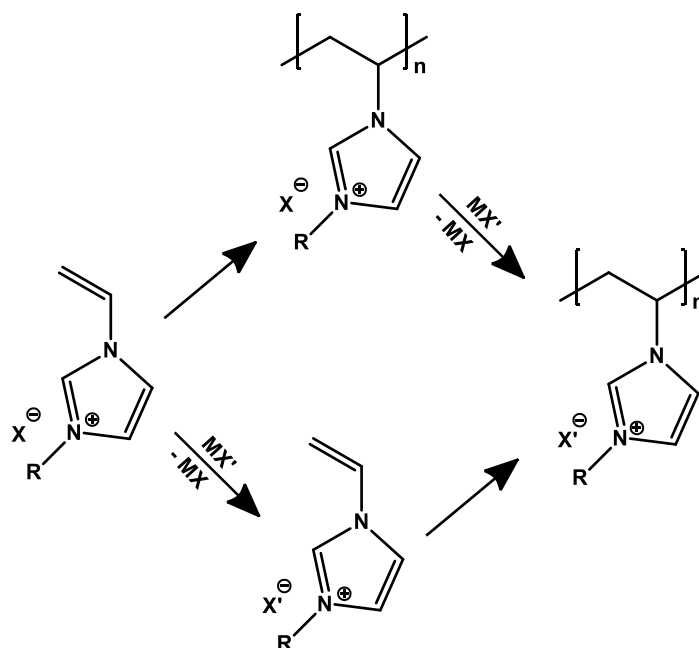
Figure 2. Synthetic routes towards anion exchanged PILs (R - alkyl substituent, X^-, X'^- - counterions; MX, MX′ - salts).

Among the polymerization methods employed in the preparation of PILs, free radical polymerization of vinyl, styrenic or methacrylic ILMs is the most frequent one. Its popularity arises from the synthetic simplicity and high tolerance to a wide range of functional groups and impurities. As a consequence, a variety of hydrophilic and hydrophobic PILs and their copolymers has been synthesized by free radical polymerization. It includes cationic and anionic PILs as well as polyzwitterions. Typically, such reactions are performed in a medium, which is a good solvent for both, the monomer and the corresponding PILs. However, some interesting structures like nanoparticles and fibers can be obtained for instance by precipitation polymerization. As an example, this method was utilized by Yuan *et al.* for the synthesis of polymeric nanoparticles with side-chain length dependent unilamellar or multilamellar morphology. In addition, free radical polymerization provides a synthetic platform for the preparation of cross-linked PIL nanoparticles, gels or even monolithic porous structures.[37, 38] Such polymeric structures of satisfying cross-linking density can be accessed by

the utilization of multivalent ILMs or non-ionic cross-linking agents and their subsequent copolymerization with ILMs.

The synthetic methods employed in PIL research are not limited to free radical polymerization. Polycondensation reactions,[39] "click chemistry",[34] and ring opening metathesis polymerization[40] have been applied for the preparation of some PILs as their unique structures are often not accessible by free radical polymerization. Yet, all the above-mentioned methods fail when more sophisticated polymeric architectures, for example block copolymers, are desired. In addition, they bring poor control over molar mass and molar mass distribution of the synthesized PILs. Thus, controlled radical polymerization (CRP) techniques like reversible addition-fragmentation transfer polymerization,[41, 42] atom transfer radical polymerization[43, 44] and cobalt-mediated radical polymerization[14, 45] have been investigated for the synthesis of PILs. CRP methods are powerful tools towards polymers of defined and tunable molar masses and narrow molar mass distributions. They can be also used for synthesis of (multi)block copolymers, which are of great importance for instance in studies of their self-assembly behavior. The utilization of multifunctional initiators for CRP may yield polymers with sophisticated architecture (for example branched or star-shaped). Moreover, the novel coupling method developed by Detrembleur *et al.* provides access to symmetric, triblock copolymers of PILs.[46] In addition to the polymerization in solution or bulk, synthesis of PILs in emulsions, microemulsions and dispersions have also been reported. Generally speaking, the synthetic toolbox for PILs has been broadened with convenient methods towards nanoparticles, (micro)gels, and even open-cell porous materials.

Whereas polymerization of ILMs dominated the research on PILs, postpolymerization modification of some conventional polymeric precursors provides an alternative. It requires the synthesis of polymers which bear in their structure certain groups (for instance tertiary nitrogen

atoms, imidazole rings or trialkylamine groups), which can be subsequently converted into IL-type, charged species. These macro-precursors of PILs are accessible by typical synthetic methods developed for conventional polymers. However, non-quantitative post-polymerization modification reactions of these precursors are a major drawback of this method.[36]

1.3 Applications of PILs in materials chemistry

The abundance of accessible structures of PILs and high versatility of their properties yields a multitude of applications for which PILs have been successfully tested. The physicochemical properties of PILs strongly depend on the choice of counterion, but the role of the type of cations or anions covalently incorporated into the polymeric main-chain cannot be overlooked. PILs having imidazolium-cations were utilized for various applications, like components of light emitting electrochemical cells or field effect transistors, coatings, and solid-phase microextraction.[47] They were also successfully incorporated into porous polyelectrolyte membranes. This type of membranes is scientifically and industrially attractive due to its potential usefulness in areas like gas separation, controlled release, sensors or catalyst support.[48] Thus, pH sensors and actuators were prepared from porous imidazolium based PILs.[48, 49] Imidazolium-type PILs can be used as precursors for nitrogen doped carbon materials.[50] Moreover, their application as catalysts for benzoin condensation has been reported.[51, 52] Imidazolium PILs have been also recognized as efficient stabilizers for various nano- and micro-objects in aqueous and organic media. The dispersions of gold nanorods, silver nanoparticles, as well as single and multi-walled carbon nanotubes were effectively stabilized and reversibly transferred between water and various organic solvents.[53, 54] Analogously, the simultaneous role of PILs as stabilizers and phase transfer agents

for sub-micron sized particles of conductive polymers, like polypyrrole, polyaniline, and poly(ethylenedioxythiophene) has been studied.[22] In addition, ILMs were photopolymerized as a method for *in situ* stabilization of gold nanoparticles within the PIL matrix.[55] Paillard *et al*. obtained electrochemically stable, imidazolium-containing PIL nanoparticles with TFSI$^-$ counterion which serve as binder materials for lithium-ion battery electrodes.[56]

Apart from imidazolium-containing polymers, PILs bearing other cations and anions are also useful in materials chemistry. It was reported that for certain usages, the tailored choice of ions connected to the polymeric backbone may play a crucial role to enhance the materials properties. PILs bearing specific tetraalkyl phosphonium and 4-styrenesulfonate groups were employed as stabilizers for nanomaterials. Interestingly, their solutions possess lower critical solution temperatures which equips the obtained dispersions with stimuli responsive features (e.g. to ionic strength and temperature).[54, 57-59] Moreover, due to its relevance in preventing the global warming, the research on CO_2 sorption and storage has recently attracted much attention. PILs are intensively studied for this purpose. Their performance strongly depends on the type of cationic moieties incorporated into the structure of polymers and decreases in the following order: tetraalkyl ammonium > pyridinium > phosphonium > imidazolium.[60] Thus, PILs were successfully engaged in the studies on CO_2 sorption, in general outperforming the corresponding ILs in terms of CO_2 uptake regarding both, absorption kinetics, and capacity. In addition, tetraalkyl ammonium-containing PILs were successfully processed into CO_2 sensors.[29] Polymers bearing tetraalkyl ammonium species are potentially better materials for microwave absorption compared to imidazolium-type PILs, since they possess higher dielectric constant and dielectric loss factor values.[61] Recently, cholinium-based PILs were obtained for the applications in biocompatible ion gels and cellulose coatings.[62] Photosensitive supramolecular liquid crystalline materials were synthesized from pyridinium-type PILs.[63]

Polymers bearing this cations were also studied for their anti-microbial activity.[64] Even though most of PILs decompose at high temperatures without achieving liquid state, recently a PIL which is a viscous liquid below 100 °C has been reported. This PIL containing anionic sulfonate groups in the main chain and alkylammonium-based counterions of the tailored structure can be employed in the synthesis of metal nanoparticles for dual purpose, simultaneously as solvents and stabilizers.[65] Moreover the synthesis of paramagnetic PILs based on pyrrolidinium as well as imidazolium was presented.[66] In general, the careful choice of the chemical structure of PILs may determine their performance in materials applications. Triggered by this knowledge, the synthetic methods for novel PIL structures are established as a part of this work in order to further widen the application scope of polyelectrolytes.

1.4 Motivation

The motivation of the present work embraces the development of new PIL structures for the applications as stabilization, phase transfer, and gas storage agents. The potential usage of such polymers in areas like batteries and CO_2 adsorption is also in the scope of interest. The secondary objective of this thesis is to make PIL synthesis more sustainable, for instance by using chemicals produced from biomass and mild reaction conditions. This is relevant, since depleting resources of fossil fuels and the "greenhouse effect" are socially significant issues. The methods towards PILs and PIL-containing hybrid materials which feasibly harness bio-derived components, energy-efficient procedure, and environmental-friendly conditions are established.

In Chapter 2, the capability of PILs to act as simultaneous phase transfer agents and stabilizers for cellulose nanofibers (CNFs) is investigated. CNFs are water-dispersible bio-

products with superior mechanical properties. Nevertheless, difficulties in processing CNFs in organic media limit their applicability. To overcome this obstacle, the method for grafting imidazolium-type PILs onto the surface of CNFs is designed, yielding stable dispersions either in water or organic solvents. Subsequently, grafting PILs onto the surface of CNFs improved compatibility of the latter with the polyelectrolyte membranes, enabling application of this novel hybrid material as reinforcing agents.

The work presented in Chapter 3 aims to develop new chemical structures of PILs, which bear thiazolium functionalities among their polymeric backbone. Establishing of new synthetic routes is followed by the investigation of their performance as stabilizing agents. Thus, they are examined in applications as binders of the electrode components and as stabilizers for carbon nanotubes (CNTs) in water and organic solvents.

Finally, in Chapter 4 the synthesis of novel main-chain imidazolium-type PILs which are partly or fully obtained from bio-derived components is described. In the first part, imidazolium-type diester synthesized by the modified Debus-Radziszewski method is employed as a precursor of partly bio-derived polyesters. These PILs are found to exhibit satisfactory CO_2 sorption capacity. In the second part, the modified Debus-Radziszewski method is applied for the one-pot synthesis of bio-derived, main-chain imidazolium-type PILs. Such energy efficient and "green" method towards PILs is explored in order to synthesize PILs of different charge density and to introduce novel-functionalities into their main chains. Moreover, the synthesis of PILs possessing aromatic spacers between imidazolium functionalities is developed, proving the versatility of the newly developed synthetic procedure.

2. OMNIDISPERSIBLE PIL-FUNCTIONALIZED CELLULOSE NANOFIBRILS

Nanocellulose is a unique class of nanomaterials which stems from renewable resources. It has recently attracted rapidly growing attention in fundamental science and industry due to outstanding material properties and a multitude of potential applications. Its utilization perfectly matches a general trend of using bio-derived products as a possible solution for saving depleting resources of fossil fuels, reducing environmental pollution, and limiting the "greenhouse effect". Nanocellulose possesses several intrinsic, particular features, such as low thermal expansion, functional surface groups, versatile chemical-modification capacity and excellent mechanical properties. All of them are combined with a high surface-to-volume ratio – a characteristic attribute of all nanomaterials. Among the applications of nanocellulose, barrier films, composites, aerogels, and multifunctional foams are the most striking.[67, 68]

Scientists distinguish three major forms of nanocellulose materials: cellulose nanofibrils (CNFs), cellulose nanocrystals, and bacterial cellulose. All of them have different properties due to variations in dimension and mechanical flexibility. CNFs are wire-like anisotropic particles composed of crystalline cellulose nanodomains connected by amorphous cellulose linkers. Their dispersions possess interesting viscoelastic behavior that can be attributed to a high aspect ratio of rods (diameter in the range from 5 to 60 nm and length up to several micrometers). CNFs are prone to gelation even at low concentration.[68] They display a good capability of film formation and consequently were employed in order to produce nanopapers with high tensile strength (up to 250 MPa).[68] Moreover, CNFs are applied (or being implemented) in such branches of industry as food, hygiene and packaging, as well as scaffold materials in tissue engineering, and as additives in cosmetic products and pastils.[68, 69] Currently,

in the case of CNFs obtained *via* common synthetic methods, their surface is highly charged. In this way, CNFs can be readily stabilized in water, but aggregate in most of organic media. However, their processing in organic solvents is absolutely essential for certain applications. This factor is one of the major obstacles limiting the scope of usages of CNFs. The state-of-the-art methods employed to make CNFs dispersible in organic solvents and/or polymeric matrixes are based on adsorption or grafting of surfactants, polymers, and coupling agents,[70-73] or alternatively corona treatment.[74-76] Other methods include hydophobization of CNFs' surface by acetylation, silylation, or "click chemistry".[77-79] Those routes are often associated with certain limitations, including lack of versatility and a risk of damaging the fibrillar structure of CNFs (especially in the case of silylation).[80] Therefore, there is a necessity to develop alternative functionalization methods which are straightforward, non-damaging for the surface of CNFs, and allow for easily transfer and processing of CNFs in organic solvents.

As presented in the introduction part, PILs can be efficiently used as stabilizers and phase-transfer agents.[36, 38, 53, 58] In addition, a simple pathway for the preparation of porous membranes by triggering ionic complexation between PIL and poly(acrylic acid) (PAA) has been developed by Zhao *et al*.[48] The potential applications of such membranes are gas separation, controlled release, sensors, and catalyst support. However, they possess insufficient mechanical properties. Thus, as a part of this doctoral work, a method for one-step grafting of PILs onto CNFs has been developed. Such CNF@PIL nanocomposites show tunable dispersity in water and organic solvents of different dielectric constants. Moreover, the hybrid material was introduced into the porous PIL/PAA membranes in order to enhance their mechanical properties. The overall synthetic route for the preparation of such hybrids and reinforced membranes is presented in Figure 3. Part of this chapter has been published in Chemical Communication, 2014, 50, 12486-12489.
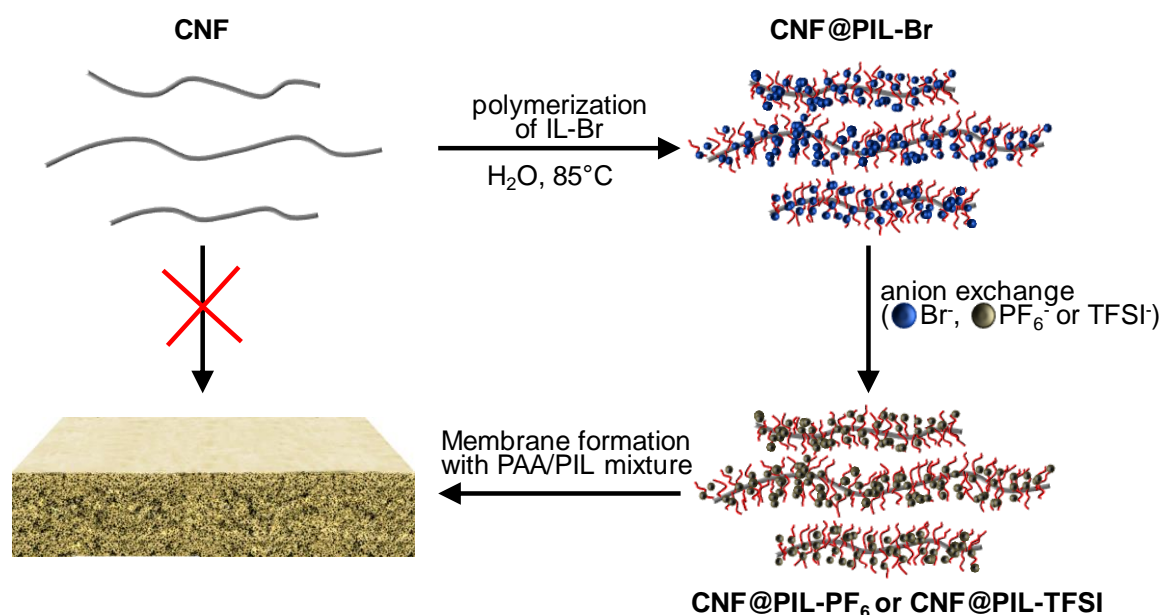
Figure 3. Synthetic route to the CNF@PIL hybrid nanomaterials and CNF-reinforced porous polyelectrolyte membranes (IL-Br - ionic liquid monomer with Br$^-$ anion).[81]

2.1 Synthesis of CNF@PIL nanocomposites

Successful grafting of dense PIL chains on the surface of CNFs plays a crucial role in the synthesis of hybrid material. As a prerequisite, high-quality suspension of untangled CNFs in water must be obtained prior to the grafting process. Thus, the CNF suspension was sonicated using a highly efficient ultrasonic horn device. Good quality of dispersion was confirmed *via* atomic force microscopy (AFM, Figure 4A). Cationic PIL chains were grafted onto the negatively charged surfaces of 2,2,6,6-tetramethylpiperidine-1-oxyl - oxidized (TEMPO-oxidized) CNFs, rich in carboxylate functionalities. The grafting was performed *via in situ* polymerization of an ILM [1-ethyl-3-vinylimidazolium bromide (EVIm$^+$Br$^-$)] in water in the presence of CNFs. During the synthesis, a large excess of EVIm$^+$Br$^-$ was used (40:1 weight ratio of EVIm$^+$Br$^-$:CNF) in order to achieve high grafting efficiency. Meanwhile, the concentration of CNF dispersions was kept at 0.05 w% to maintain relatively low viscosity.

15

It was necessary, since a too high viscosity could impede effective stirring of the reaction mixture. After polymerization a gel-like mixture was subjected to ultrafiltration (pore size: 50 nm), using water as eluent to eliminate the unanchored, free polymer chains, and non-reacted monomer. The ultrafiltration process was performed until a monomer- and polymer-free filtrate was eluting from the system. It is important to mention that a straightforward, direct mixing of a PIL solution and the CNF dispersion led to the creation of interpolyelectrolyte complexes which precipitate from the solvent and aggregate even under sonication treatment. Finally, counteranion metathesis reactions were performed in order to exchange Br^- anions of CNF@PIL-Br to more hydrophobic PF_6^- and $TFSI^-$ anions, forming CNF@PIL-PF$_6$ and CNF@PIL-TFSI hybrids, respectively. Anion-exchange was achieved by the addition of corresponding aqueous salt solutions to the aqueous dispersion of CNF@PIL-Br. Incorporation of hydrophobic anions into the hybrid structure turned it insoluble in water, consequently causing rapid precipitation from reaction mixture. The obtained precipitate was eventually purified from excess of salt by ultrafiltration.

2.2 Characterization of CNF@PIL hybrid nanomaterial

AFM images visualized that bundle-free morphology of CNFs remains well preserved after the grafting of PILs (Figure 4 A,B). In addition, it confirms that no degradation of CNFs due to possible dissolution in reaction media occurred during the *in situ* polymerization of the IL monomer (Figure 4B). It is important to highlight that the ability of ILs to dissolve cellulose is widely known. However, this feature applies only for certain ILs, typically at very high purity or under specifically chosen conditions.[82]
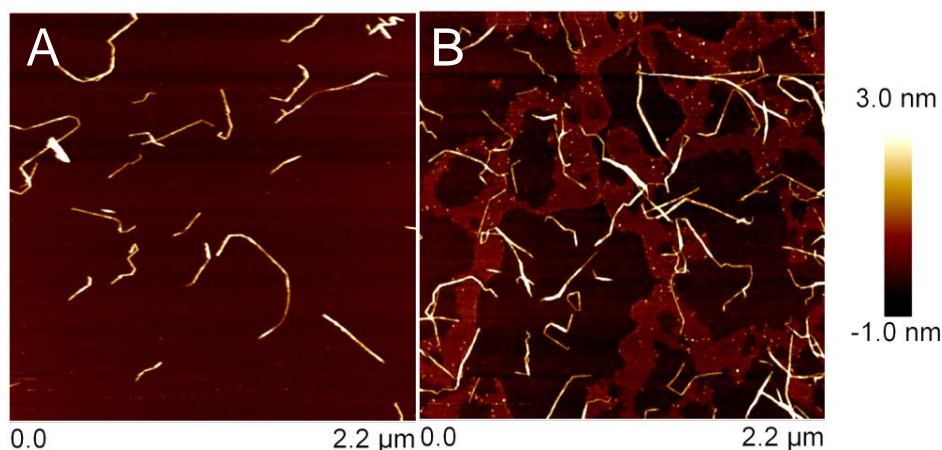
Figure 4. AFM height images of A - CNF; B - CNF@PIL-Br hybrid adsorbed from their corresponding aqueous suspensions.

Successful grafting of PIL onto the surface of CNFs was confirmed by attenuated total reflection Fourier transform infrared spectroscopy (ATR-FTIR), ζ-potential measurements as well as elemental analysis. In ATR-FTIR spectra of the hybrid material, characteristic peaks of both components – PIL and CNFs can be clearly distinguished (Figure 5). Sharp bands at 1160 and 1550 cm^{-1} are assigned to C-N stretching of imidazolium rings as well as CH$_2$(N), CH$_3$(N)CN, and asymmetric ring in-plane stretching vibrations, respectively. Peak at 1050 cm^{-1} is due to C-O stretching vibration of CNF. This clearly verifies the presence of both components in the hybrid material.[83] Moreover, ζ-potential measurements showed that negatively charged CNFs (-45.4 ± 4.7 mV) bear positive surface charge after the polymerization (37.3 ± 4.2 mV), which can be explained by the existence of polycationic brushes on CNFs' surface. Elemental analysis measurement was employed in order to determine the CNF/PIL weight ratio in the hybrid material. The measured C/N weight ratio of CNF@PIL-Br hybrid was 4.23. It was confirmed that CNFs do not contain nitrogen (< 0.05 wt%). For the calculation of the amount of grafted polymer, C/N for the hybrid material was compared with the C/N value in pure PIL-Br polymer. Hence, according to the obtained data, the CNF/PIL weight ratio in the final product was calculated to be 1:2.5. The existence of ca. 70 wt% of PILs in the hybrid proves successful and highly efficient grafting of PILs onto the CNF surface. Dynamic light scattering

(DLS) measurement was applied to characterize aqueous suspensions of CNFs and CNF@PIL-Br hybrids. The hydrodynamic radius of CNFs showed a size expansion from 500 to 700 nm after polymerization process. This can be attributed to stretching of CNFs due to the enhanced steric and electrostatic repulsion among the grafted PIL chains on the CNF surface.
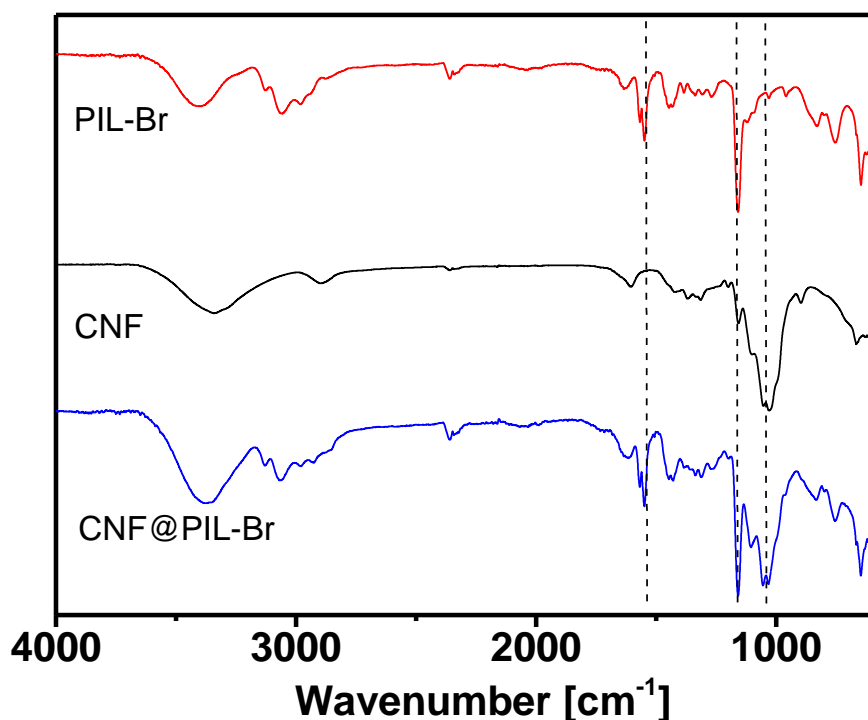

Figure 5. ATR-FTIR spectra of PIL-Br, CNF   and the CNF@PIL-Br hybrid.

It is worth noting that the stabilization of CNFs *via in situ* polymerization of IL monomer does not require any further pre-functionalization of the surface of TEMPO-oxidated CNFs. As it was presented before, direct mixing of PIL solution and CNF dispersion failed in the synthesis of well dispersible hybrid CNF@PIL material, forming indispersible precipitate instead. Such aggregates are interpolyelectrolyte complexes of two oppositely charged species. The possible explanation why *in situ* polymerization method is so efficient is that after addition of several monomeric units to the radical, the short polymer chains were adsorbed onto CNFs due to electrostatic interaction. This attachment locally neutralizes the negative charge of CNFs, but at this step PILs chains are still active in the radical propagation. Further addition of monomeric

18

units leads to the inversion of the surface charge of CNF material from negative to positive, which stabilizes dispersions of the hybrids. Good quality of the suspensions can be related to two factors. The first one is the short length of oligomeric PIL chains at the adsorption step. PILs interact with individual fibers, rather than create inter-CNF network that would lead to electrostatically crosslinked products. Therefore, the hybrids retain their fibrillar structure at the grafting step. Additionally, positively charged PIL brushes growing on the surface of CNFs introduced electrostatic repulsions between individual fibers. Both factors efficiently suppress undesirable crosslinking of the hybrid material and improve colloidal stability of this system. According to the above-mentioned anticipated mechanism of electrostatic grafting PIL on CNFs, individual polymeric chains exhibit multivalent interactions with the surface of CNFs but repel each other during the grafting process. Therefore, a polymeric layer of medium or low grafting density should be expected. In order to estimate the value of grafting density, firstly a sample of the free polymer (obtained from the filtrate of ultrafiltration process) was characterized by gel permeation chromatography (GPC) measurement in 0.2M aqueous solution of Na_2SO_4 with 1% of acetic acid used as eluent. The performed experiment revealed that molar mass of the PIL-Br sample amounted to 35 kg/mol, having molar mass dispersity index (Đ) of 1.5 (the values were calculated to pullalan standards). For the further calculations, it was assumed that the molar mass of PIL electrostatically attached to the surface of CNF was similar to the one of free polymer. This opened up a possibility to estimate a grafting density of PIL-Br chains on CNFs (the method is described in section B of Appendix). According to the performed calculations, CNF@PIL-Br hybrid contains 0.15 PIL-Br chains per each 1 nm^{-2} of CNFs' surface. Such created PIL layer can be considered as a middle density polymer brush which is in agreement with anticipated grafting mechanism. However, one must take into account that pullalan standards which were used to determine molar mass of the free polymer do not fully

19

mimic its solution behavior. Therefore, the obtained value of the grafting density should be considered as an estimation rather than an absolute value.

The thermal stability of CNF@PIL was determined by thermogravimetric analysis (TGA) under nitrogen and compared with the results obtained for pure PIL-Br and CNFs. The results indicated that grafting of PIL did not cause any deterioration in the thermal stability of CNFs (Figure 6). Moreover, a slight increase in the threshold decomposition (in this thesis defined as 10 wt% of mass loss) was observed for the hybrid material, when correlated to bare CNFs. At the temperature range between 330 and 900 °C the residual mass for CNF@PIL-Br is lower than that for CNFs, but higher than that for pure PIL. This verifies again the presence of both components in the hybrid.
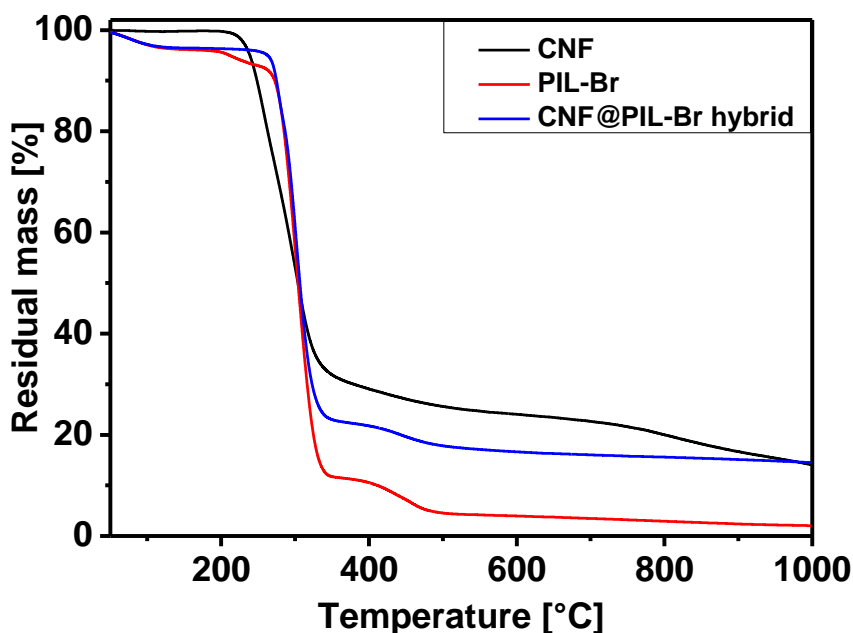
Figure 6. TGA curves of CNF, PIL-Br and CNF@PIL-Br hybrid (heating rate 10 K·min^{-1}, under nitrogen atmosphere).

The striking advantage of the CNF@PIL hybrid materials over bare CNFs is their dispersibility in a broader range of organic solvents. Tuning the dispersion behavior can be achieved *via* extensively studied anion-effect of PILs.[13] Such properties of hybrid materials

20

were tested and compared with that of bare CNFs. The results are summarized in Table 2. The CNF@PIL-Br hybrid is dispersible in water but only partially in DMSO. Replacing the Br$^-$ with more hydrophobic TFSI$^-$ counter anion leads to the formation of a hybrid, which precipitates from water, but can be readily dispersed in DMSO. Interestingly, CNF@PIL-PF$_6$ display dispersibility not only in DMSO, but also in volatile organic solvents such as MeOH and acetone, which are poor solvents for bare CNFs (Figure 7). This is a significant advantage in terms of material processing in organic media. The performed experiments indicate that dispersibility of CNF@PIL hybrids can be easily tuned without the necessity of changing chemical structure of the polymeric backbone, which would involve complicated reactions. Instead, the experimentally facile anion-exchange reactions were applied for the synthesis of omnidispersible and versatile hybrid material.

Table 2. Dispersibility tests of CNF and CNF@PIL hybrids with different anions in various solvents.

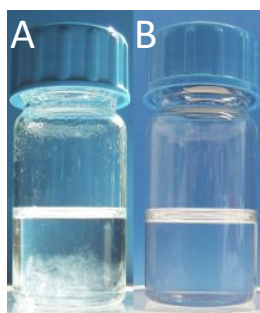| Material	Water	MeOH/EtOH	DMSO	Acetone
CNF	+	-	+	-
CNF@PIL-Br	+	-	+/-	-
CNF@PIL-PF$_6$	-	+	+	+
CNF@PIL-TFSI	-	-	+	-

Figure 7. Photographs of: A - CNF and B - CNF@PIL-PF$_6$ hybrid dispersions in acetone.

2.3   CNF@PIL hybrids as reinforcing agent

The omnidispersible hybrid material combines properties of CNFs with the versatile solubility of PILs. It is widely known that excellent mechanical properties are one of the intrinsic features of CNFs. Hence, CNF@PIL appeared to be potentially efficient reinforcing agent for materials which must be processed in organic solvents. Very recently, Zhao *et al.* described a straightforward, template-free approach for the preparation of porous membranes composed of PILs and PAA.[48] In detail, such materials were obtained by mixing both PAA and a PIL in a non-protic organic solvent, followed by film casting on a glass plate, drying, and subsequent immersion of the film into an aqueous ammonia solution to form pores. To further improve the mechanical stability of membranes, a reinforcing agent compatible with their matrix became imperative. The structural similarity and high charge density of the grafted PILs with the matrix of the membrane made CNF@PIL hybrids perfect candidates for this purpose. The preparation of reinforced membranes follows the procedure illustrated in Figure 8. In the first step, different amounts of the CNF@PIL-PF$_6$ hybrid were mixed with PAA and poly(1-cyanomethyl-3-vinylimidazolium PF$_6$) (the imidazolium/COOH molar ratio was fixed to 1:1) in DMSO to form a stable dispersion. The mixtures were then cast onto a glass slide, followed by drying in the air at 80 °C for 3 h. Afterwards, the dry films were immersed in aqueous ammonia solution, which triggered pore formation within their bulk. This pore formation process has been well described in the aforementioned work of Zhao *et al.*[48] In agreement with their studies, after the steps of film casting and drying, the developed film was dense, non-porous, and tightly adhered to the glass substrate. Creation of pores took place when the glass slide covered with the polymer blend was immersed in 0.2 wt % aqueous ammonia solution (pH 10.8). Diffusion of aqueous ammonia into the film causes deprotonation of carboxylic acid groups in PAA chains. The PAA chains create inter-polyelectrolyte complexes with PILs and

lead to the restructuration of the bulk of the film into a porous, electrostatically cross-linked arrangement.
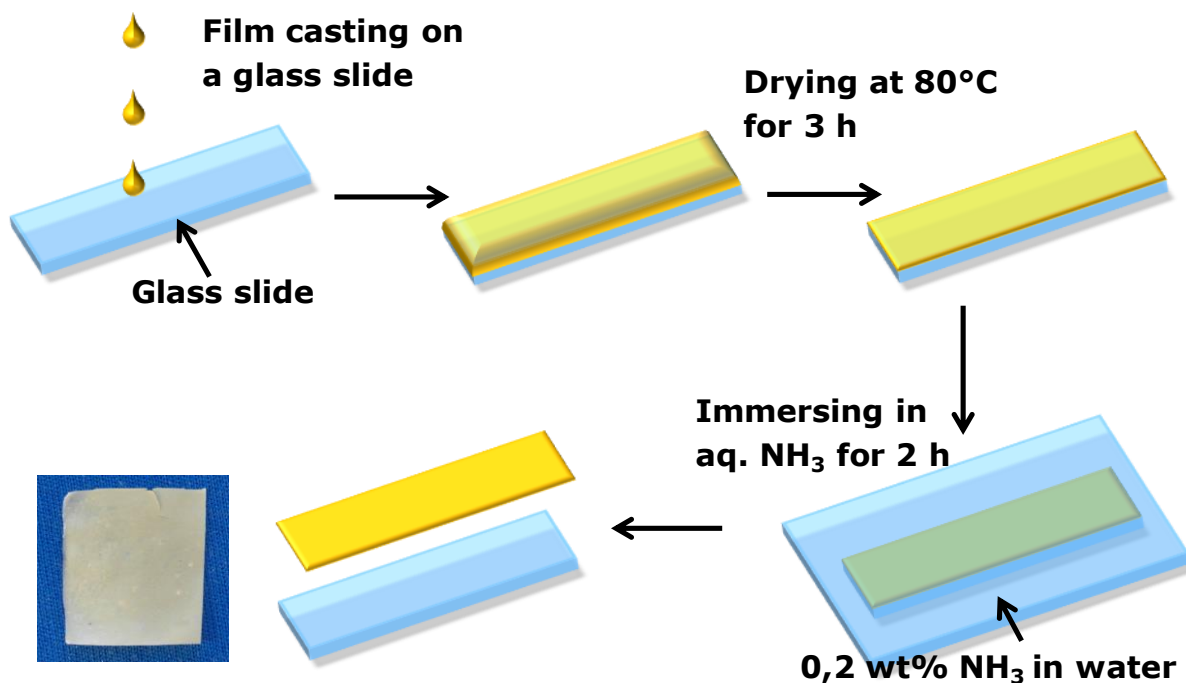

Figure 8. The preparation method of porous membranes and a photograph of such reinforced material.

As shown in the scanning electron micrographs (SEM, Figure 9), three-dimensionally interconnected porous structures were formed in both hybrid-free and hybrid-reinforced membranes. Both membranes display a similarly structured two-zone morphology (white lines in Figure 9 A and C), consisting of a micrometer-sized porous top zone and a bulk bottom zone with pores of 150 ± 50 nm for the CNF-free (Figure 9 B) and 250 ± 40 nm for the reinforced membranes (Figure 9 D). The structural similarity of grafted polymer and the PIL component of the membrane prevents phase separation of reinforcing agent from the polymeric matrix during the membrane formation. Thus, homogenous porous materials can be efficiently processed in the analogous manner as its precursors, presented by Zhao et al.[48] Unfortunately, a spatial distribution of CNF@PIL fibers within the membrane cannot be determined using SEM. Individual fibers in the bulk of the membrane cannot be distinguished even at high

magnification. This can be explained by the thin diameter (ca. 5 nm by TEM characterization) of CNFs and the presence of the polymeric brush on its outer layer which reduces the contrast between CNFs and the bulk membranes. Surprisingly, there are also no fibers protruding from the cross-section of the reinforced membrane.
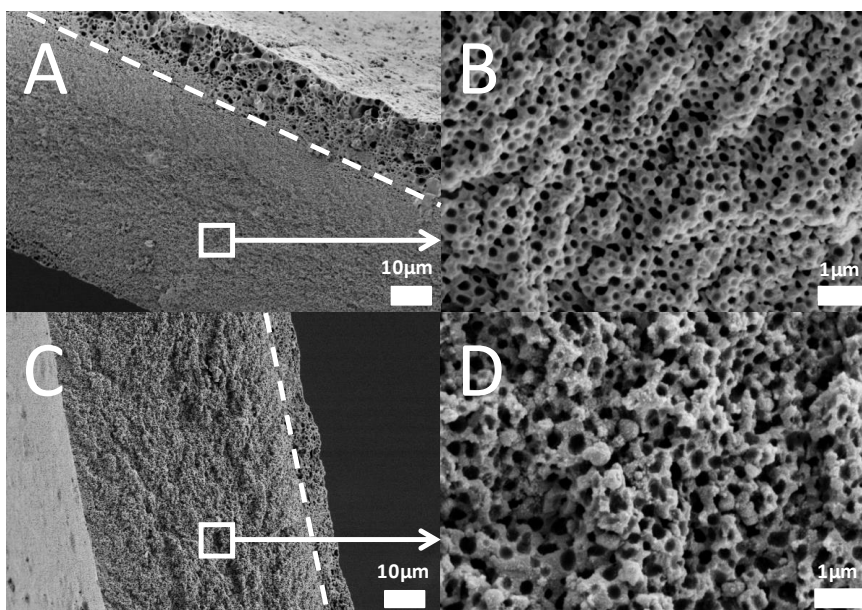

Figure 9. SEM images of membranes containing: A, B – 0 wt %; C, D – 5 wt % of CNF@PIL-PF$_6$.

Reinforcement of the porous membranes obtained by the incorporation of CNF@PIL-PF$_6$ hybrids was evaluated by tensile tests. It was anticipated that wet conditions are a potential environment at which membranes can be practically used. Hence, to acquire the data which is representative and brings an insight into the performance of the membranes at the conditions of their application, the test was performed at the wet state. In order to obtain quantitative results, thin strips of membrane (14 x 2 x 0.1 mm, at least 5 measurements for each type of membrane) were stressed in tension in a custom-made device. Due to the presence of hybrid materials within the bulk of the membrane, Young's modulus and stress at failure values increased from ~470 to ~610 MPa and from ~7.8 to ~10.4 MPa, respectively (Figure 10, Figure 11). The results show that incorporation of even 5 wt% of CNF@PIL-PF$_6$ (1.4 wt% of CNFs)

yields in the material with substantially better mechanical performance. Such a substantial reinforcement in the mechanical properties of membranes can be associated with the twofold structure of CNF@PIL-PF$_6$ hybrids. Their inner part is constituted of CNF rods which due to high tensile strength are good materials for application in reinforcing agents. PIL-PF$_6$ brush on the surface of hybrid has a high charge density and is structurally similar to the matrix of the membrane. It is anticipated that such a structure prevents the separation of CNFs from the polymeric matrix at the stage of membrane preparation, leading to the homogenous distribution of CNF@PIL and creating a reinforcing scaffold within the membrane.
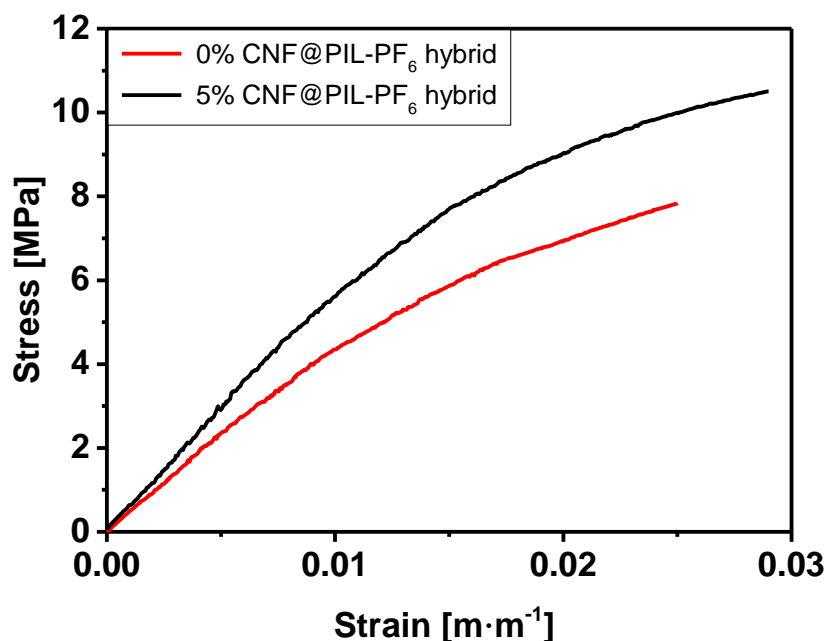
Figure 10. Average stress - strain curves of porous membranes composed of CMVImPF$_6$/PAA matrix containing 0 wt% (red line) and 5 wt% (black line) of CNF@PIL-PF$_6$.
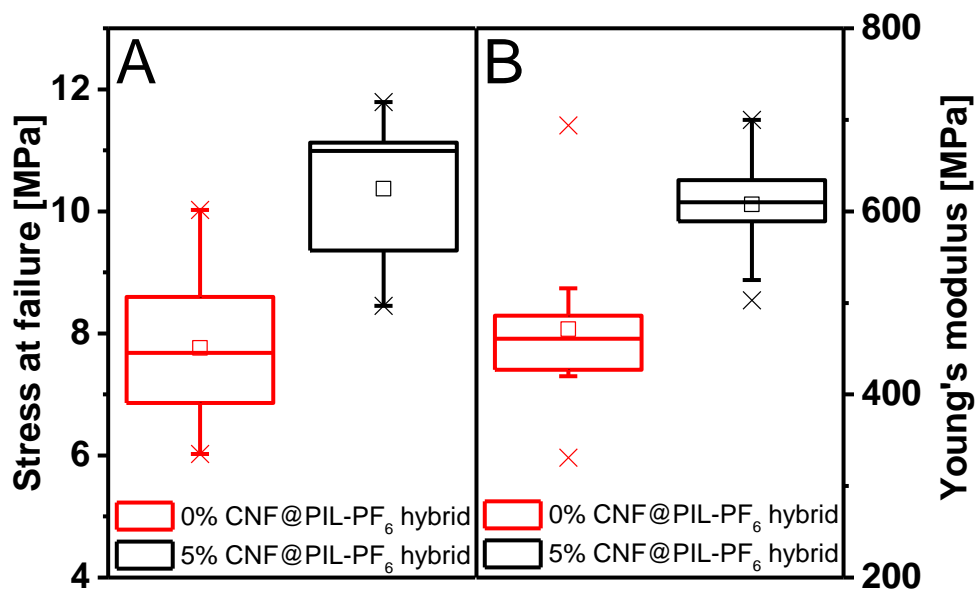
Figure 11. Box plots illustrating (A) stress at failure and (B) Young's modulus values obtained for porous membranes composed of PCMVImPF$_6$/PAA matrix and containing 0 wt% (red) and 5 wt% (black) of CNF@PIL-PF$_6$ hybrids (crosses represent maximum and minimum measured values, whiskers are 5th and 95th percentile, 25th and 75th percentile are represented as top and bottom lines of the boxes, medians are shown by the line inside the box and squares inside boxes correspond to average values).

Due to its hybrid composition, porous structure, and mechanical properties, CNF@PIL-PF$_6$ reinforced membrane can be considered as potential separation or supporting membrane. Thus, stress at failure and Young's modulus values measured for the reinforced porous membrane were collated with the literature results obtained for other porous, polyelectrolyte membranes (Table 3). The CNF@PIL-PF$_6$ containing porous film outperforms most of these membranes in terms of stress at failure values. It is worth noting that the obtained results are around 50 to 80 % higher than that of polyethersulfone, polysulfone, and poly(styrene sulfonate) complexes. Moreover, the CNF@PIL-PF$_6$ reinforced membrane resists stress two times higher than its counterparts composed of cellulose acetate and poly(ether–ether–sulfone). A membrane of chitosane-alginate complexes again breaks at stress almost 7 times lower than the reinforced PILs/PAA material. Only several reported values obtained for the membranes composed of poly(vinyl alcohol) and poly(vinylidene fluoride) outmatch the PILs/PAA reinforced porous films in terms of stress at failure values. However, the poly(vinyl alcohol)

26

based membranes possess Young's modulus around 13 times lower than the one obtained within this work. The poly(vinylidene fluoride) membrane, in turn, has very low porosity, so the direct comparison to the PIL/PAA complexes is misleading. In addition, with the measured value of 610 MPa, the PIL/PAA membrane containing CNF@PIL-PF$_6$ outperforms all above-mentioned porous materials in terms of Young's modulus. This comparison clearly allows the conclusion that PIL/PAA membranes reinforced with CNF@PIL hybrids possess very good mechanical features, which make it competitive with other existent porous polyelectrolyte analogues.

Table 3. Literature values of stress at failure and Young's modulus of selected porous membranes.

Polymer	Stress at failure [MPa]	Young's modulus [MPa]
Poly(vinyl alcohol)[84]	13.5	48
Poly(vinyl alcohol)[84]	4.3	110
Polyvinylidene fluoride[85]	7,5	-
Polyvinylidene fluoride[85]	17,7 (10% of porosity)	-
Polyethersulfone[86]	6.97 ± 0.23	228.30 ± 49.56
Polyethersulfone[86]	5.88 ± 0.27	273.80 ± 21.58
Polysulfone[87]	6.04	194.9
Poly(diallyldimethylammonium)-poly(styrene sulfonate) complex[88]	6.0	-
Cellulose acetate + poly(ether–ether–sulfone)[89]	4.87	247.30
Chitosan-Alginate complex[90]	1.54	-

2.4 Conclusion

In summary, an efficient method for facile grafting PILs onto the surface of CNFs by a simple *in situ* one-step polymerization has been developed. Such CNF@PIL hybrids display

excellent and tunable dispersibility in water and various organic media *via* anion exchange. The omnidispersibility of the PIL-functionalized CNFs enables processing them in organic solvents, which was used to implement such nanohybrids into porous polyelectrolyte membranes. Addition of CNF@PIL hybrids even at a low fraction of 5 wt% substantially affects mechanical properties of porous PIL membranes, improving both, ultimate tensile strength and Young's modulus values. The PIL-functionalization of CNFs offers a versatile and straightforward way to create omnidispersible nanoparticles from highly charged components.

3. THIAZOLIUM-BASED PIL STABILIZERS

The thiazolium cation as a part of vitamin B_1 (thiamine) is produced in nature within bacteria, plants and fungi (Figure 12) as a catalyst for biochemical processes. Its catalytic activity (for instance in nucleophilic acylation) is explained by the presence of nucleophilic carbene, which can be generated on thiazolium ring under special conditions.[91]
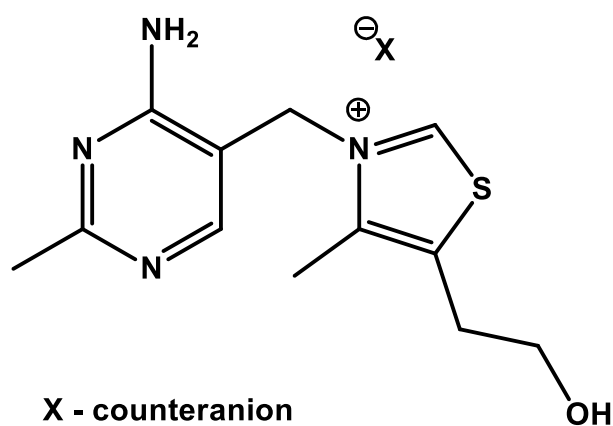
Figure 12. Chemical structure of thiamine.

The catalytic activity of thiazolium cation has attracted attention of material scientists. Several examples of ILs containing thiazolium ring in their structure have been reported for the catalytic applications in benzoin condensation[92] and the Stetter reaction.[93] The commonly accepted mechanism of benzoin condensation by thiazolium salts was proposed by Breslow (Figure 13).[91] In detail, the thiazolium salt undergoes deprotonation at the C2 position of thiazolium ring due to its acidic character. The formed thiazolin-2-ylidene (Figure 13, compound 2) can act as a nucleophile and attack an aldehyde to form a resonance-stabilized enaminol-type Breslow intermediate (Figure 13, compound 5). Subsequently, compound 5 can react with another molecule of electrophile (e.g. the carbonyl group of aldehyde), followed by elimination of benzoin and carbene catalyst.[91] Additionally, thiazolium-containing ILs can be used for gas separation and extractive desulfurization of fuel oil.[94, 95] Even though several

examples of thiazolium-type ILs have been reported previously, thiazolium-based ionic polymers are rare cases and they have not been extensively studied so far. It is one of the main aims of this PhD work to merge thiazolium-type compounds and PIL chemistry in order to produce new PIL structures and functional polymer materials. In this work, along with the focus of this thesis such structures were investigated as stabilizers for nanomaterials and binders for battery application.
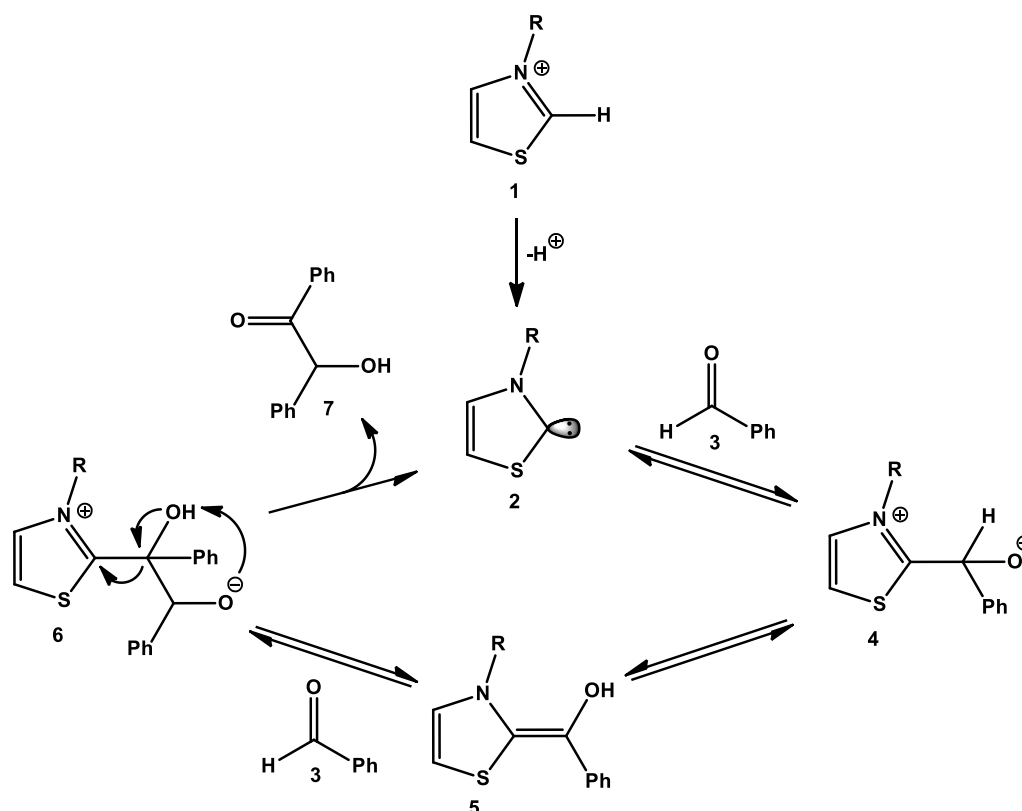

Figure 13. Thiazolium salt-catalyzed benzoin condensation.[91]

3.1 4-Methyl-3-(4-vinylbenzyl)thiazolium-type PILs for stabilization of carbon nanotubes

4-Methylthiazole was selected as a model starting compound for the synthesis of thiazolium-containing PILs (Figure 14) due to its relatively low price compared with its other

commercial counterparts. It has been reported in the literature that the nitrogen atom of the thiazole ring can readily undergo a quaternization reaction with alkyl halides, leading to the corresponding ILs. Thus, the attachment of a polymerizable unit to the thiazole ring *via* the nitrogen atom was a potential method to prepare an ILM, which can be subsequently polymerized in order to form PILs.
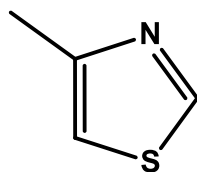
Figure 14. The chemical structure of 4-methylthiazole.

Among potential applications of thiazolium-containing ionic polymers, stabilization of carbon nanotubes (CNTs) was especially appealing. CNTs, as one of the most popular nanomaterials, have been extensively studied for their unique mechanical, thermal, electrical, chemical, and optical properties. A broad range of usages of CNTs have been explored, including drug delivery, nanoelectronics and optical sensors.[96] A common problem associated with applications of CNTs is that they are prone to agglomeration due to strong hydrophobic interactions. For the purpose of dispersing CNTs in liquid phase, stabilization or deaggregation agents can be used to prevent CNTs from re-agglomeration after exfoliation from bundles into individual tubes. The state-of-the-art methods for the stabilization of CNTs are often divided into two main groups, named "covalent" and "physical" ones. The first one relies on anchoring stabilization agents on the surface of CNTs by covalent bonding. The major drawback of this method is the risk of damaging the CNT, causing disruption of π-networks which decreases their mechanical and electronic properties. The latter approach involves strong, non-covalent interactions of stabilization agents with the CNT surface.[97, 98] This method critically preserves the physical properties of the CNT. However, the necessity of using the stabilizer in large excess is recognized as an inherent disadvantage. Several organic compounds, including polymers and

surfactants, are capable of acting as efficient physical stabilizers for CNTs. [99-102] Part of this chapter has been published in Macromolecular Symposia, 2014, 342, 1, 67-77.

3.1.1 Synthesis of 4-methyl-3-(4-vinylbenzyl)thiazolium-type PILs

The synthetic route to thiazolium ionic monomers and polymers is presented in Figure 15. 4-Methyl-3-(4-vinylbenzyl)thiazolium chloride (MVBT$^+$Cl$^-$), a water soluble ionic monomer, was obtained by a quaternization reaction of 4-methyl thiazole with 4-vinylbenzyl chloride in ethyl acetate at 70 ºC. Since such a high temperature during synthesis could lead to undesired radical reactions of styrene groups, a polymerization inhibitor 2,6-di-t-butyl-4-methylphenol was included in the reaction mixture. Subsequently, MVBT$^+$Cl$^-$ after purification was polymerized in aqueous media using a water soluble non-ionic thermal initiator 2,2'-azobis[2-methyl-N-(2-hydroxyethyl) propionamide] (VA86), to form poly[4-methyl-3-(4-vinylbenzyl)thiazolium) chloride] [P(MVBT$^+$Cl$^-$)]. In order to tune the physical properties of the synthesized ionic monomer and polymer, a series of anion exchange reactions were performed. The chloride counterions of MVBT$^+$Cl$^-$ and P(MVBT$^+$Cl$^-$) were replaced with more hydrophobic, fluorinated anions, such as triflurosulfonate (TFO$^-$), PF$_6^-$, and TFSI$^-$. Two main methods were employed in the anion exchange reactions of MVBT$^+$Cl$^-$ and P(MVBT$^+$Cl$^-$). In the synthetic pathway, the synthesis of monomers and polymers containing TFSI$^-$ and PF$_6^-$ counter anions was performed by adding an aqueous solution of the corresponding salt dropwise into the aqueous solutions of MVBT$^+$Cl$^-$ and P(MVBT$^+$Cl$^-$), respectively. The precipitation was observed immediately after the addition of the salt solution. This is macroscopic evidence that the hydrophilic Cl$^-$ of the monomers and polymers was replaced by hydrophobic, fluorinated TFSI$^-$ and PF$_6^-$. A different method was employed in order to exchange anions from Cl$^-$ towards BF$_4^-$ and TFO$^-$, as the previously described protocol failed

here due to the non-negligible solubility of the monomer and polymer with these two anions in water. The exchange reaction was performed by mixing MVBT⁺Cl⁻ or P(MVBT⁺Cl⁻) with a 1.1 molar equivalent of the corresponding sodium salt in dry acetonitrile. Slow dissolution of sodium salts and simultaneous precipitation of NaCl from acetonitrile due to its low solubility (0.003 g in 1 kg of acetonitrile at 25°C) took place along the course of the reaction.[103] After removal of NaCl by filtration, the monomer and polymer with TFO⁻ and BF₄⁻ anions were isolated by evaporation of acetonitrile under high vacuum at room temperature. Unfortunately, in spite of multiple attempts, direct radical polymerization of non-halide monomers failed to yield polymers of high molar mass. Thus, the synthesis of non-halide polymers was only performed *via* post-polymerization modification of P(MVBT⁺Cl⁻) though anion exchange.
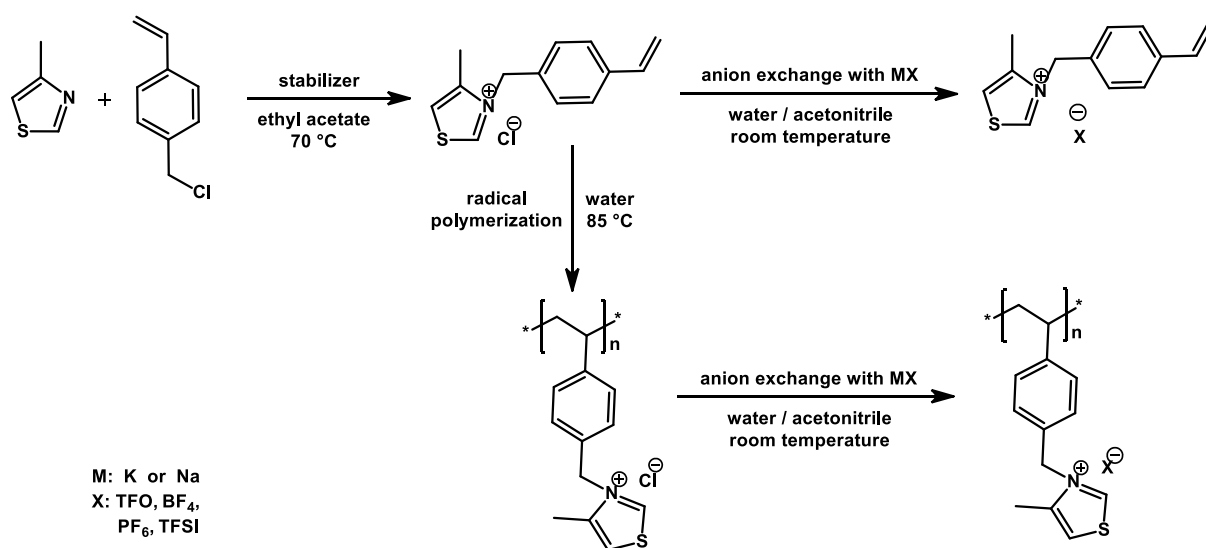
Figure 15. Synthetic route and chemical structures for the obtained thiazolium-type monomers and ionic polymers.

3.1.2 Characterization of 4-methyl-3-(4-vinylbenzyl)thiazolium-type monomers and polymers

For the thiazolium monomer, a quaternization reaction on nitrogen is preferred to a reaction on the sulfur atom. In order to confirm the chemical structure and purity of the synthesized monomer, proton-carbon heteronuclear single quantum coherence spectroscopy (^{1}H-^{13}C HSQC) and proton-carbon heteronuclear multiple bond correlation (^{1}H-^{13}C HMBC) spectroscopy measurements were employed (Figure 16, Figure 17). The spectral data fits well with the proposed product of the reaction. ^{1}H-^{13}C HSQC spectrum was initially employed to confirm the correct assignment of signals belonging to carbons and protons of the synthesized product. Afterwards, ^{1}H-^{13}C HMBC spectrum was used to detect multiband coupling between proton and carbons and therefore resolve the structure of the thiazolium monomer. The coupling between proton 10 and carbon 2 can be observed, but no coupling between proton 10 and carbon 8 was found. ^{1}H-^{13}C HMBC reveals that carbon 10 is coupled to proton 1, but not to proton 8. This clearly indicates that the 4-methyl thiazole underwent a reaction with the 4-vinylbenzyl group exclusively on the nitrogen atom of the thiazolium ring, but not on the sulfur atom.
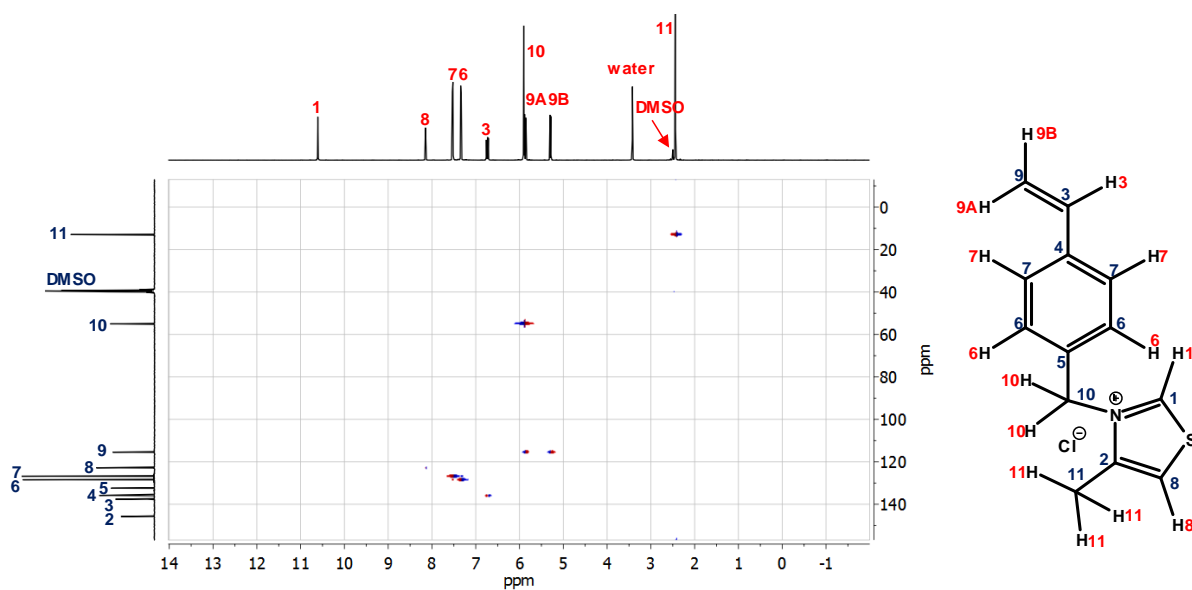
Figure 16. ^{1}H-^{13}C HSQC spectral data of MVBT$^+$Cl$^-$.

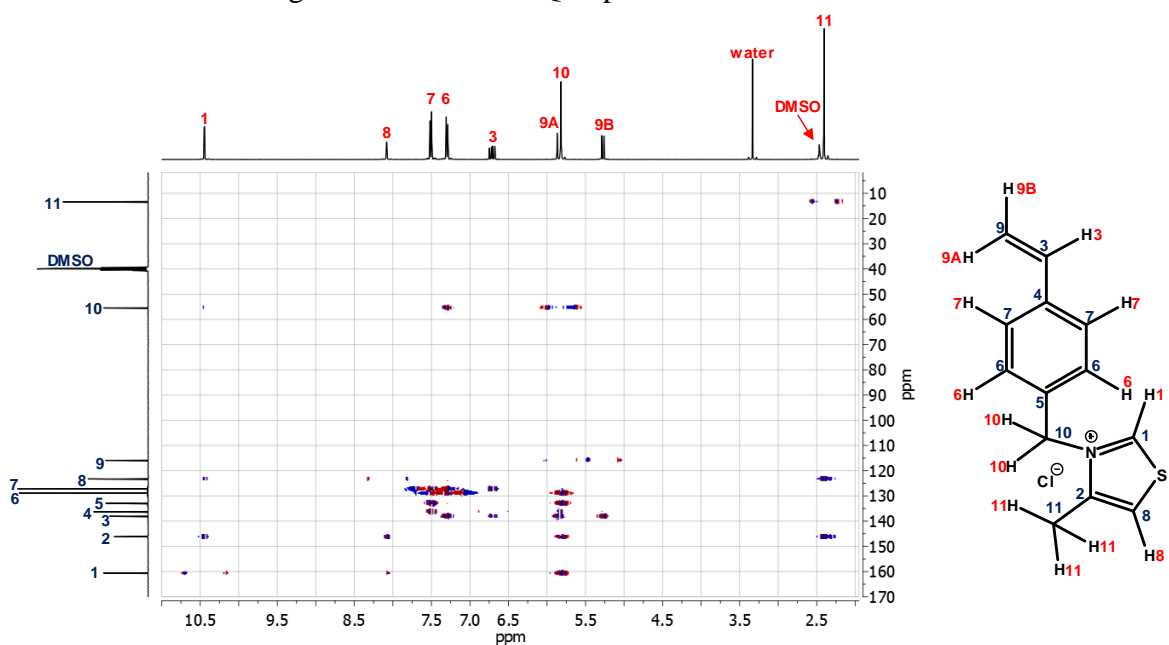Figure 17. ^{1}H-^{13}C HMBC spectral data of monomer MVBT$^+$Cl$^-$.

After polymerization of MVBT$^+$Cl$^-$, the product was characterized by proton nuclear magnetic resonance spectroscopy (^{1}H-NMR) and GPC. The disappearance of the peaks of vinyl group (at 6.73, 5.84, and 5.29 ppm) and the new broad signal in the high field range (between 1 and 2 ppm) which can be assigned to protons of polymeric backbone, indicate that the desired polymer structure was formed (Figure 21). Moreover, broadening of particular signals in ^{1}H-NMR spectrum, which is typically observed for polymers, further confirms that a reasonably high molar mass polymer was obtained. To analyze the molar mass GPC measurements were

35

performed using a Novema column with a water/methanol mixture in the presence of an acetic buffer as eluent (Figure 18). These conditions were purposely chosen in order to avoid the possible binding of the polymers to the GPC column. P(MVBT$^+$Cl$^-$) displayed a monomodal molar mass distribution and an apparent number average molar mass of 15 kg/mol (calculated using PEO standard). Its Đ equals to 3.0, which is in the reasonable range for typical free radical polymerizations. Owing to the fact that other ionic polymers were synthesized *via* an anion exchange of P(MVBT$^+$Cl$^-$), their degree of polymerization should be identical to that of P(MVBT$^+$Cl$^-$).
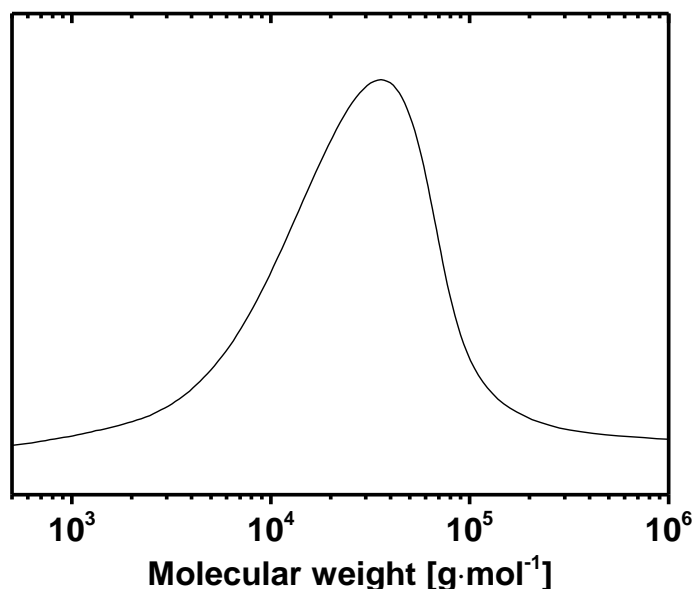
Figure 18. Molar mass distribution of P(MVBT$^+$Cl$^-$) obtained from GPC measurements.

Anion exchange reactions can be conveniently characterized by ATR-FTIR spectroscopy (Figure 19). The FTIR pattern of MVBT$^+$Cl$^-$ stems from the thiazolium cation, since Cl$^-$ is not visible in the IR range. After the anion exchange reaction, recorded spectra were examined for the presence of new peaks of the corresponding counter anions. In the case of MVBT$^+$BF$_4$$^-$ the broad signal with two absorption maxima at 1038 and 1049 cm^{-1} can be associated with the asymmetric stretching of the BF$_4$$^-$ anion. The presence of the PF$_6$$^-$ anion of MVBT$^+$PF$_6$$^-$ is clearly indicated by the strong, broad band at 825 cm^{-1}, which is due to the

antisymmetric stretching of PF_6^-.[104] When the Cl^- anion is replaced by TFO^-, the new vibration bands of the CF_3 group ($\delta_a CF_3$ at 572 cm^{-1}, $\delta_s CF_3$ at 756 cm^{-1}, $\nu_s CF_3$ at1153 cm^{-1}, and $\nu_a CF_3$ at 1223 cm^{-1}) can be detected. Additionally, signals resulting from vibrations of SO_3 groups (δSO_3 at 634 cm^{-1}, $\nu_s SO_3$ at 1027 cm^{-1} and $\nu_a SO_3$ at 1256 cm^{-1}) further confirm the efficient anion exchange. Finally, in a similar manner, exchange of Cl^- with $TFSI^-$ was confirmed. Three sharp bands of CF_3 groups ($\nu_a CF_3$ at 1182, $\delta_s CF_3$ at 741 and $\delta_a CF_3$ at 569 cm^{-1}) as well as bands from the SO_2 group of $TFSI^-$ ($\nu_a SO_2$ at 1346, $\nu_s SO_2$ at 1134, and $\delta_a SO_2$ at 609 cm^{-1}) indicate successful incorporation of $TFSI^-$ into the structure of the thiazolium monomer. In addition, asymmetric (1047 cm^{-1}), and symmetric (763 cm^{-1}) stretching bands of the S-N-S group and symmetric stretching of C-S bond (792 cm^{-1}) further confirm that anion exchange towards $MVBT^+TFSI^-$ took place.
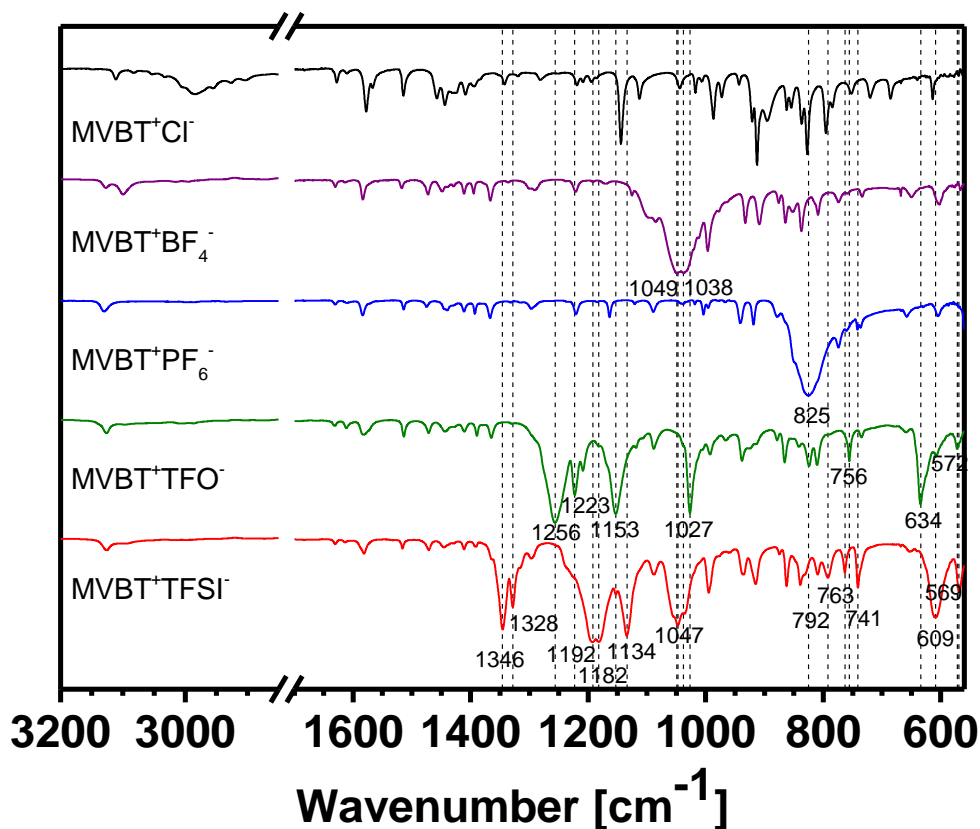

Figure 19. ATR-FTIR spectra recorded for $MVBT^+X^-$ monomers (X - PF_6, BF_4, TFO, and TFSI).

Analogously, the new ATR-FTIR bands were used to confirm the anion exchange reaction of P(MVBT$^+$Cl$^-$) (Figure 20). From the spectrum, the asymmetric stretching vibration of BF$_4^-$ anion gives broad bands of two absorption maxima at 1033 and 1051 cm^{-1}. In the ATR-FTIR spectrum of P(MVBT$^+$PF$_6^-$) a strong, broad signal at 821 cm^{-1} from the antisymmetric stretching vibration of PF$_6^-$ is observed. When TFO$^-$ is introduced into the structure of the thiazolium polymer, sharp vibrational signals of the CF$_3$ group (δ_aCF$_3$ at 573, δ_sCF$_3$ at 756, ν_sCF$_3$ at 1152 and ν_aCF$_3$ at 1223 cm^{-1}) as well as of SO$_3$ groups (δSO$_3$ at 634, ν_sSO$_3$ at 1026 and ν_aSO$_3$ at 1252 cm^{-1}) are detected. Finally, the successful reaction of a polymer containing the TFSI$^-$ anion is indicated by the presence of peaks from CF$_3$ groups (ν_sCF$_{3-}$ shoulder at 1220, ν_aCF$_3$ at 1176, δ_sCF$_3$ at 740 and δ_aCF$_3$ at 569 cm^{-1}) and SO$_2$ (ν_aSO$_2$ at 1345, ν_sSO$_2$ at 1131, δ_aSO$_2$ at 610 and δ_sSO$_2$ at 599 cm^{-1}). Moreover, the presence of bands as a result of vibrations of S-N-S (ν_aSNS at 1051 cm^{-1} and ν_sSNS at 762 cm^{-1}) and C-S bond (ν_sCS at 788 cm^{-1}) also indicate that polymer underwent anion exchange reaction towards TFSI$^-$.
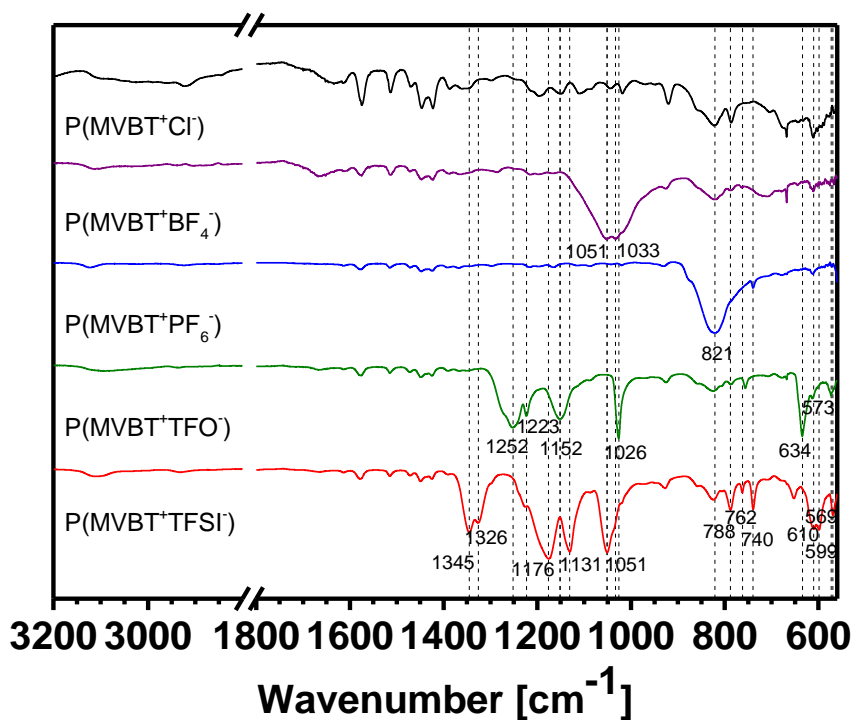

Figure 20. ATR-FTIR spectra recorded for P(MVBT$^+$X$^-$) polymers (X - PF$_6$, BF$_4$, TFO, and TFSI).

The anion exchange reaction from Cl^{-} to fluorinated counterions also causes change in deshielding of protons belonging to thiazolium ring. ^{1}H-NMR spectroscopy measurements were employed in order to confirm anion exchange in the synthesized monomers and polymers. As an example, in MVBT[+]TFSI[-], peaks assigned to protons of imidazolium ring shifted from 10.59 and 8.14 ppm to 10.14 and 8.05 ppm, respectively, when compared to MVBT[+]Cl^{-} (Figure 21). Analogous changes in the ^{1}H-NMR spectrum were also observed when Cl^{-} anions of P(MVBT[+]Cl^{-}) became replaced by TFSI[-]. In this case, the resonance signals of protons of the thiazolium ring at 11.0 and 8.3 ppm as well as the peak of the -CH$_2$- group at 6.1 ppm are all shifted towards lower ppm values at 10.1, 8.0 and 5.6 ppm respectively. The ^{1}H-NMR spectra of the other anion-exchanged monomers and polymers resemble that of MVBT[+]TFSI[-] and P(MVBT[+]TFSI[-]), a further evidence to suggest a successful anion exchange reaction.
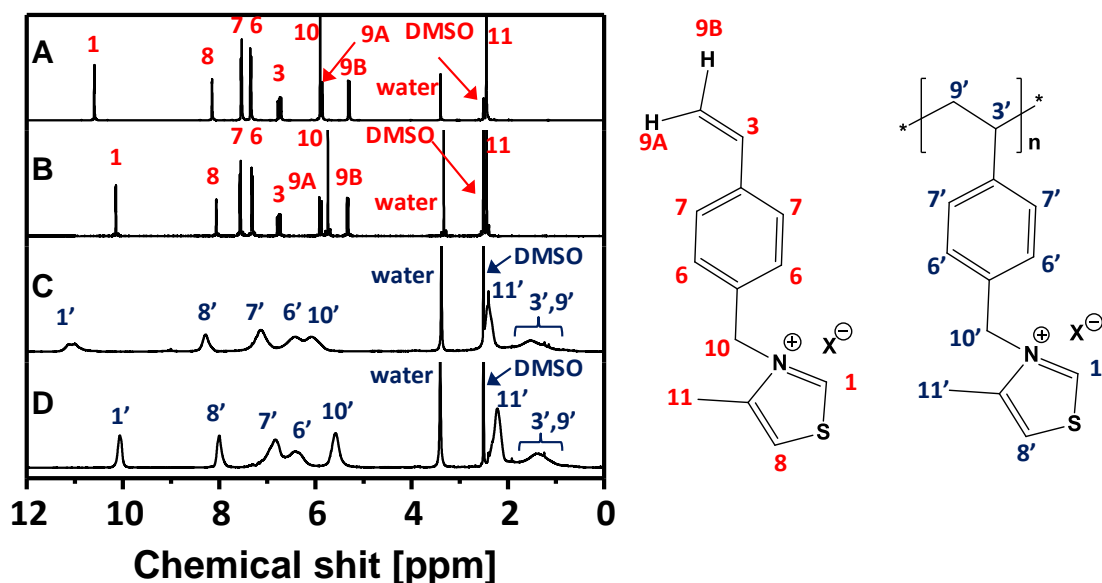
Figure 21. ^{1}H-NMR spectra of: A - monomer MVBT[+]Cl^{-}; B - monomer MVBT[+]TFSI[-]; C - polymer P(MVBT[+]Cl^{-}); D) polymer P(MVBT[+]TFSI[-]).

According to the conventional definition of PILs, their corresponding monomers must be an IL, *i.e.* liquid at temperatures below 100 °C. Therefore all synthesized thiazolium monomers were characterized by differential scanning calorimetry (DSC) (Figure 22) to determine their melting point. Recorded thermograms revealed that exchanging counter

anions from Cl$^-$ to TFSI$^-$ and TFO$^-$ yields ionic products being in a liquid state at 60 and 70 °C (Figure 22, Figure 23), respectively. Hence, MVBT$^+$TFSI$^-$, and MVBT$^+$TFO$^-$ can be indeed classified as classic ILs and their corresponding polymers as PILs. It is worth noting that the melting temperatures of MVBT$^+$Cl$^-$, MVBT$^+$BF$_4^-$ and MVBT$^+$PF$_6^-$ exceed 100 °C. Thus, the latter 3 monomers are only considered within the general scope of organic salts and their polymers in the strict sense can be defined as ionic polymers rather than PILs.
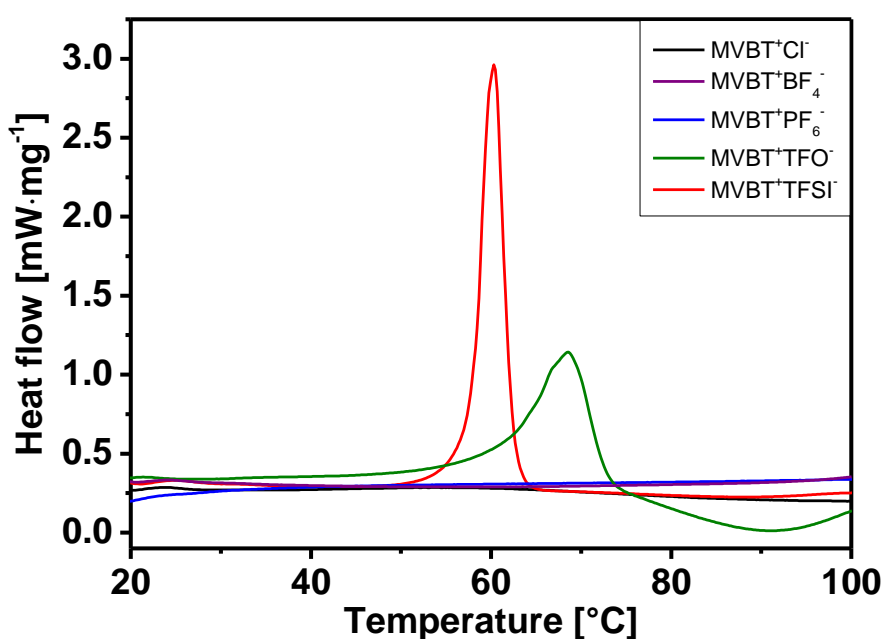

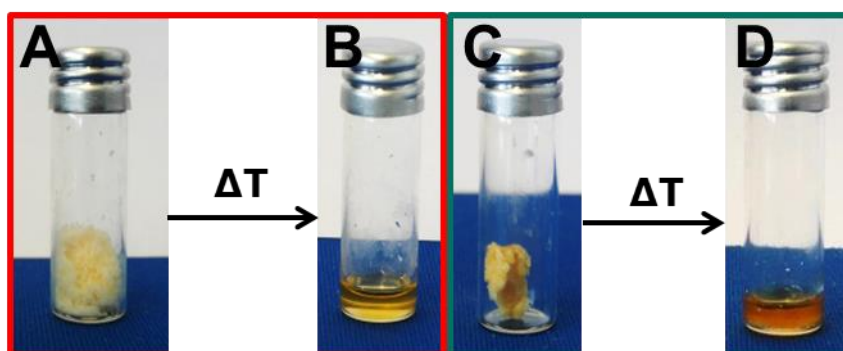Figure 22. DSC curves recorded for thiazolium-based ionic monomers.

Figure 23. Photographs of MVBT$^+$TFSI$^-$ in the left red frame; and MVBT$^+$TFO$^-$ in the right green frame at room temperature (A, C) and at 80 °C (B, D).

Among several interesting features of PILs, a high, tunable thermal stability is of great importance when potential applications of PILs are considered. Therefore it was necessary to analyze the decomposition temperature of the newly synthesized family of thiazolium-type PILs and ionic polymers. The thermal stability of $MVBT^+Cl^-$ and all other synthesized PILs and ionic polymers were determined by TGA measurement (Figure 24). $MVBT^+Cl^-$ decomposes at 170 °C (temperature of 10 % of weight loss). The initial weight loss of the $MVBT^+Cl^-$ monomer at the temperature range 100-150 °C is associated with the evaporation of a trace amount of moisture due to limited drying temperature, which must remain low to avoid its thermal polymerization. The decomposition temperature of $P(MVBT^+Cl^-)$ was found to be 200 ºC, that is, 30 °C higher than its monomer. It is in agreement with typical observation that PILs are slightly thermally more stable than corresponding ILMs. Analogously, decomposition temperatures of thiazolium-containing polymers can be also tuned by the choice of counterion. When Cl^- is replaced with $TFSI^-$, the thermal stability of the polymer increases substantially by 80 ºC, *i.e.* the decomposition temperature of this polymer by a 10 % weight loss is 280 ºC. Surprisingly, $P(MVBT^+BF_4^-)$ is even more stable than the polymer bearing $TFSI^-$, which decomposes at 295 °C. Decomposition temperatures of $P(MVBT^+PF_6^-)$ and $P(MVBT^+TFO^-)$ are also higher than $P(MVBT^+Cl^-)$, reaching values of around 260 ºC. Thus, thermal stability of thiazolium-containing PILs and ionic polymers decreases in the sequence of $BF_4^- > TFSI > PF_6^- \sim TFO^- > Cl^-$.
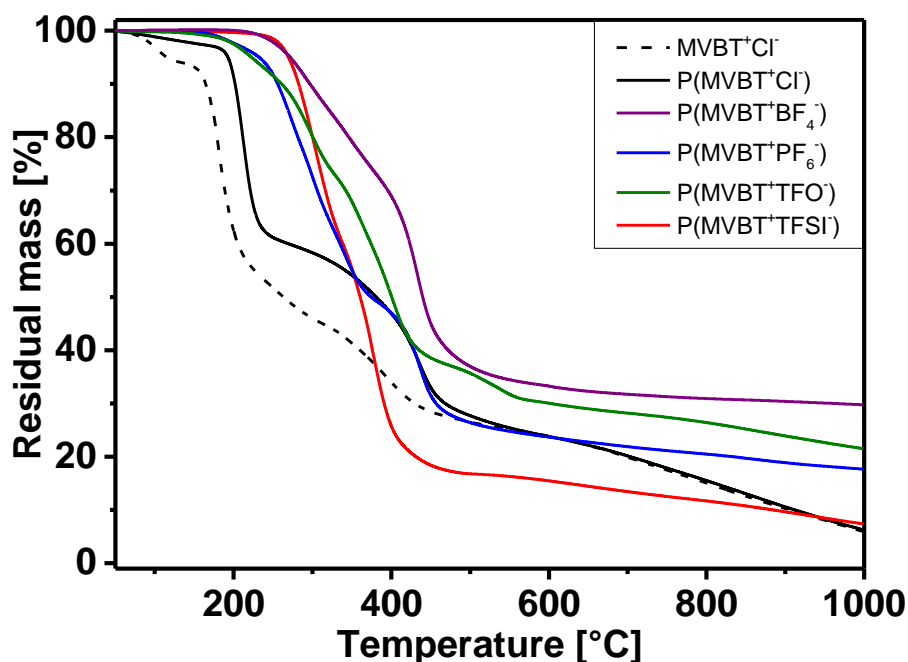
Figure 24. TGA curves of the synthesized ionic polymers (measured at heating rate 10 K·min^{-1} and under nitrogen atmosphere).

Another features of PILs which strongly depends on the type of counterion are their solubility properties. The solubility of thiazolium polymers in water and various organic solvents were tested and the results are presented in Table 4. The thiazolium polymer bearing a hydrophilic Cl$^-$ counteranion can be readily dissolved in water and in polar organic solvents, for instance in methanol. Organic solvents of moderate and low polarity are poorly suited for P(MVBT$^+$Cl$^-$). Unexpectedly, this polymer was insoluble in DMF, typically a good solvent for most of PILs. Thiazolium polymers bearing more hydrophobic counterions (PF$_6^-$, TFO$^-$ and TFSI$^-$) turn out to be well soluble in DMF but are no longer soluble in water. Additionally, P(MVBT$^+$PF$_6^-$) and P(MVBT$^+$TFSI$^-$) show good solubility in acetone, while only P(MVBT$^+$TFSI$^-$) and P(MVBT$^+$TFO$^-$) remain soluble in MeOH. Surprisingly, P(MVBT$^+$BF$_4^-$) can be dissolved only in DMSO and DMF. It is worth noting that all synthesized polymers dissolve in DMSO. Moreover, none of them was soluble in organic solvents which have a relatively high dielectric constant, such as THF, EtAc, toluene, and chloroform (CHCl$_3$).

Table 4. Solubility table of P(MVBT$^+$X$^-$) in different solvents.

P(MVBT$^+$X$^-$)	H$_2$O	MeOH	Acetone	DMF	DMSO	THF, EtAc, Toluene, CHCl$_3$
Cl$^-$	+	+	-	-	+	-
TFO$^-$	-	+	-	+	+	-
PF$_6$$^-$	-	-	+	+	+	-
BF$_4$$^-$	-	-	-	+	+	-
TFSI$^-$	-	+	+	+	+	-

3.1.3 Applications of 4-methyl-3-(4-vinylbenzyl)thiazolium-type polymers

In the TGA analysis, a high content of residues obtained from P(MVBT$^+$Cl$^-$) above 500 °C, (> 20 wt%, Figure 24) and the existence of sulfur and nitrogen atoms in the thiazolium ring suggest that such polymers may be interesting precursors for sulfur-nitrogen co-doped carbon materials. Carbonization of P(MVBT$^+$Cl$^-$) at 500, 800 and 1000 °C under nitrogen atmosphere was performed, and the resulting carbon materials were characterized by elemental analysis. The yield of P(MVBT$^+$Cl$^-$) carbonized at 500 °C was as high as 28.2 %, but it showed downturn as the carbonization temperature was increased of (20 % at 800 °C and 18 % at 1000 °C, Figure 25). Elemental analysis revealed that the nitrogen content is around 2.5 % and only slightly depends on the carbonization temperature in the analyzed range of temperatures (Figure 25). Conversely, the sulfur content in the final product depends strongly on the carbonization temperature. It decreases from 2.5 % for carbons obtained at 500 °C to less than 1.0 % at 1000 ºC.
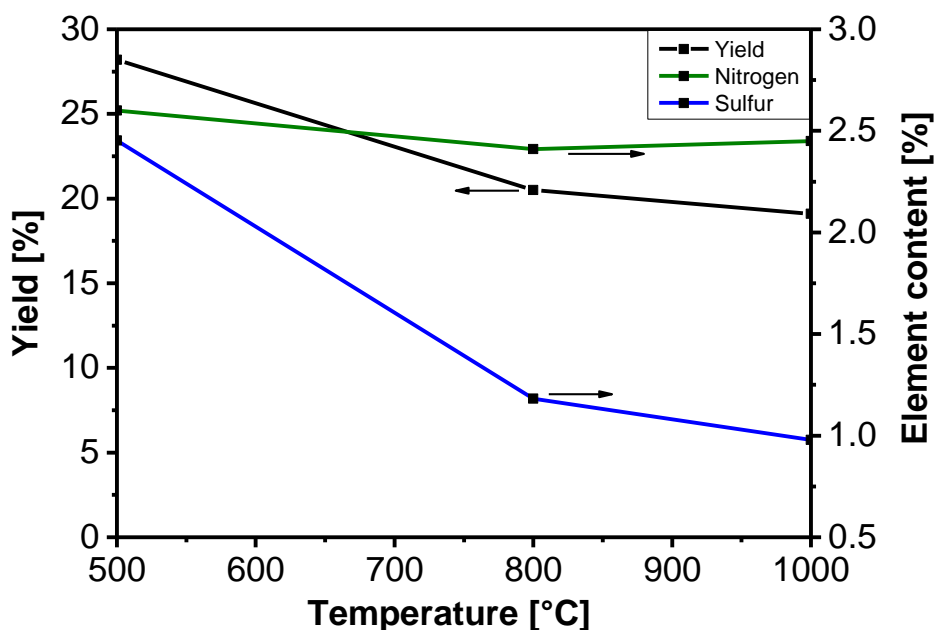
Figure 25. Carbonization yield, sulfur and nitrogen content of P(MVBT$^+$Cl$^-$) as a function of the carbonization temperature.

Finally, the potential of thiazolium-based ionic polymers to stabilize multiwalled carbon nanotubes (MWCNTs) as well as single walled carbon nanotubes (SWCNTs) in aqueous and organic media was investigated. The same feature was previously described for imidazolium-type cation PILs. Following a reported procedure, MWCNTs and P(MVBT$^+$Cl$^-$) were sonicated in water, forming a dark suspension which was stable for weeks (Figure 26 A, B). TEM measurements confirmed very good quality of obtained dispersions (Figure 26 C, D). The observed MWCNTs were well separated, free of the existence of large agglomerates. In a control experiment, MWCNTs were dispersed in water using an ultrasonic horn without the presence of P(MVBT$^+$Cl$^-$). A precipitate of MWCNTs formed shortly after the sonication (Figure 26 A, B). Analogous results were obtained for SWCNTs. Unfortunately, due to low contrast between SWCNTs and carbon film of TEM grids, stable dispersions of SWCNTs were barely visible by TEM. The proposed stabilization mechanism of CNTs by thiazolium-containing polymers involves cation-π interaction, which has been previously suggested for PILs with imidazolium cations. Moreover, P(MVBT$^+$Cl$^-$) adsorbed on the surface of MWCNTs can be used to transfer MWCNTs to organic solvents. In an exemplary

experiment, the MWCNTs/P(MVBT$^+$Cl$^-$) hybrids were precipitated from their aqueous dispersion by addition of KPF$_6$ solution (Figure 26 E). This caused an anion exchange reaction of P(MVBT$^+$Cl$^-$), forming P(MVBT$^+$PF$_6^-$). Subsequently, the hydrophobic MWCNTs/P(MVBT$^+$PF$_6^-$) hybrids precipitated from water, which after separation were dispersible in acetone (Figure 26 F).
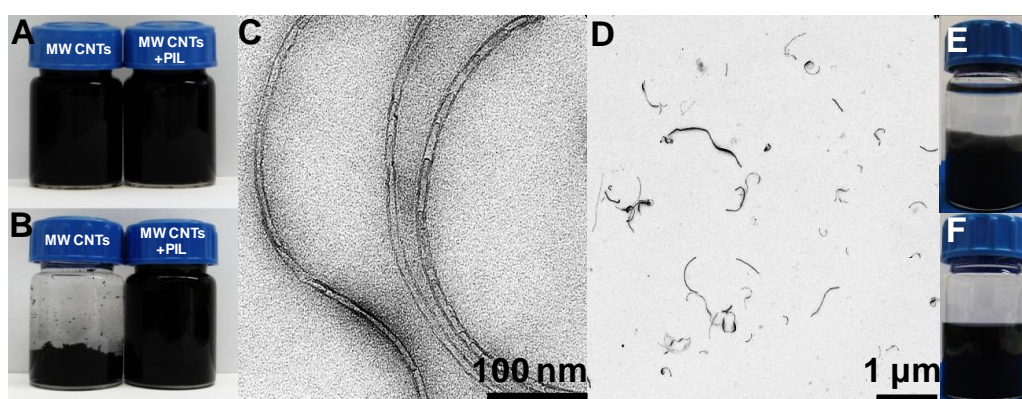

Figure 26. A - Photographs of MWCNTs dispersion and P(MVBT$^+$Cl$^-$) stabilized MWCNTs dispersion immediately after sonication; B - Photographs of MWCTs suspension and P(MVBT$^+$Cl$^-$) stabilized MWCNs dispersion 24 h after sonication; C and D - TEM images of P(MVBT$^+$Cl$^-$) stabilized MWCNTs dispersion. E - P(MVBT$^+$Cl$^-$) dispersion in water after the addition of KPF$_6$ salt solution; F - P(MVBT$^+$PF$_6^-$) dispersion in acetone.

3.2 3,4-Dimethyl-5-vinylthiazolium containing PILs

The previous section described the method for obtaining thiazolium-type ionic polymers and PILs. However, it should be highlighted that the established synthetic route has several flaws. First of all, it failed in the attempt to produce PILs containing fluorinated counterions directly from their IL monomers. Instead, anion exchange reactions for polymers were employed which always bear a risk of non-quantitative anion replacement. Secondly, the synthesized thiazolium monomers contain a large phenylene group which makes their structure more bulky and rigid. Owing to this fact, only two of the IL monomers were liquids below 100 °C fulfilling the definition of ILs. Finally, in addition to these nomenclature

divagations, the complex structure of the MVBT⁺X⁻ monomers reduced the concentration of effective IL species in the final material, *i.e.* the styrenic unit stands for a large weight fraction. This in turn, may limit the potential to utilize such polymers in the production of nitrogen/sulfur co-doped carbons. These disadvantages triggered the follow-up work to prepare IL monomer with more compact structure and high fraction of thiaozolium cations. For this reason 4-methyl-5-vinyl thiazole was used as monomer precursor. Such compound has the advantages of being structurally simple and commercially available. A direct consequence of this design of the chemical structure is an access to new monomers with lower melting points and PILs with higher charge density and boosted sulfur-nitrogen content.

3.2.1 Synthesis of 3,4-dimethyl-5-vinylthiazolium containing PILs

The synthetic route towards novel thiazolium-containing monomers as well as their corresponding polymers is presented in Figure 27. Firstly, the nitrogen atom of 4-methyl-5-vinyl thiazole underwent quaternization reaction with methyl iodide, in order to obtain 3,4-dimethyl-5-vinylthiazolium iodide (MVT⁺I⁻). Afterwards, monomers containing PF_6^-, TFSI⁻ and BF_4^- counter anions were synthesized by anion exchange reaction of MVT⁺I⁻. Similarly in the previous section, two methods were employed in anion exchange reactions. For the synthesis of 3,4-dimethyl-5-vinylthiazolium hexafluorophosphate (MVT⁺PF₆⁻) and 3,4-dimethyl-5-vinylthiazolium bis(trifluoromethane sulfonate)imide (MVT⁺TFSI⁻) aqueous solutions of corresponding salts were added dropwise into that of MVT⁺I⁻. The immediate precipitation was a sign that hydrophilic I⁻ of the monomers were replaced by hydrophobic, fluorinated TFSI⁻ and PF_6^-. Anion exchange from I⁻ to BF_4^- was performed by adding a AgBF₄ solution in a water/acetone mixture to a MVT⁺I⁻ solution in water/acetone. The precipitate, i.e. AgCl salt, was centrifuged out, and the supernatant was collected, followed by evaporation of

acetone and subsequent lyophilization. MVT$^+$BF$_4^-$ appears as a light yellow solid. The polymer

containing I$^-$ counterions was accessed by free radical polymerization of MVT$^+$I$^-$ in water. Other

polymers containing fluorinated counterions were synthesized by two methods: bulk

polymerization of the corresponding monomers and by solution polymerization in DMF.

Moreover, polymers having PF$_6^-$ [P(MVT$^+$PF$_6^-$)], TFSI$^-$ [P(MVT$^+$TFSI$^-$)], and BF$_4^-$

[P(MVT$^+$BF$_4^-$)] counterions can be accessed by counterion exchange of P(MVT$^+$I$^-$) making the

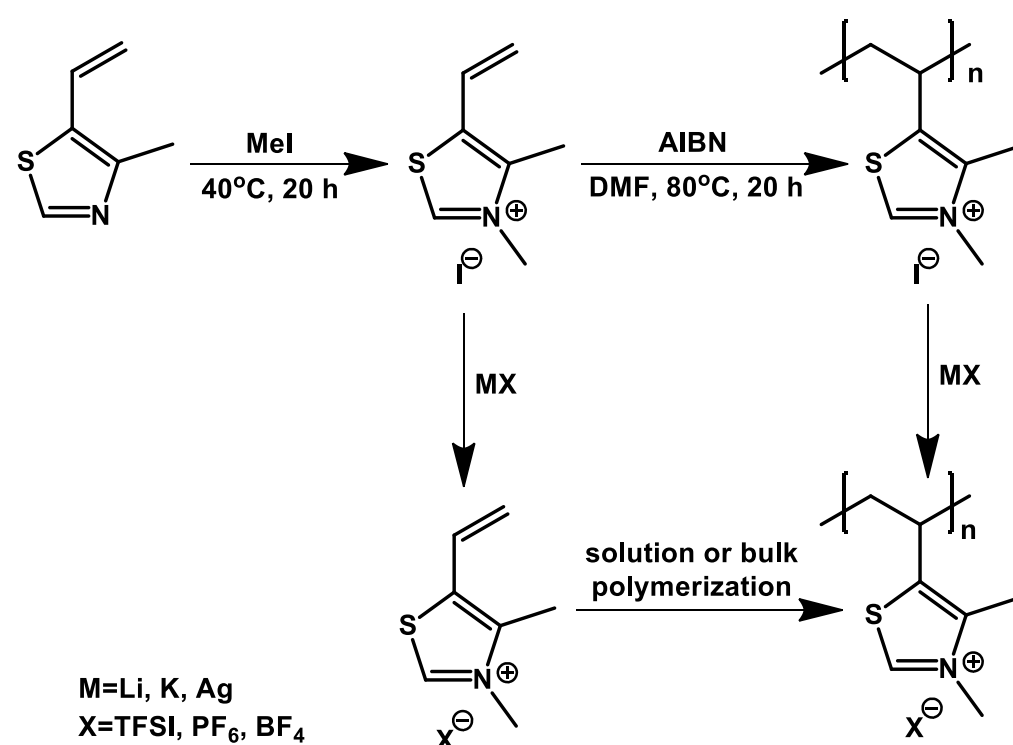synthetic route for the different PILs straightforward and highly versatile.

Figure 27. The synthetic route to thiazolium-type PILs and ionic polymers.

3.2.2 Characterization of 3,4-dimethyl-5-vinylthiazolium containing monomers and polymers

When the thiazole compounds are reacted with alkyl halides, an addition of alkyl chain to the

nitrogen atom is typically expected.[105] Such a synthetic pathway was verified using

^{1}H-^{13}C HSQC and ^{1}H-^{13}C HMBC spectroscopy (Figure 28, Figure 29). ^{1}H-^{13}C HSQC spectrum was initially employed to confirm assignment of signals belonging to carbons possessing directly attached protons. However, in order to analyze the position of methyl adduct, the prior assignment of ^{13}C nuclear magnetic resonance (^{13}C-NMR) signals of carbons 2 and 3 (Figure 29) was essential. This problem cannot be solved using ^{1}H-^{13}C HSQC spectroscopy alone since the mentioned carbons are not directly connected to any protons. For this reason the structure of the obtained product was resolved using ^{1}H-^{13}C HMBC spectroscopy. Initially, the analysis of coupling between protons of the vinyl group with carbons of thiazolium ring was studied. In the ^{1}H-^{13}C HMBC spectrum, coupling between proton 4 and carbon 3 instead of carbon 2 can be detected. Moreover, carbon 3 is coupled with proton 5A, while no coupling between carbon 2 and protons of vinyl group is observed. This confirms that signal 3 is due to the carbon atom, which is directly bounded to the vinyl group. Subsequently, coupling between protons 6 of the methyl adduct and carbons in the thiazolium ring was analyzed. If the above-mentioned methyl group was bound to sulfur, protons 6 would be coupled with carbon 3. The quaternization of nitrogen would couple protons 6 with carbon 2. The latter is true in the analyzed spectrum which clearly proves that reaction of 4-methyl-5-vinyl thiazole with methyl iodide leads exclusively to quaternization of the nitrogen atom of the thiazole ring.
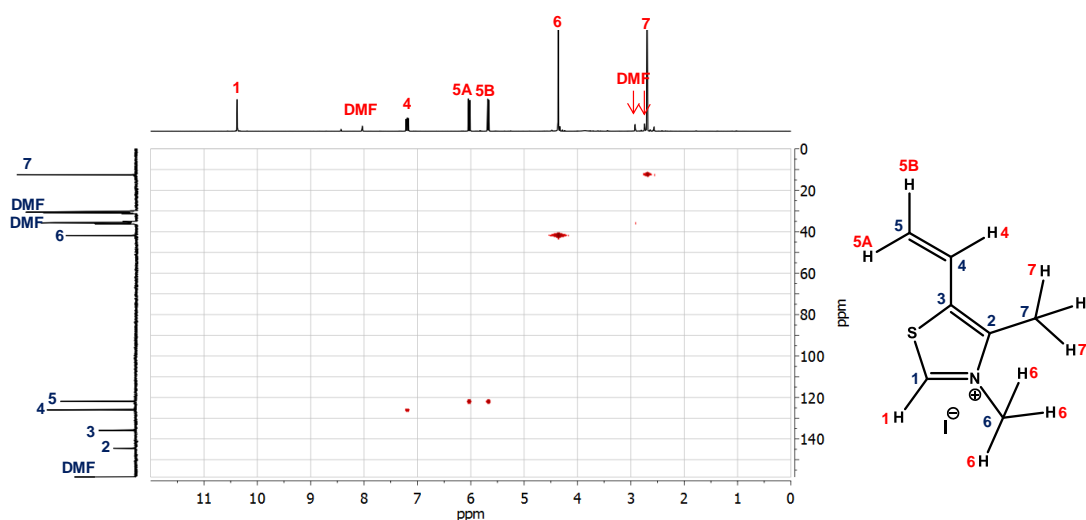

Figure 28. ^{1}H-^{13}C HSQC spectrum of MVT$^+$I$^-$.

48

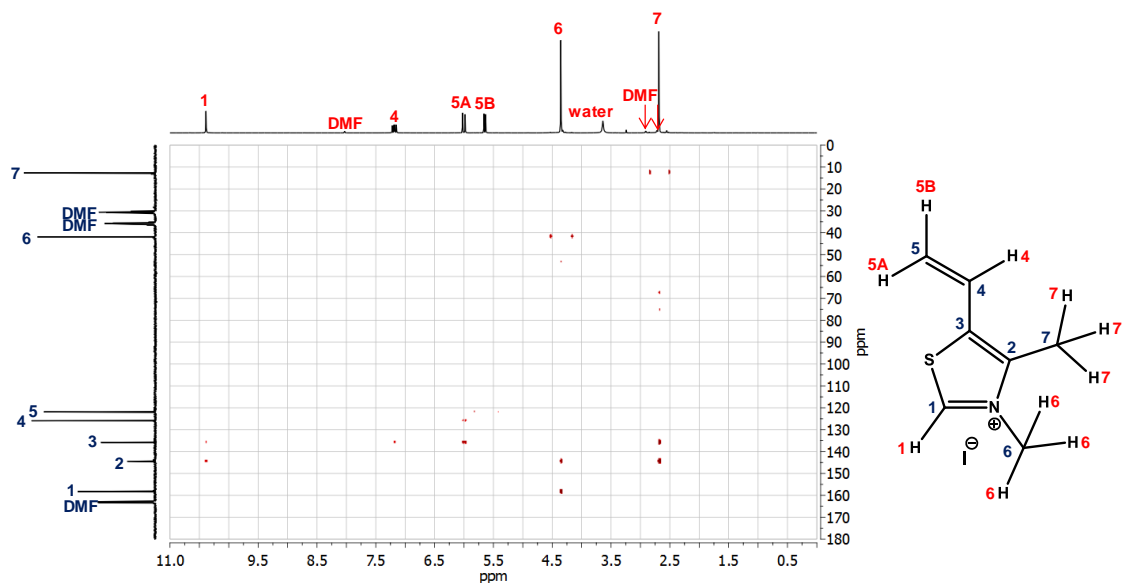Figure 29. ^{1}H-^{13}C HMBC correlation spectra of MVT^{+}I^{-}.

The performed reactions were controlled by ^{1}H-NMR spectroscopy. This method allowed validating the chemical structure of products and their purity. In addition to the analysis of ^{1}H-^{13}C HMBC spectrum, quaternization reaction of 4-methyl-5-vinyl thiazole was further verified *via* comparison of ^{1}H-NMR spectra of the product and its precursor. After the reaction, all the protons of monomer become more deshielded and appear at higher chemical shift values (Figure 30). Moreover, the new peak at 2.69 ppm, assigned to 3 protons of methyl group attached to the quaternary nitrogen, further proves that the targeted compound was synthesized. After polymerization of MVT^{+}I^{-}, the peaks assigned to the protons of vinyl group (B', C' and D' at 7.19, 6.02 and 5.66 ppm, respectively, Figure 30) were not observed any more. In P(MVT^{+}I^{-}), these protons are converted into ones of the polymer backbone and consequently are observed in the high field range (peaks B", C", Figure 30). Thus, the successful polymerization reaction of MVT^{+}I^{-} was confirmed. Importantly, the synthesized polymer was free of non-reacted monomer.
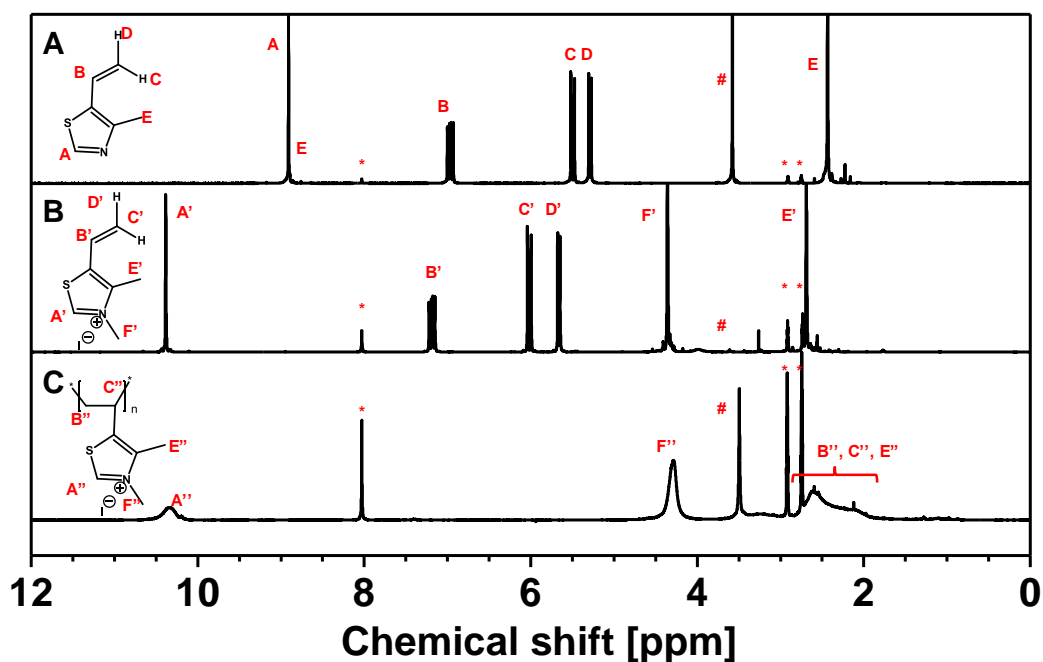
Figure 30. ^{1}H-NMR spectra of: A) 4-methyl-5-vinyl thiazole, B) MVT$^+$I$^-$ and C) P(MVT$^+$I$^-$) (signals on ^{1}H-NMR spectra: * - DMF, # - water).

MVT$^+$I$^-$ was then subjected to several anion exchange reactions for the synthesis of ILMs having fluorinated counterions. The replacement of counterions often causes substantial changes in ATR-FTIR spectra of ILs and PILs. Consequently, such spectra were recorder for all the synthesized monomers (Figure 31). Iodide counterion does not give any adsorption band in the IR range. Hence, in the spectrum of MVT$^+$I$^-$ only the 4-methy-5-vinylthiazolium moiety is responsible for the recorded adsorption pattern. However, the presence of PF$_6^-$, TFSI$^-$ and BF$_4^-$ anions can be easily detected by FTIR. For MVT$^+$BF$_4^-$ the broad signal at 1024 cm^{-1} corresponds to the asymmetric stretching of BF$_4^-$ anion. In the case of MVT$^+$PF$_6^-$ a strong signal at 823 cm^{-1} can be distinguished which is due to antisymmetric stretching of PF$_6^-$. IR spectra of ILs and PILs having TFSI$^-$ counterion are widely reported in the scientific literature. Four signals of stretching (ν_aSO$_2$ at 1343 cm^{-1}, ν_sSO$_2$ at 1133 cm^{-1}) and bending (δ_aSO$_2$ at 611 cm^{-1} and shoulder at δ_sSO$_2$ at 600 cm^{-1}) of SO$_2$ groups of TFSI$^-$ can be detected. Three sharp peaks at 1177, 740 and 569 cm^{-1} are assigned to ν_aCF$_3$, δ_sCF$_3$, δ_aCF$_3$, respectively. Finally symmetric stretching of C-S bond (790 cm^{-1}) as well as asymmetric (1051 cm^{-1}) and symmetric (764 cm^{-1})

stretching bands of S-N-S group are observed, further proving the existence of TFSI⁻ counterion.
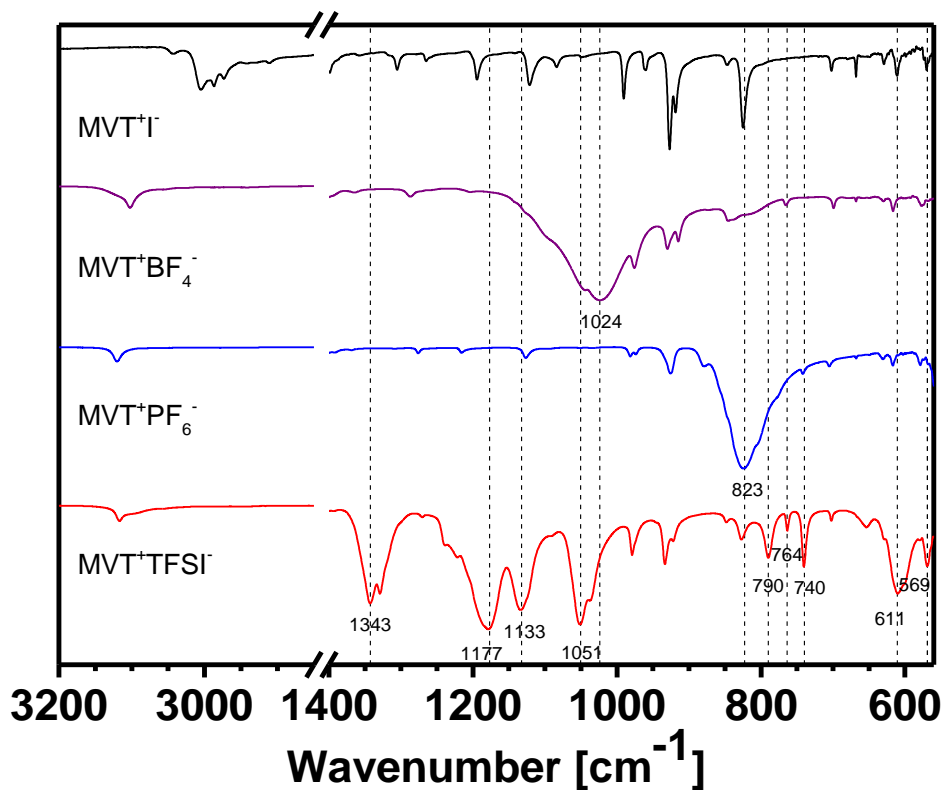

Figure 31. ATR-FTIR spectra recorded for all synthesized thiazolium monomers.

To follow the strict classification of ILs, the melting points of these monomers were determined by DSC measurements (Figure 32). The trace recorded for MVT$^+$I$^-$ revealed that it becomes liquid around 120 °C, followed by rapid, spontaneous thermal polymerization. MVT$^+$PF$_6^-$ and MVT$^+$BF$_4^-$ display analogous behavior but their melting points are shifted to 135 °C and 60 °C, respectively. MVT$^+$TFSI$^-$ becomes liquid at the temperature as low as 45 °C, but shows satisfactory thermal stability up to 150 °C. According to the DSC thermograms, MVT$^+$BF$_4^-$ and MVT$^+$TFSI$^-$ are liquids below 100 °C, thus belonging to the scope of ILMs while MVT$^+$I$^-$ and MVT$^+$PF$_6^-$ can be described as organic salts.
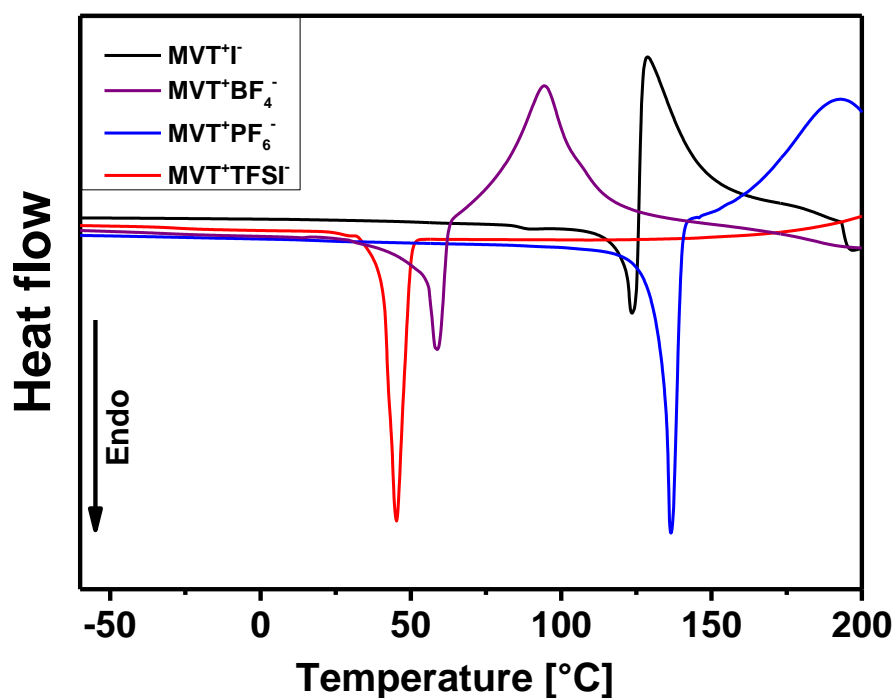
Figure 32. DSC thermograms recorded for all synthesized thiazolium monomers.

As it was previously presented, high and anion-dependent thermal stability of PILs and ILs belongs to their intrinsic features and most significant advantages. It was scientifically intriguing to evaluate such properties of all the synthesized monomers and polymers. As the TGA measurement revealed, MVT^+I^- starts decomposing at 220 °C (decomposition temperature defined as temperature of 10 % weight loss, Figure 33). It is well-known from previous studies that exchanging counterions to large, fluorinated species leads to monomers of much higher thermal stability. Hence, I^- was replaced by PF_6^-, BF_4^-, or $TFSI^-$. Monomers bearing such anions do not decompose up to 345 °C, 355 °C, and 385 °C, respectively. Typically PILs possess slightly better thermally stability than their corresponding monomers. Unexpectedly, the thermal behavior of thiazolium-type PILs was opposite to the general trend reported in literature. Polymers, independent of the polymerization condition in bulk or in the solution were thermally less stable than their monomers. In the case of $P(MVT^+I^-)$ polymerized in water, decomposition temperature is around 10 °C lower than its monomer. $P(MVT^+BF_4^-)$ synthesized either by solution polymerization or in bulk decomposes at 310 °C, 45 °C lower than the

corresponding monomer. Polymer containing PF_6^- anion decomposes at 270 °C when synthesized in bulk and at 315 °C when synthesized in solution. Those temperatures are much lower than that of $MVT^+ PF_6^-$. Only in the case of thiazolium polymer containing $TFSI^-$ counterion its thermal stability is similar to its monomer (obtained results are within the experimental errors). These results are unexpected and the exact reason responsible for such a thermal instability of thiazolium-type polymers, compared to their monomers, remains unclear yet and will be of interest for future study. It is worth noting that $P(MVT^+TFSI^-)$ and $P(MVT^+BF_4^-)$ are more thermally stable than their prototypes synthesized in the first part of this chapter [$P(MVBT^+TFSI^-)$ and $P(MVBT^+BF_4^-)$] outmatching them in the terms of decomposition temperature for 100 °C and 15 °C, respectively (Figure 24). It can be summarized that simplification of the structure of thiazolium polymer led to a significant increase in thermal stability of such materials.
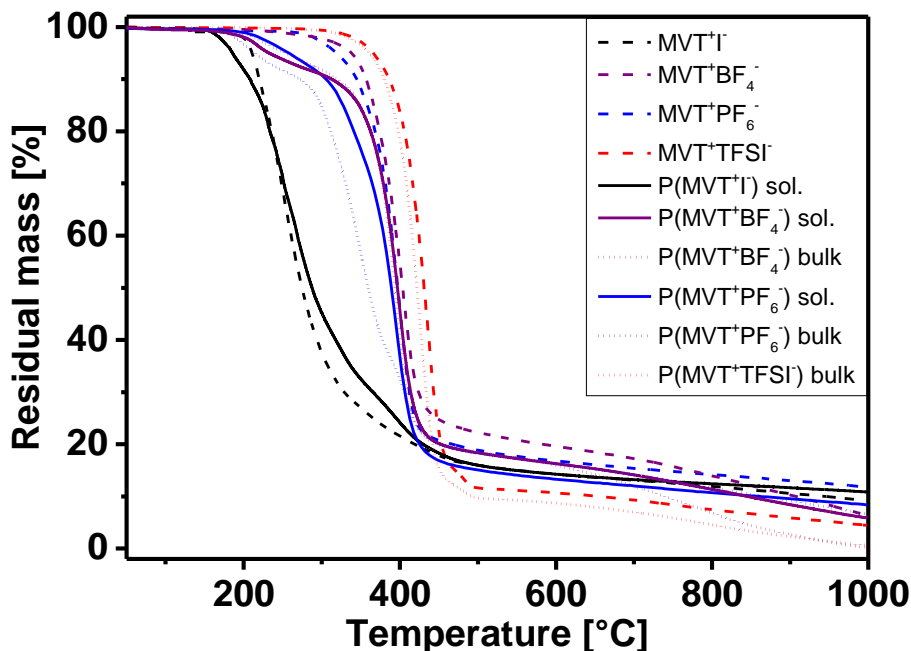

Figure 33. TGA thermograms of all synthesized monomers and polymers (sol – polymer synthesized by solution polymerization; bulk – polymer synthesized by bulk polymerization).

Not only bulk, but also solution properties of ILs and PILs are strongly affected by the choice of counterion. In the present work, the solubility of these synthesized monomers

and polymers in water and various organic solvents was tested at room temperature at the concentration of 1.0 wt% (Table 5). MVT^+I^- can be dissolved in water and MeOH. When a hydrophobic counterion BF_4^- is introduced into the monomer structure, the product becomes soluble in acetonitrile while preserving its solubility in water. Reacting MVT^+I^- with KPF_6 leads to the monomer $MVT^+PF_6^-$, which is soluble in acetone but insoluble in water. $MVT^+PF_6^-$ possesses also certain solubility in THF and MeOH (between 0.1 wt% and 1.0 wt%). In the case of other tested solvents, the solubility of $MVT^+PF_6^-$ is analogous to the solution properties of $MVT^+BF_4^-$. Eventually, introducing $TFSI^-$ to the monomer structure leads to the hydrophobic product which can be dissolved in all tested organic solvents (including chloroform, EtAc, and THF). After polymerization, the products are generally more hydrophobic and less soluble in most of the solvents that can dissolve the corresponding monomers. For example, polymerization of $MVBT^+I^-$ leads to the ionic polymer which is not soluble in MeOH at the concentration of 1.0 wt% while its monomer shows good solubility in this solvent. Solubility of $P(MVT^+BF_4^-)$ is analogous to its monomeric precursor. However, $P(MVT^+PF_6^-)$ is insoluble in MeOH and THF. Chloroform and MeOH are bad solvents for $P(MVT^+TFSI^-)$ yet they can dissolve its monomer. To be noted, all synthesized thiazolium-containing monomers and polymers possess good solubility in DMSO and DMF.

Table 5. Comparison of solubility properties of thiazolium-containing monomers and polymers in various solvents ("+"– soluble at 1 wt%,"+ -" – soluble at the concentration between 1 wt% and 0.1 wt%, "-" – insoluble at 0.1 wt%).

Compound	H$_2$O	MeOH	Acetone	DMF	DMSO	THF	EtOAc	CHCl$_3$	Acetonitrile
MVT$^+$I$^-$	+	+	-	+	+	-	-	-	-
MVT+BF$_4^-$	+	-	-	+	+	-	-	-	+
MVT$^+$PF$_6^-$	-	+ -	+	+	+	+ -	-	-	+
MVT$^+$TFSI$^-$	-	+	+	+	+	+	+	+	+
P(MVT$^+$I$^-$)	+	-	-	+	+	-	-	-	-
P(MVT$^+$BF$_4^-$)	+	-	-	+	+	-	-	-	+
P(MVT$^+$PF$_6^-$)	-	-	+	+	+	-	-	-	+
P(MVT$^+$TFSI$^-$)	-	-	+	+	+	+	+	-	+

3.2.3 Application of 3,4-dimethyl-5-vinylthiazolium containing polymers

Recently, a potential of PIL nanoparticles to play a role as high performance binders for lithium-ion battery electrodes has been shown.[56] Triggered by this research, P(MVT$^+$TFSI$^-$) was examined as a candidate for the binder in lithium-ion batteries (this part was performed in collaboration with Dr. Ken Sakaushi and Dr. Jung-Soo Lee). It is important to mention that when compared to the previous research not only the chemical composition of PIL was altered but a homogenous solution of a linear PIL was used instead of polymer nanoparticles. The reason to select P(MVT$^+$TFSI$^-$) is based on previous studies that ILs and PILs with TFSI$^-$ anion possess superior electrochemical stability among their counterparts. The performance of a P(MVT$^+$TFSI$^-$) binder was collated with the results obtained for a commercial binder poly(vinylidene fluoride) (PVDF). The full charge/discharge cycle tests (performed at 1C rate, that is charging to the full theoretical capacity of 170 mAh/g in the time of 1 hour) were

conducted in order to examine stability and specific capacity of electrodes composed of 80 wt% of LiFePO$_4$, 10 w% of acetylene black and 10 wt% of binder material. P(MVT$^+$TFSI$^-$) favorably outperforms PVDF in terms of specific capacity and durability. Specific capacity of P(MVT$^+$TFSI$^-$) reached 140 mAh/g at 6th cycle and without a significant capacity loss after 100 cycles (Figure 34, Figure 35). In comparison, the specific capacity value of PVDF achieves only 120 mAh/g and requires a long activation process (maximum specific capacity first at 20th cycle). Moreover, PVDF suffers from relatively high capacity loss of 1% after 100 cycles. A possible explanation of the improved performance in the case of P(MVT$^+$TFSI$^-$) ties this effect with better wettability of PIL than PVDF by electrolyte.

Finally, the long term stability test (performed at 5C rate correlates to charging to full capacity in 12 minutes, Figure 36) reveals that electrodes composed of individual binder materials - P(MVT$^+$TFSI$^-$) and PVDF are stable over the period of 400 cycles. Nevertheless, the specific capacity of electrode using P(MVT$^+$TFSI$^-$) binder is over 15 % higher than using PVDF binder, reaching a value over 100 mAh/g at the 400th cycle. Bearing these results in mind, the conclusion can be drawn that P(MVT$^+$TFSI$^-$) is a better candidate as binder for lithium ion battery than the current default choice PVDF.
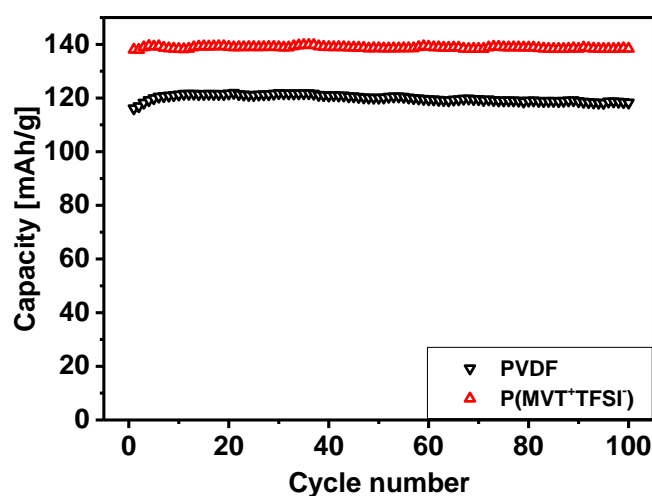

Figure 34. Stability test of P(MVT$^+$TFSI$^-$) and PVDF (results obtained for 1C test).
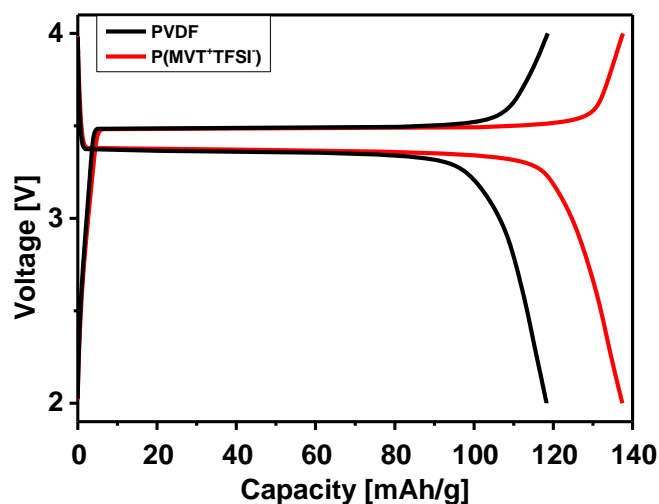
Figure 35. Voltage profile of P(MVT⁺TFSI⁻) and PVDF.
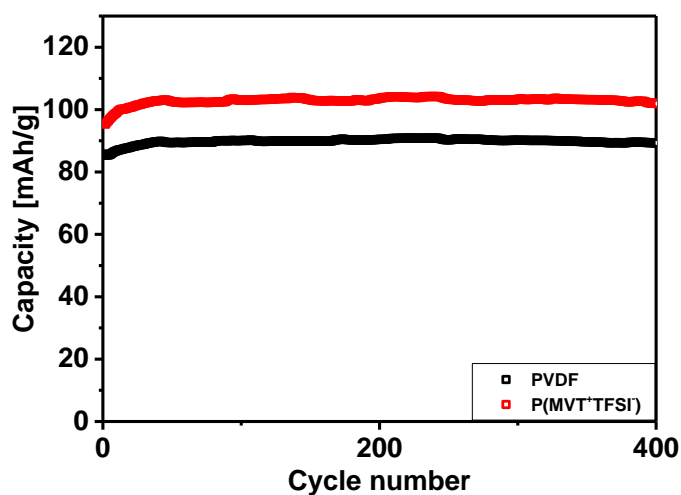
Figure 36. Long term stability test of P(MVT⁺TFSI⁻) and PVDF (results obtained for 5C test).

3.3 Conclusion

In summary, a series of thiazolium-containing ILMs and ionic monomers and their corresponding polymers were successfully synthesized and characterized. Quaternization of 4-methyl thiazole with 4-vinylbenzyl chloride led to the formation of MVBT⁺Cl⁻, whose structure was verified by ^{1}H-^{13}C HMBC NMR spectroscopy. Subsequently, such monomer was polymerized in water yielding P(MVBT⁺Cl⁻). Hydrophilic MVBT⁺Cl⁻ and its corresponding

polymer underwent further anion exchange reactions towards hydrophobic products bearing fluorinated counterions affecting thermal stability and solution properties of thiazolium materials. Eventually, sonication of the synthesized PILs with CNTs led to the stable dispersion of such CNTs which can be readily transferred into organic solvents. In the second part of this chapter, 4-methyl-5-vinyl thiazole was utilized as a structurally simple precursor of thiazolium monomer. Its quaternization with methyl iodide and subsequent counteranion exchange led to the series of thiazolium monomers. Each of them was then polymerized in solution and/or bulk to give corresponding polymers of high purity. These materials possess high thermal stability and solubility in a broad range of solvents outperforming previously described thiazolium-type counterparts. In addition, satisfactory electrochemical stability of $P(MVT^+TFSI^-)$ enabled its application as a binder for electrodes in lithium-ion batteries.

4. BIO-DERIVED, TASK-SPECIFIC MAIN-CHAIN IMIDAZOLIUM-TYPE PILS

Industry consumes around 4 % of world oil production as the feedstock for the plastic materials.[106] This amount is even doubled when fossil fuels used as the energy sources in their manufacturing processes are taken into account. Thus, the production of polymers has a large share in the total release of CO_2 which amounted to 31 Gt in 2011 (and is estimated to increase up to 37 Gt in 2035), contributing to the "greenhouse effect".[107] A possible way to reduce the overall dependence of the society on fossil fuels is the production of plastics from renewable resources. For this reason, the alternative and green synthetic pathways involving products exclusively or partially derived from biomass are highly demanded.[108] A significant effort has already been made to produce bio-polymers for the common as well as sophisticated applications in such areas as packaging, electronics, medicine, and adhesives, to name only a few.[109-111] The synthesis of more sustainable ILs and PILs has also attracted an increasing attention. For example, fructose-derived room-temperature ILs were reported by Dickenson *et al.* as good solvents for the Heck reaction of aryl iodides.[112] Moreover, bio-derived ILs assembling into an amphotropic liquid crystalline phase and possessing anisotropic ion conductivity were described by Devaki *et al*.[113] Rapid dissolution of DNA was achieved using cholinium type bio-derived ILs.[114] Cholinium cations were also introduced into the polymer chains of PILs in order to obtain biocompatible ion gels and amphiphilic block copolymers of PIL and polylactide.[62, 115] In addition, examples of PILs having bio-derived carboxylic acids as counterions were reported.[62, 116] Hence, the growing interest of researchers to produce bio-derived ILs and PILs is currently becoming more pronounced.

4.1 PILs from biomass – turning biomass into polyester stabilizers

Recently, a green and straightforward synthetic route towards bifunctional imidazolium compounds deriving from biomass has been reported by Esposito *et al.*[117] Imidazolium zwitterions were prepared *via* a modified Debus-Radziszewski reaction from various amino acids and bio-derived carbohydrates.[118] This imidazolium zwitterion was consequently esterified with ethanol to form a room temperature IL which in the present study was used as a PIL precursor. The synthetic route to the ILM utilizes mostly substrates (such as amino acid glycine, pyruvaldehyde, formaldehyde, acetic acid, and ethanol) which can be accessed from renewable resources according to the following methods. The production of pyruvaldehyde involves the oxidation of glycerol, a byproduct of biodiesel production, followed by its dehydration.[119, 120] Alternatively, pyruvaldehyde is an intermediate in the hydrothermal synthesis of lactic acid from sugars and can be accessed *via* retro-aldol mediated fragmentation of C_6-carbohydrates (derivatives of cellulose).[121] The synthesis of formaldehyde from bio-sources involves fast pyrolysis of cellulosic biomass or catalytic oxidation of methanol.[122, 123] The common industrial way to obtain methanol requires the usage of synthetic gas or methane. However, it can be alternatively accessed from biomass by its gasification.[124] Finally, ethanol is currently produced by fermentation of sugars or starch.[125, 126] Moreover, plants producing lignocellulosic ethanol have recently come into operation. The synthesis of ILM from the above-mentioned compounds was developed and performed by Sarah Kirchhecker and Dr. Davide Esposito. As a part of this work, the described imidazolium diester was converted into bio-derived PILs by polycondensation with 1,3-propanediol, an alcohol that can be obtained in biotechnological processes from glycerol and corn syrup.[127, 128]

4.1.1 Synthesis of polyester type PILs

Main chain imidazolium-type polyesters were synthesized by transesterification reaction of the imidazolium-type diester, 1,3-bis(2-ethoxy-2-oxoethyl)-5-methylimidazolium trifluoromethanesulfonate (denoted as $ImDE^+TFO^-$) and 1,3-propanediol, followed by anion exchange reactions (Figure 37). Synthesis of PIL from $ImDE^+TFO^-$ (abbreviated as $PImDE^+TFO^-$) was performed in two steps. Firstly, one molar equivalent of diester, three molar equivalents of diol, and tin octanoate $[Sn(Oct)_2]$ as transesterification catalyst were reacted at 160 °C for 3 h under inert atmosphere. The aim of this step was to perform a transesterification reaction, replacing at least part of ethoxy groups of the $ImDE^+TFO^-$ with 3-oxypropan-1-ol. At this stage only products having low molar mass can be obtained, since a large excess of diol inhibits the formation of polymeric products. In the following step, high vacuum was applied and the reaction was continued for 4 h at 215 °C. The goal was to induce condensation of oligomeric chain-ends, generating products having higher molar mass and co-products of polycondensation reaction (ethanol, 1,3-propanediol, and possibly water). At these conditions the non-reacted diol and low molar mass byproducts of the transesterification reaction were being constantly removed under reduced pressure. Therefore, the initial excess of diol in regard to $ImDE^+TFO^-$ was being gradually reduced leading to the increase in the molar mass of the product. The reaction temperature was optimized to be sufficiently high to obtain a satisfactory molar mass of polymers but to avoid *in-situ* thermal degradation.

The polymer obtained directly from the transesterification of $ImDE^+TFO^-$ carried TFO^- as counterion. The PIL bearing hydrophilic Br^- counterion ($PImDE^+Br^-$) was synthesized by anion exchange of $PImDE^+TFO^-$. The reaction was performed by addition of a $PImDE^+TFO^-$ solution in acetone into tetra-*n*-butylammonium bromide (T*n*BABr) dissolved in a mixture of water/acetone (volume ratio ~ 1/1) and the precipitate of $PImDE^+Br^-$ was filtered off. PILs with

PF$_6^-$ (PImDE$^+$PF$_6^-$) and TFSI$^-$ (PImDE$^+$TFSI$^-$) counterions were synthesized by addition of an aqueous solution of corresponding salt, KPF$_6$ or LiTFSI into a solution of PImDE$^+$Br$^-$ in water, yielding precipitates of corresponding polymers.
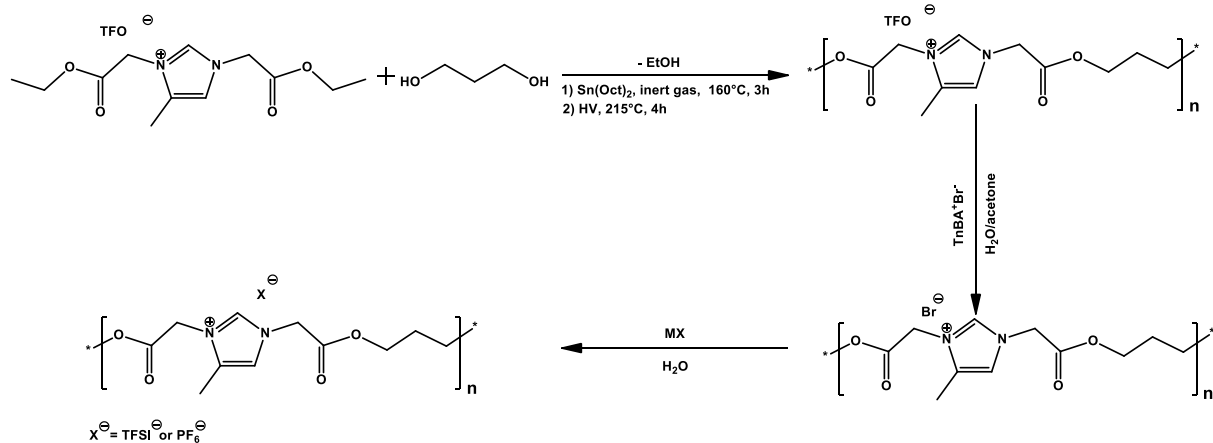

Figure 37. The synthetic route towards ImDE and PImDEs.

4.1.2 Characterization of polyester type PILs

At room temperature ImDE$^+$TFO$^-$ is a viscous liquid of a brown color. The DSC thermogram revealed that its T_g occurs at -15 °C (Figure 38). The presence of the endothermal peak over the baseline at the transition temperature can be associated with enthalpy relaxation.[129] A thermal scan over a complete temperature range up to the thermal decomposition threshold reveals no detectable melting point. Hence, this monomer belongs to the general scope of ILs.
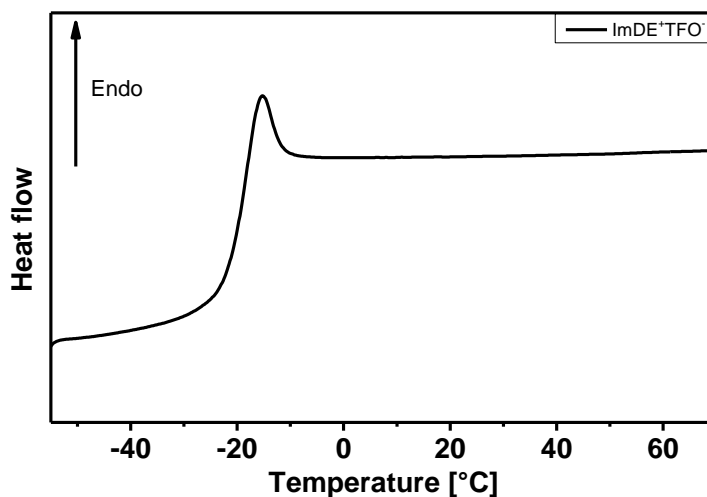
Figure 38. DSC thermogram of ImDE⁺TFO⁻.

The transesterification reaction of ImDE⁺TFO⁻ with 1,3-propanediol accompanied by a slow, continuous removal of low molar mass byproducts yielded PImDE⁺TFO⁻. The vanishing of ethoxy groups and the incorporation of 1,3 propanediol into the structure of product were confirmed by ^{1}H-NMR and ^{13}C-NMR spectroscopy. In the monomer spectrum, peaks of protons and carbon belonging to -CH$_3$ groups of ethoxy substituents are clearly distinguished. In contrast they cannot be detected in the product of polycondensation, which confirms the removal of ethanol during the reaction. Moreover, the spectral data of PImDE⁺TFO⁻ reveals the presence of new peaks at 1.8, 2.1 and 3.5 ppm (^{1}H-NMR) and at 28.3, 27.2 and 66.3 ppm (^{13}C-NMR), which are due to the incorporation of methylene (-CH$_2$-CH$_2$OH, -CH$_2$-CH$_2$-COO-) and hydroxymethyl groups, respectively. The first step of the polycondensation reaction at 160 °C was carried out in a large excess of 1,3 propanediol. Therefore, the generated oligomer chain-ends are composed of diol moieties being terminated with hydroxymethyl groups. In principle, the molar mass of the oligomer can be calculated on the basis of ^{1}H-NMR data from the chain end fraction. Unfortunately, peaks of protons D (Figure 39), belonging to the terminal group, cannot be used to determine the molar mass of the product, since they overlap with signals of water or/and solvent in most of the common NMR solvents, such as DMSO-d_6, MeOD and

DMF-d_7. Instead, the peak C (Figure 39) is well separated from other peaks and was therefore used as reference to calculate the molar mass.
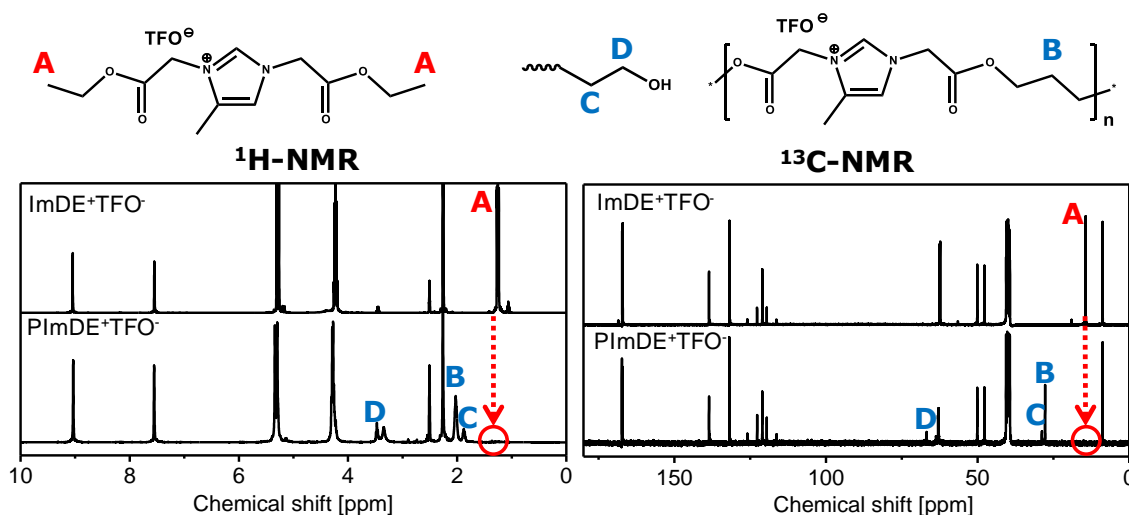

Figure 39. ^{1}H-NMR and ^{13}C-NMR spectra of ImDE$^+$TFO$^-$ and PImDE$^+$TFO$^-$.

As it was presented in the previous chapters, ATR-FTIR spectroscopy is an efficient and convenient method to confirm anion exchange reactions of PILs. Replacing counterions from TFO$^-$ to Br$^-$ causes the disappearance of IR bands of TFO$^-$ anion (Br$^-$ cannot be detected by FTIR). In the ATR-FTIR spectrum of PImDE$^+$TFO$^-$ sharp peaks of the vibrations assigned to the CF$_3$ group can be observed (δ_aCF$_3$ at 573 cm^{-1}, δ_sCF$_3$ at 756 cm^{-1}). In the case of PImDE$^+$Br$^-$ they cannot be detected anymore. Moreover, the decrease in the intensity of bands at 1157 cm^{-1} (ν_sCF$_3$) and at 1221 cm^{-1} (ν_aCF$_3$) further confirms successful anion exchange reactions. In the same region, the presence of less intensive bands in PImDE$^+$Br$^-$ is due to symmetric and asymmetric stretching of imidazolium ring as well as of stretching of C=C and (N)CH$_2$ bonds which also contribute to the peaks in the range from 1100 to 1250 cm^{-1}. Lack of signals of vibrations of SO$_3$ groups (δSO$_3$ at 636 cm^{-1}, ν_sSO$_3$ at 1027 cm^{-1} and ν_aSO$_3$ at 1251 cm^{-1}) is a further confirmation of the successful replacement of TFO$^-$ by Br$^-$.[130-134] The exchange of Br$^-$ counterions of PImDE$^+$Br$^-$ to fluorinated PF$_6^-$ and TFSI$^-$ was also detected by ATR-FTIR spectroscopy. PF$_6^-$ counterion gives a strong, broad signal at 821 cm^{-1}, confirming the efficiency

of the employed methodology in anion metathesis reaction.[104] For the PImDE$^+$TFSI$^-$, the shoulder peak at 1221 cm^{-1} as well as three sharp bands at 1170, 740 and 569 cm^{-1} can be assigned to ν_sCF$_3$, ν_aCF$_3$, δ_sCF$_3$ and δ_aCF$_3$ vibrations, respectively. Furthermore, strong peaks caused by stretching (ν_aSO$_2$ at 1346 cm^{-1}, ν_sSO$_2$ at 1131 cm^{-1}) and bending (δ_aSO$_2$ at 613 cm^{-1} and δ_sSO$_2$ at 599 cm^{-1}) vibrations of SO$_2$ groups of TFSI$^-$ are present in the FTIR spectrum of PImDE$^+$TFSI$^-$. Eventually asymmetric (1051 cm^{-1}), symmetric (763 cm^{-1}) stretching bands of the S-N-S group and symmetric stretching of C-S band (789 cm^{-1}) are also observed, proving the successful counterion exchange towards TFSI$^-$.[104, 130, 135]

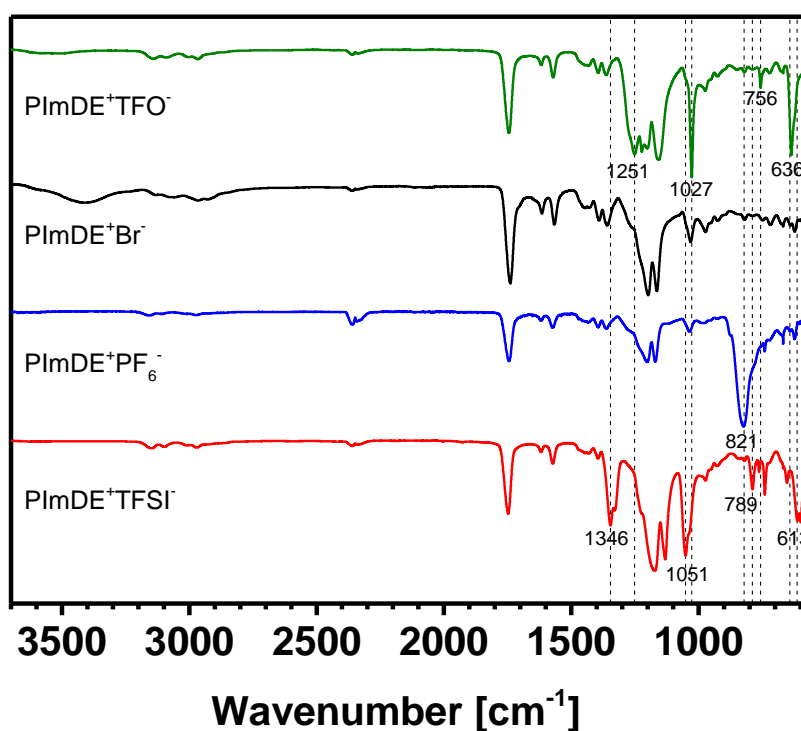Figure 40. ATR-FTIR spectra recorded for the synthesized PImDEs.

The molar mass of PImDE$^+$Br$^-$, calculated using end-group analysis of ^{1}H-NMR (according to the above mentioned method), amounted to 3400 g/mol. For comparison, GPC measurement was performed. The number average molar mass (M_{nGPC}) was equal to 5700 g/mol. The disagreement of obtained values can be explained by the use of poly(ethylene

glycol) standards for the GPC data evaluation, whose solution behavior differs from that of the imidazolium polymers.

DSC thermograms were recorded for all synthesized polymers as a method to characterize their T_g (Figure 41). When the Br⁻ counterion was implemented into the structure of PILs, its T_g was detected at 80 °C. Exchanging counterion from Br⁻ to PF$_6$⁻ only slightly affected the T_g of synthesized polymer, shifting it to 70 °C. In contrast, introducing TFSI⁻ and TFO⁻ anions was an efficient method to lower the T_g of PImDEs to 20 °C and 55 °C, respectively. Obtained results are in agreement with previous reports for structurally different types of PILs, where a strong dependence of T_g on the type of counterion was observed.[36]

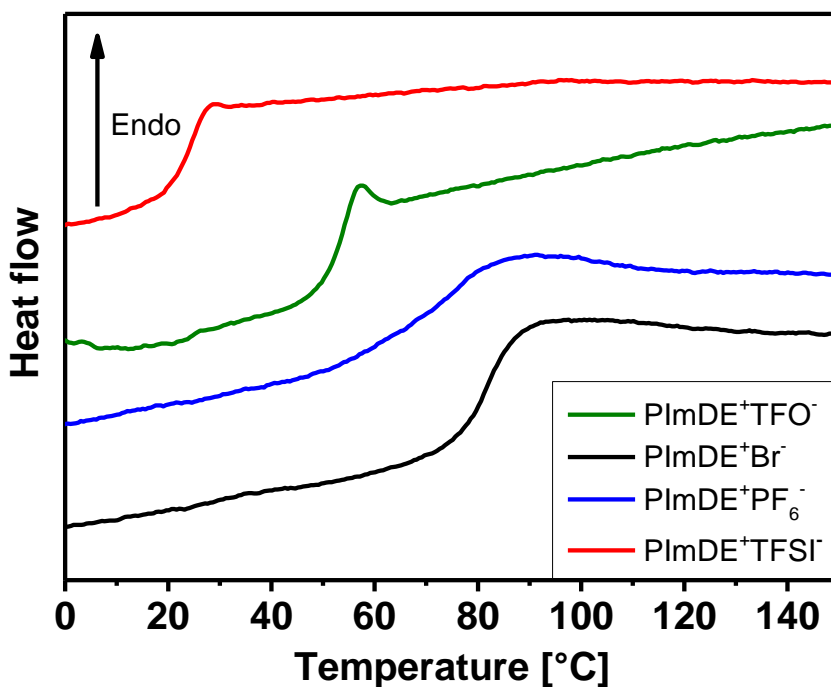Figure 41. DSC curves recorded for PImDEs.

Thermal stability of the synthesized products was investigated by TGA. The recorded thermograms revealed that decomposition temperature of PImDEs differs only slightly when compared to its monomer. More substantial variations of the thermal stability were caused by the exchange of the counterion. According to similar observations reported in the literature,

PILs bearing halide as counterions possess relatively low decomposition temperature (when compared to other PILs). Herein, PImDE$^+$Br$^-$ decomposes readily at 270 °C (Figure 42). Implementing of fluorinated counterions into the structure of PImDE substantially alters its thermal stability. For PImDE$^+$PF$_6^-$, the weight loss of 10 % was found at 340 °C. Introducing of TFSI$^-$ and TFO$^-$ counterions causes an increase of the decomposition temperature of PILs up to 385 and 360 °C, respectively. Interestingly, for the stability of the polymer, the order in the dependence of counterion (TFSI>TFO>PF$_6$>Br) is an inverse sequence when compared to their T_g.
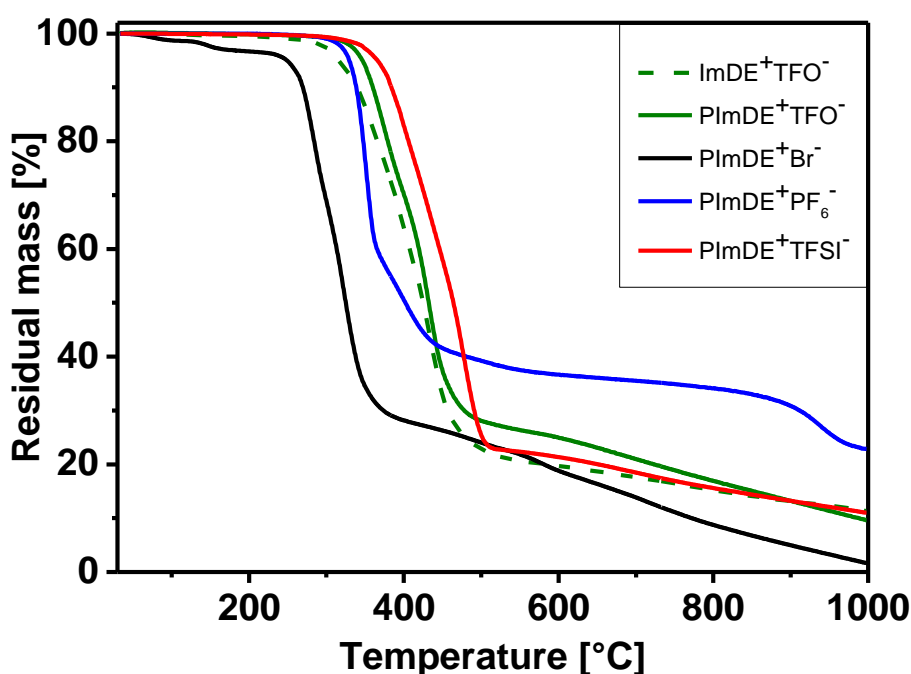
Figure 42. TGA thermograms recorded for ImDE$^+$TFO$^-$ and PImDEs.

Solution properties of PImDEs match the general scheme observed for PILs. PImDE with Br$^-$ counterion is a hydrophilic polymer, soluble in water and MeOH. Polymers with hydrophobic, fluorinated counterions like TFO$^-$ and TFSI$^-$ are not soluble in water, but soluble in polar oganic solvents, for instance in MeOH and acetone. Exchanging the counterion to PF$_6^-$ leads to an even more hydrophobic material, which cannot be dissolved in MeOH anymore. None of the synthesized polymers was soluble in comparably more apolar

organic solvents like THF, EtOAc and CHCl₃, which are good solvents for ImDE⁺TFO⁻. In addition, all the synthesized polymers were soluble in DMSO, but none of them nor the monomers can be dissolved in highly apolar solvents, like toluene. Thus, the simple anion exchange reactions lead to products with highly tunable solution properties.

Table 6. Solubility table of ImDE and synthesized PImDEs (performed at 1 wt% of IL or PIL sample in the solvent).

Compound	H_2O	MeOH	DMSO	Acetone	THF	EtOAc	CHCl₃	Toluene
ImDE⁺TFO⁻	-	+	+	+	+	+	+	-
PImDE⁺TFO⁻	-	+	+	+	-	-	-	-
PImDE⁺Br⁻	+	+	+	-	-	-	-	-
PImDE⁺PF₆⁻	-	-	+	+	-	-	-	-
PImDE⁺TFSI⁻	-	+	+	+	-	-	-	-

4.1.3 CO_2 sorption of the polyester type PILs

Due to the presence of imidazolium-cations and carbonyl groups in the structure of polyester-type PILs, they were considered as potential materials for CO_2 sorption. To verify their performance, polymeric samples of PImDE⁺Br⁻ and PImDE⁺PF₆⁻ were placed in closed cells and gas sorption data points were acquired by monitoring the pressure drop after an addition of certain doses of CO_2 (the measurements were performed at 0 °C). When the equilibrium between sorption and desorption is achieved, no further decrease in the gas pressure inside the cell is observed ($\Delta p = 0$, where Δp is defined as p_0-p; p_0 – pressure at the beginning of the measurement period, p – final pressure). An equilibrium is assumed when within the certain measurement time (Δt) the pressure drop is lower than the arbitrary set value, which depends on the accuracy of Quantochrome instrument (for the purpose of the measurement $\Delta p = 0.0008$ atm). Since an equilibration time has a strong effect on the CO_2

uptake, the measurements were performed independently at two different settings of the equilibration period ($\Delta t = 3$ min - named fast measurement and $\Delta t = 99$ min – named slow measurement). The CO_2 sorption isotherms obtained for $PImDE^+Br^-$ and $PImDE^+PF_6^-$ are presented in Figure 43. Both of the investigated polymers display large desorption hysteresis as well as slow sorption. The latter is indicated by the higher measured sorption capacity in the slow than in the fast measurements, which arises from long required equilibration times. Moreover, especially in the slow measurements, the absorbed CO_2 cannot be fully desorbed even at low pressure, which may indicate that CO_2 capture is due to its chemisorption. It is in agreement with previously reported studies by Yuan *et al*. where authors proposed CO_2 sorption mechanism for imidazolium-type PILs.[136] Analogously to above mentioned studies, it can be assumed that counterions of PImDEs can act as a base which leads to deprotonation of imidazolium rings at C2 position. Subsequently, a transient N-heterocyclic carbene is formed, which can reversibly react with CO_2 to yield a carboxylate-imidazolium zwitterion (Figure 44). The interactions of carbonyl groups of PImDEs with CO_2 however cannot be excluded. It was already reported that the presence of electron-donating functional groups may cause Lewis acid-base interactions with CO_2, improving the CO_2 capture capacity of polymers.[137] At the pressure of 760 mmHg, a significantly higher CO_2 uptake value was obtained for both polymers in the slow measurements (0.32 mmol CO_2/g of $PImDE^+Br^-$ and 0.31 mmol CO_2/g of $PImDE^+PF_6^-$) than in the fast measurements (0.074 mmol CO_2/g of $PImDE^+Br^-$ and 0.091 mmol CO_2/g of $PImDE^+PF_6^-$). This is understandable, since diffusion of CO_2 in the bulk of non-porous polymers is a slow process, which requires long equilibration time. The absorption power of $PImDE^+Br^-$ and $PImDE^+PF_6^-$ is in the same range of values. A deduction from this experiment is that the choice of counterions in the polyester-type PILs only slightly affects the CO_2 sorption capacity.

In order to evaluate the obtained results, CO_2 sorption capacity of PImDEs was collated to the literature data recorded for comparable PILs of low surface area. As an example, in the study of Yuan *et al.*1-cyanomethyl-3-vinyl imidazolium PILs having Br^- counterion shows CO_2 sorption capacity of 0.12 mmol CO_2/g (results obtained at the condition identical to the described here as the slow measurement).[136] Owing to this fact, PImDE possessing the same counterion has more than 2.5 higher CO_2 uptake (per gram of polymer) than 1-cyanomethyl-3-vinyl imidazolium PILs. However, in the latter case, exchanging counterion to acetate increases its CO_2 sorption capacity up to 0.6 mmol CO_2/g, significantly outmatching the performance of PImDEs. This indicates that the proper choice of counterion plays an important role in the CO_2 sorption efficiency. In another study, structurally similar to PImDEs, main-chain imidazolium polyester-type PILs were studied for CO_2 uptake.[138] At the CO_2 pressure of 650 mmHg and the temperature of 25 °C such PILs with PF_6^- and BF_4^- counteranions showed CO_2 sorption of 0.10 and 0.12 mmol CO_2/g, respectively. At the pressure of 650 mmHg CO_2, PImDEs synthesized in this thesis showed the CO_2 uptake of 0.22 mmol CO_2/g. Unfortunately, these results cannot be directly compared, since the temperature of the measurements differed as much as 25 °C (it was presented by Yuan *et al.* that CO_2 uptake is sensitive to the temperature[136]).
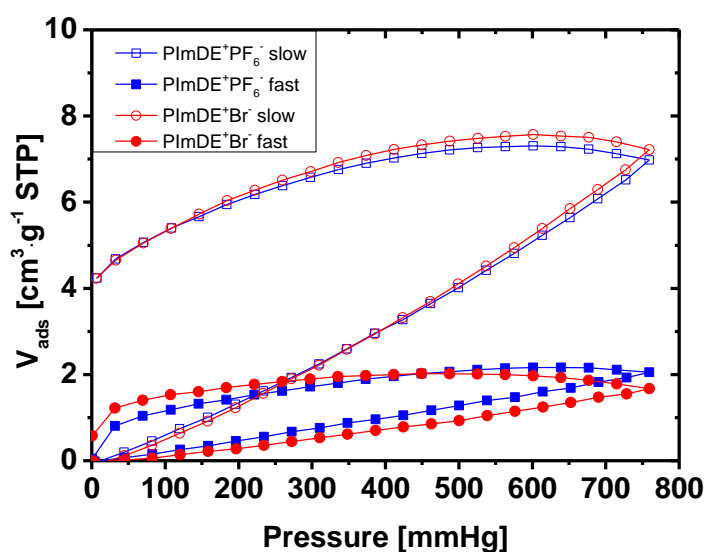

Figure 43. CO_2 adsorption/desorption isotherms of $PImDE^+Br^-$ and $PImDE^+PF_6^-$) obtained at 0 °C, at different equilibration time (fast and slow measurements); STP – standard temperature and pressure.
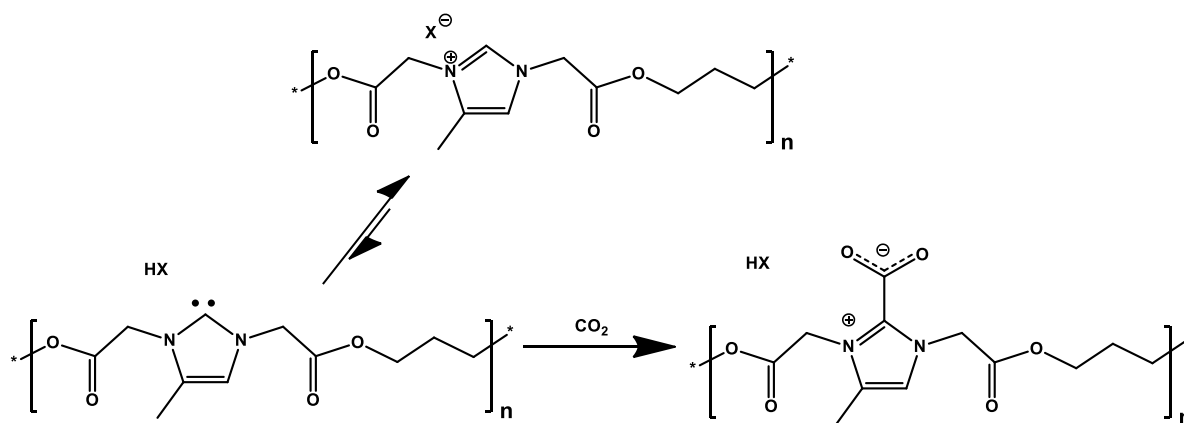
Figure 44. Proposed mechanism of CO_2 absorption in the synthesized PImDEs.

4.2 One-pot synthesis of PILs *via* Debus-Radziszewski reaction

The previous chapters contain a description of state-of-the-art methods which are employed in the preparation of PILs. It can be concluded that the formation of PILs typically requires at least several synthetic steps of a different level of complexity. For instance, imidazolium-type polymers can be accessed from basic, structurally simple molecules as follows. In the industrial method, imidazole is firstly synthesized from glyoxal, formaldehyde, and ammonia *via* Debus-Radziszewski reaction.[139] This is followed by a base-catalyzed addition of acetylene to imidazole which yields vinyl imidazole. Vinyl imidazole in turn, is a commercially available chemical, frequently utilized for the synthesis of ILMs. Such monomers are typically accessed by a quaternization of vinyl imidazole with alkyl halide. In order to synthesize PILs, ILMs can either be directly polymerized or beforehand an additional step, anion exchange is performed. Complicated synthetic pathways impose obvious effect on the final cost of PILs, which is considered as one of the key factors to limit their applicability. In addition, the employment of organic solvents and toxic chemicals which usually derive from fossil fuels leave the footprint on the environment. Certain efforts to synthesize PILs in a more sustainable fashion have been done, albeit they do not yield products which can be described as

fully bio-derived. As an attempt to improve the current synthetic state, the development of a completely new synthetic approach is described in this section. In order to decrease the final cost as well as the synthetic complexity, imidazolium-type main chain PILs are synthesized in water *via* one-pot modified Debus-Radziszewski reaction utilizing simple compounds. Moreover, such a method can be employed to synthesize PILs exclusively from bio-derived (although not always bio-friendly) molecules.

The industrially applied Debus-Radziszewski reaction is widely-known in organic chemistry as a synthetic route towards tri-substituted imidazole compounds. It is based upon the condensation of an aldehyde, 1,2-dicarbonyl compound, and ammonia. In the first step, the dicarbonyl molecule reacts with ammonia to yield diimine (Figure 45). Subsequently, the diimine undergoes a condensation with an aldehyde eventually forming an imidazole ring. By varying the type of dicarbonyl and aldehyde species a wide range of imidazoles bearing different substituents are accessible.
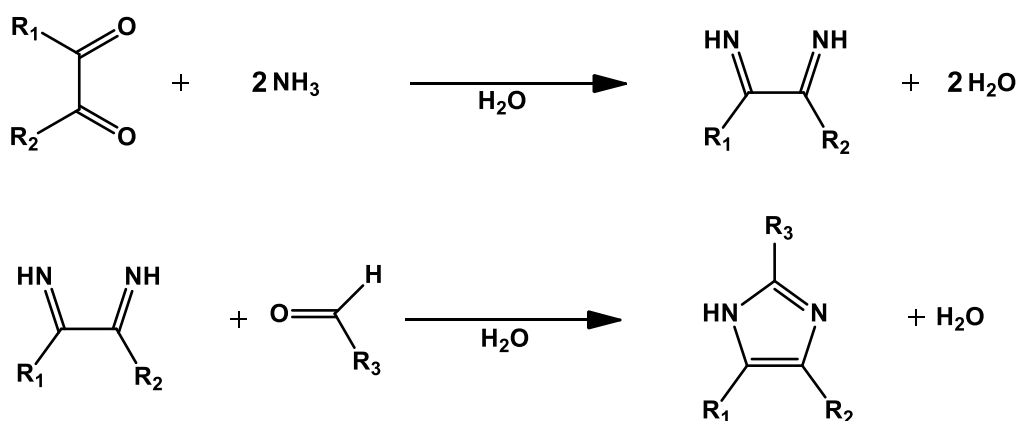
Figure 45. Debus-Radziszewski imidazole synthesis (R_1, R_2, R_3 – H or alkyl chains).

Recently, a convenient and green synthetic route towards ILs *via* modification of the Debus-Radziszewski reaction was reported (Figure 46).[117] In contrast to the standard approach, in this method ammonia was replaced with amines (in the specific case with aminoacids) and the synthesis was carried out in the presence of acetic acid. Thus,

1,3-disubtituted imidazolium-type compounds were obtained in a single step from bio-derived, small molecules. It is worth noting that in the other study, modification of Debus-Radziszewski reaction was also efficiently applied in order to cross-link polymer chains bearing pending amino groups, providing a new platform to merge such synthetic method with polymer chemistry.[140]
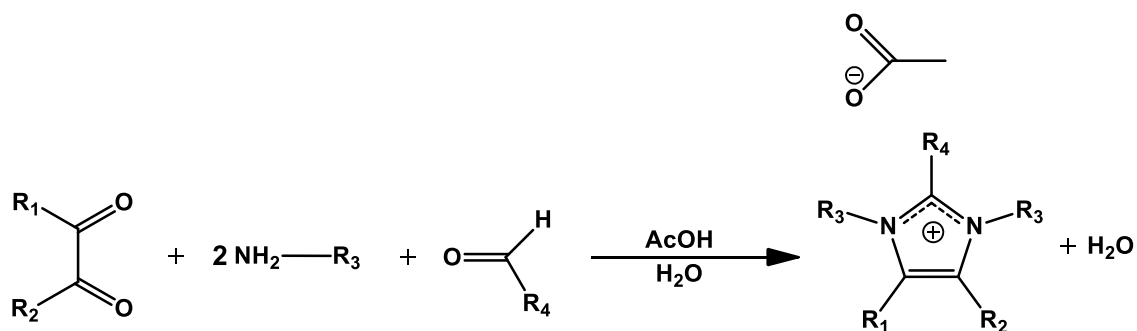
Figure 46. Modified Debus-Radziszewski imidazolium synthesis.

The above-mentioned one-pot synthesis of imidazolium compounds was accomplished at ambient conditions in water. Triggered by simplicity and high efficiency of the modified Debus-Radziszewski imidazolium synthesis, a follow-up study was performed as a part of this PhD thesis. It was anticipated that by substitution of monoamines with diamine compounds the main-chain imidazolium polymers of satisfactory high molar mass can be accessed. Moreover, since produced from bio-mass diamines (e.g. cadaverine), aldehydes, and 1,2-dicarbonyls are commercially available, this method would lead to fully bio-derived PILs. In the following sections, an investigation of a one-step synthesis of PILs *via* modified Debus-Radziszewski reaction in water (without using elevated temperature or atmosphere of an inert gas) is presented.

4.2.1 Facile synthesis of main-chain imidazolium-type PILs

The novel one-pot synthesis of the main-chain imidazolium-type PIL which is fully composed of bio-derived compounds (PILC5$^+$Ac$^-$) is presented in Figure 47. Glacial acetic acid was added dropwise under vigorous stirring to the mixture of cadaverine and water. Subsequently, the prepared solution was added to pyruvaldehyde and formaldehyde. In a standard procedure, 1.2 molar equivalents of aldehydes and 6.0 molar equivalent of acetic acid regarding cadaverine were reacted for 24 hours at room temperature. The crude product was purified by dialysis against water using the 3.5 kDa tubing. Several parameters of the above-presented synthesis were tuned in order to optimize the reaction conditions and study their influence on the molar mass of the final product. In this regard, the reaction time was varied from 15 minutes up to 3 days, the temperature was changed in the range from room temperature up to 60 °C, and the molar ratio of aldehydes in respect to amine was tuned in the range from 1.0 to 1.2. It is worth highlighting that linear, main-chain imidazolium-type PILs possessing similar structures to above-presented have been reported by Ho *et al.*[141] In their work, imidazolium cation did not have any alkyl substituent at C4 carbon and the length of the alkyl spacer varied from 3 to 6 methylene groups. However, their method did not utilize bio-derived compounds and was much more complex than the one established herein. In their exemplary synthesis, imidazole was firstly reacted with 1-bromo-5-chloropentane in the presence of Lithium hydride (LiH, the reaction was carried out under nitrogen in dry THF). The synthesis was terminated with water and the product was extracted with dichloromethane. In the final step, the monomer underwent self-polymerization in ethylene glycol at 90 °C. By the comparison to the above-mentioned study, the progress achieved by using one-step modified Debus-Radziszewski reaction is even more pronounced, since it remarkably simplifies the synthetic pathway towards PILs and makes it truly sustainable.
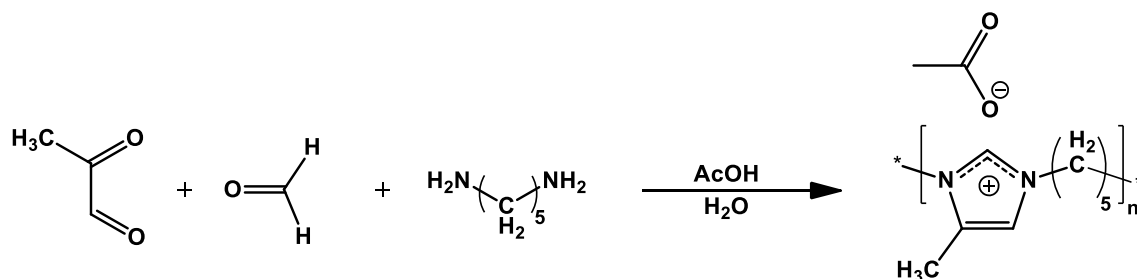
Figure 47. The one-pot synthetic route towards bio-derived PIL.

The conditions established for the reaction of cadaverine were employed in the synthesis of a series of main-chain imidazolium PILs with different charge densities. Cadaverine was replaced with other linear diamines (Figure 48) in order to investigate versatility of the new synthetic pathway. In these synthesizes, six different terminal diamines containing from two to twelve carbon atoms in their structure were reacted with 1.2 molar excess of pyruvaldehyde and formaldehyde in the presence of 6.0 molar excess of acetic acid (regarding diamines) forming PILs of different concentration of imidazolium cations (PILCX, where X is the number of carbon atoms in the structure of diamine precursor). The synthesis was performed in an analogous way to the one developed for PILC5$^+$Ac$^-$. Amines were dissolved in water/acetic acid mixture and then added dropwise to the mixture of pyruvaldehyde and formaldehyde. After 24 h, the synthesized products were diluted with water and dialyzed against MiliQ® water using 3.5 kDa dialysis tubes.
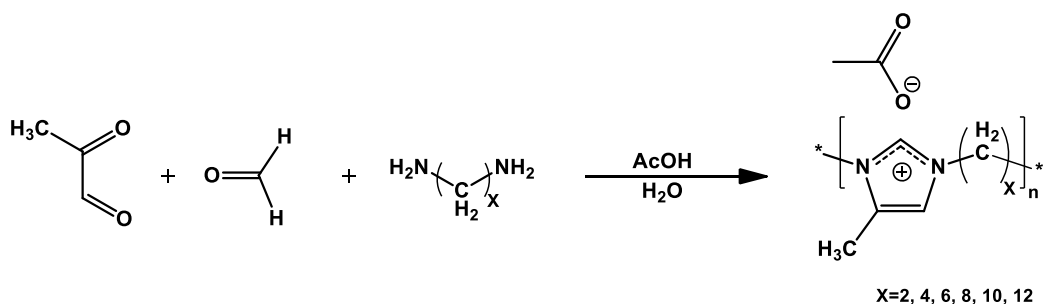

X=2, 4, 6, 8, 10, 12

Figure 48. The one-pot synthetic route towards PILs having different charge densities.

To increase the library of main-chain imidazolium PILs, the synthetic strategy was further extended to polymers which possess imidazolium as well as phenylene groups in their

backbone. For this purpose, *p*-phenylenediamine and *p*-xylylenediamine were reacted with pyruvaldehyde, formaldehyde, and acetic acid following the synthetic pathway developed for PILC5 (Figure 49). In the case of *p*-phenylenediamine, the reaction at the standard conditions led to products which possessed very low solubility in water, even upon treatment with a strong ultrasonic horn device. Owing to this fact, much lower concentrations (40 mL of water was used for 1.0 g of diamine instead of 5.0 mL as in the standard experiment) and shorter reaction time (15 min rather than 24 h) were used to slow down the process and consequently halt it at the stage of water-soluble, oligomeric product.
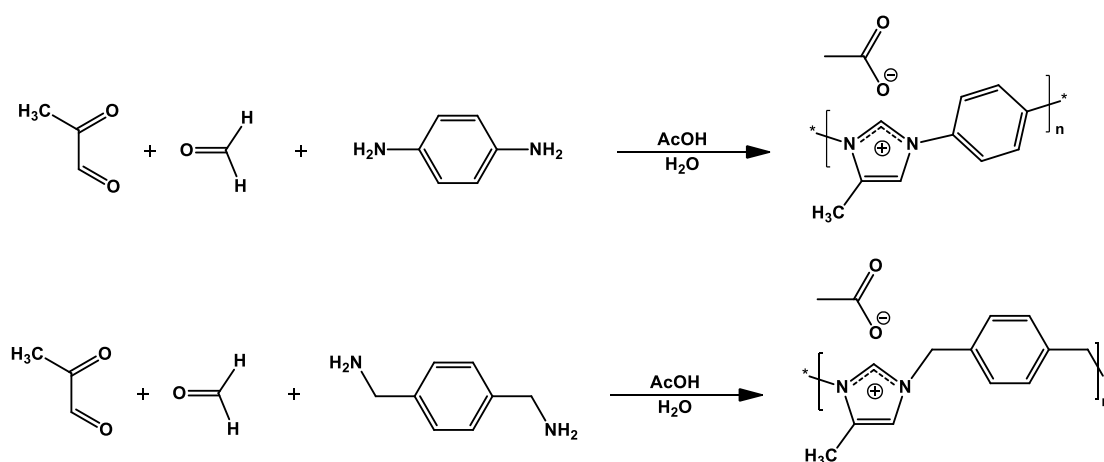
Figure 49. The one-pot synthetic route towards PILs bearing imidazolium and phenylene groups in the main chain.

Eventually, anion exchange reactions were performed to vary electrochemical and physical properties of the synthesized PILs (Figure 50). Synthesis of PILs bearing TFSI and dicyanamide [N(CN)$_2$] counterions were carried out in water. The solution of LiTFSI or NaN(CN)$_2$ (1.2 and 5 molar equivalents calculated with respect to the theoretical amount of product, respectively) was added dropwise to the solution of PILs (obtained from the dialysis according to aforementioned methods). After stirring the reaction mixture for 30 min, the brown precipitate was collected and washed several times with water.

Figure 50. The PIL anion exchange reactions.

4.2.2 Characterization of PILs and their performance

as precursors for nitrogen-doped carbon materials

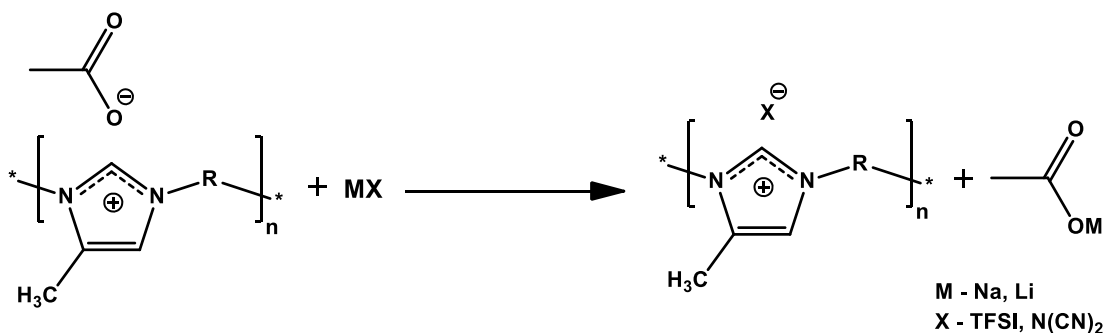The established one-pot method towards bio-derived PIL (PILC5$^+$Ac$^-$) is the first example of a direct synthesis of such polymers *via* the modified Debus-Radziszewski reaction. Thus, it was absolutely essential to precisely confirm the structure of the obtained PIL and to investigate the effect of the reaction parameters on its molar mass. ^{1}H-NMR and ^{13}C-NMR spectra of PILC5$^+$Ac$^-$ were recorded in D$_2$O. All the detected peaks can be clearly assigned to the corresponding protons and carbons of the anticipated product (Figure 51 A, B). The low intensity of the peak of proton A (at 8.37 ppm on ^{1}H-NMR spectrum) is commonly observed on ^{1}H-NMR spectra of imidazolium molecules recorded in D$_2$O. Due to the acidic character of such proton, it undergoes exchange with deuterium atoms of the solvent, leading to the loss of the intensity of the corresponding signal. This can be even amplified by the very harsh conditions (high temperature, long time) of the process of dissolution PILC5$^+$Ac$^-$ in D$_2$O (since re-dissolving a completely dried PILC5$^+$Ac$^-$ is challenging). The proton-exchange affects also the pattern of ^{13}C-NMR spectrum of PILC5$^+$Ac$^-$. The altered chemical environment around carbon A (Figure 51 B), which may occur when neighboring protons are replaced by deuterium, changes the chemical shift of its signal. It eventually leads to the splitting and loss of the

77

intensity of ^{13}C-NMR peak belonging to carbon A. Due to the complications which were caused by the proton exchange in D_2O and problems with direct dissolution of previously dried PILC5$^+$Ac$^-$ in other solvents, the ^{1}H-NMR spectrum of anion exchanged PILC5$^+$TFSI$^-$ was recorded in DMSO-d_6 (Figure 52). The presence of two explicit peaks which can be assigned to protons of imidazolium ring (protons A and C Figure 52), as well as the clear assignment of other NMR signals (except the peaks of protons E and I which overlap with the signal of water at 3.9 ppm), confirms that the proposed method can be used for the synthesis of PILC5. The signal of water in DMSO-d_6 is typically observed at 3.3 ppm. However, the blank experiment confirmed that when water content in DMSO-d_6 becomes significant, the peak of water appears at higher ppm values, which is in agreement with results presented in Figure 52. The successful formation of imidazolium rings in the synthesized products can be further confirmed using ATR-FTIR spectroscopy (Figure 53). In the collected spectrum of PILC5$^+$Ac$^-$, νC-N vibration of imidazolium rings gives a strong band at 1151 cm^{-1}. Moreover, bands of ring asymmetric in-plane stretching, νCC, and ν(N)CH$_2$ at 1390 cm^{-1} as well as peaks of CH$_2$(N), and asymmetric ring in-plane stretching vibrations at 1558 cm^{-1} can be detected.[83]
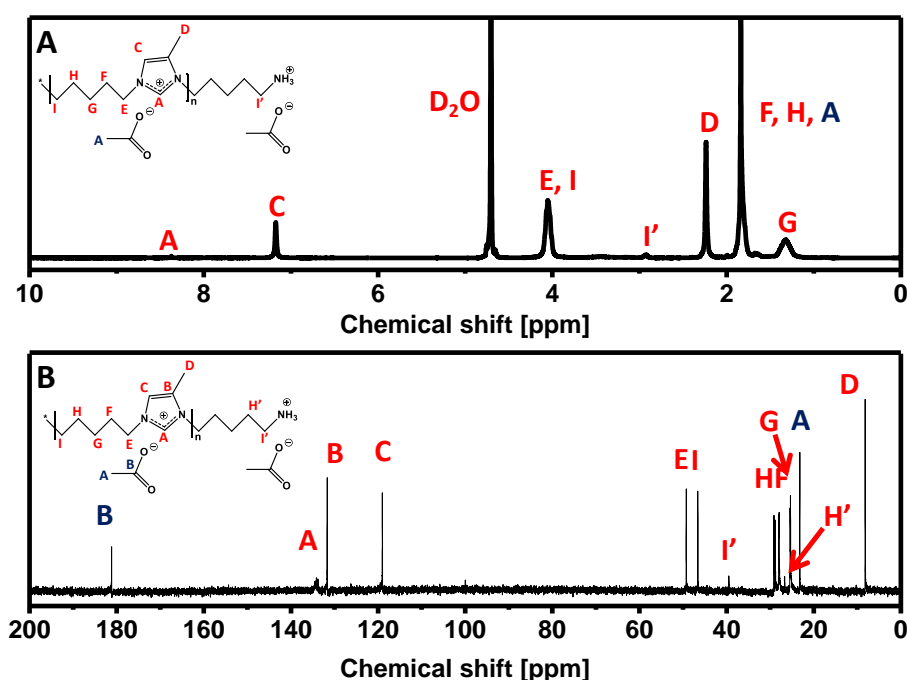
Figure 51. ^{1}H-NMR and ^{13}C-NMR of PILC5$^+$Ac$^-$ in D_2O.
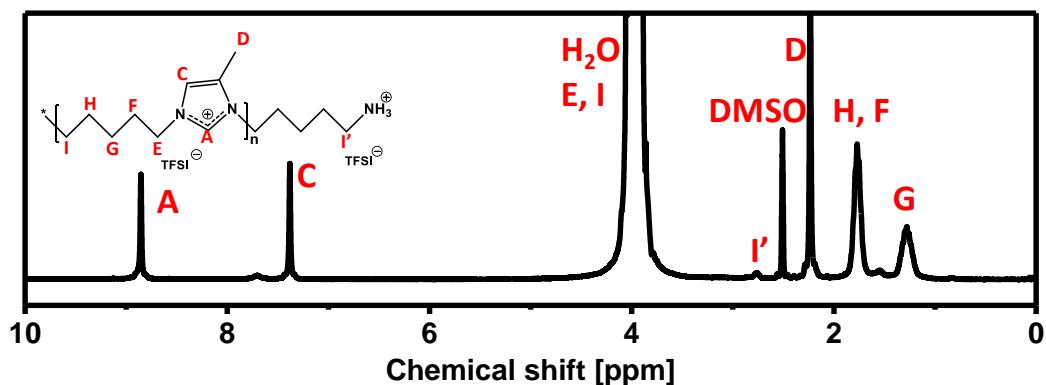
Figure 52. ^{1}H-NMR of PILC5$^+$TFSI$^-$ in DMSO-d_6.
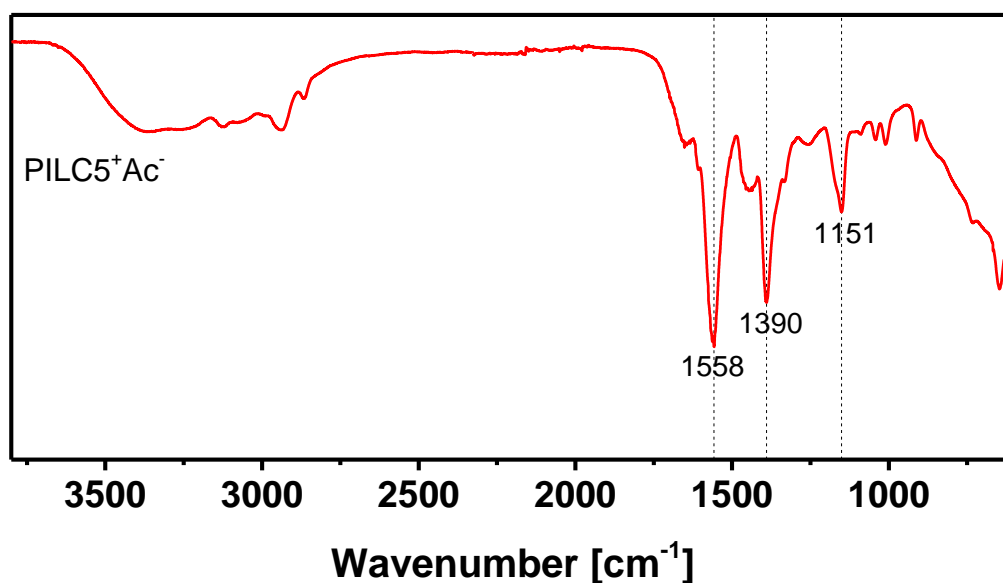
Figure 53. ATR-FTIR spectrum of PILC5$^+$Ac$^-$.

From the synthetic point of view, it was interesting to study the effect of reaction conditions, such as temperature, reactant ratio, and reaction time on molar mass of the synthesized polymer (Figure 54 A, B C). As GPC measurements revealed, the reaction develops very fast within the first hour. The polymer synthesized after 5 min of the reaction achieves $M_n = 10$ kg/mol, having dispersity index (Đ) of 1.4. Carrying out the synthesis for one hour leads to the product having M_n (19 kg/mol) almost twice of the one synthesized after 5 min. However, this is accompanied by the increase in the dispersity index of the product (Đ = 1.6). Further extension of the reaction time leads to the polymer with higher molar mass, but such increase is substantially slower than at the beginning of the reaction ($M_n = 22$ kg/mol after 8 h,

M_n = 25 kg/mol after 12 h). This is also accompanied by the steady broadening distribution of molar masses of the synthesized product ($Đ$ = 1.9 after 8 h, $Đ$ = 2.4 after 12 h of the reaction). In addition, the effect of the temperature and molar ratio of aldehyde and dicarbonyl compound in relation to diamine was studied by GPC. However, the obtained data showed that the reaction temperature only slightly affects the molar mass of the polymer. Also excess of carbonyl compounds does not induce strong effect on molar mass of the synthesized imidazolium polymers. Surprisingly, even when 1.2 molar excess of formaldehyde and pyruvaldehyde in regards to diamine was used, molar mass of the product was almost identical with the product obtained from equimolar ratio of reagents. This is in contrary to typical polycondensation reactions which are usually sensitive to non-equimolar ratio of reagents and non-equimolar ratio leads to the drop of the expected molar mass of the product. In the case of Debus-Radziszewski reaction such unusual effect can be associated with the two-step reaction mechanism, which forms imidazolium ring. First in the reversible step, diimine and water as two products are formed.[117] In the second step, a reaction of diimine with formaldehyde leads to the irreversible formation of imidazolium ring. When the synthesis is performed in water and in excess of carbonyl compounds, it can be expected that the equilibrium of the first reaction is shifted towards the substrates. However, even small amount of the diimine intermediate product can be directly consumed in the irreversible ring-closing reaction, resulting in the increase of molecular weight of polymeric product. Thus, for the rest experiments an excess of carbonyl (1.2 molar excess in regards to diamine) compounds was used. Such conditions were selected in order to assure that the propagation of polymer chain and formation of imidazolium ring will not be halted due to the lack of pyruvaldehyde or highly volatile formaldehyde.
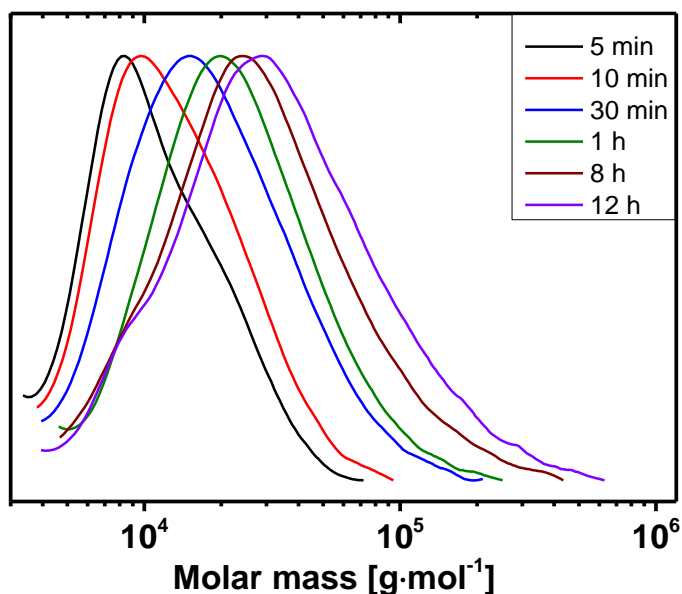
Figure 54. Molar mass distribution of PILC5$^+$Ac$^-$ obtained after various synthesis time.

The successful reaction towards PILC5$^+$Ac$^-$ initiated the follow-up studies, which targeted at broadening of the library of PILs accessed by the newly established method. For this reason, the length of the alkyl spacers which separate imidazolium moieties from each other in the PILs backbone was altered. This led to the synthesis of PILs which possess different charge densities. In regard to the synthetic route established for PILC5$^+$Ac, cadaverine was replaced by the terminal diamines possessing from 2 to 12 methylene groups between amine functionalities. The structure of the products was investigated by ^{1}H-NMR spectroscopy (Figure 55, Figure 56). ^{1}H-NMR spectra of PILs having from 4 to 12 methylene units in the alkyl linkers clearly confirm that the desired structures were obtained (Figure 55). The pronounced increase in the intensity of the peaks in the alkyl region indicates that amines of different length were successfully incorporated into the structure of PILs. The lack of the signal which could be assigned to the acidic proton denoted as A (analogously to the case of PILC5$^+$Ac$^-$) can be correlated to the exchange of such proton in D$_2$O (the process of dissolution of the samples was conducted at 90 °C for 24 h). Unfortunately, due to the insolubility of fully dried PILC2$^+$Ac$^-$ in D$_2$O (even at 90 °C), the attempts to use the same method for the preparation of the ^{1}H-NMR of this material failed. In order to overcome this obstacle, a dialyzed solution of PILC2$^+$Ac$^-$ was

concentrated, followed by the addition of DMSO-d_6 and continuous evaporation of solvents (in order to minimize the amount of water). When the desired polymer concentration was achieved, the ^{1}H-NMR spectrum was recorded. However, possibly due to the low solubility of PILC2$^+$Ac$^-$ in DMSO, this method failed to confirm the structure of the obtained polymer.
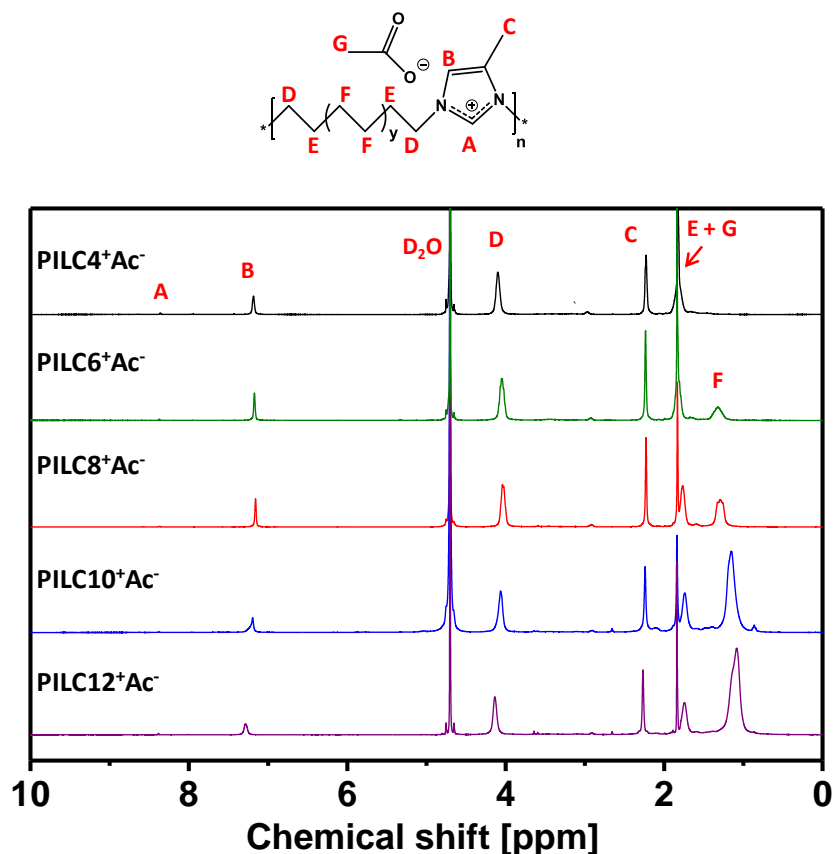

Figure 55. ^{1}H-NMR spectra of PILCX$^+$Ac$^-$ [X=4 (black line), 6 (green line), 8 (red line), 10 (blue line) or 12 (purple line)] recorded in D$_2$O [normalized to the height of the peaks at 4.02 ppm, y - number of units containing protons f; in the scheme $y = \frac{X-4}{2}$].
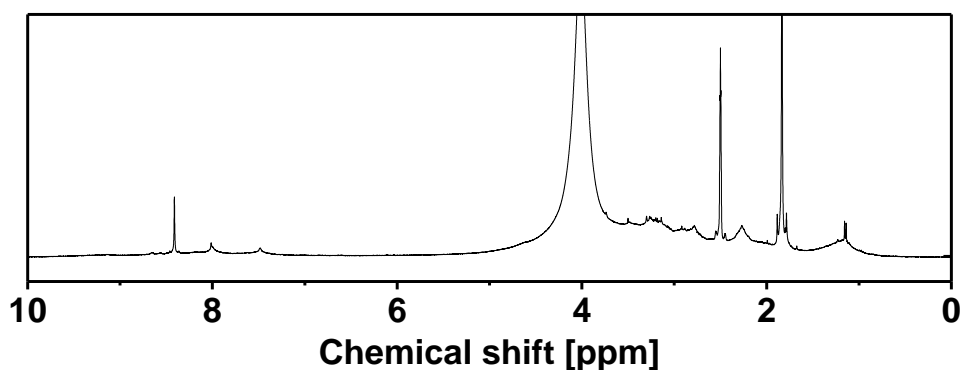

Figure 56. ^{1}H-NMR spectra of PILC2$^+$Ac$^-$ recorded in DMSO.

^{1}H-NMR samples of the products of reactions with *p*-phenylenediamine (PILPh+Ac-) and *p*-xylylenediamine (PILC2Ph+Ac-) were prepared according to the procedure described for PILC2+Ac-. The structure of PILC2Ph+Ac- can be clearly verified by this method (Figure 57). However, presumably due to the low solubility of PILPh+Ac- in DMSO, its ^{1}H-NMR spectrum does not provide a clear evidence for the formation of the designed product.
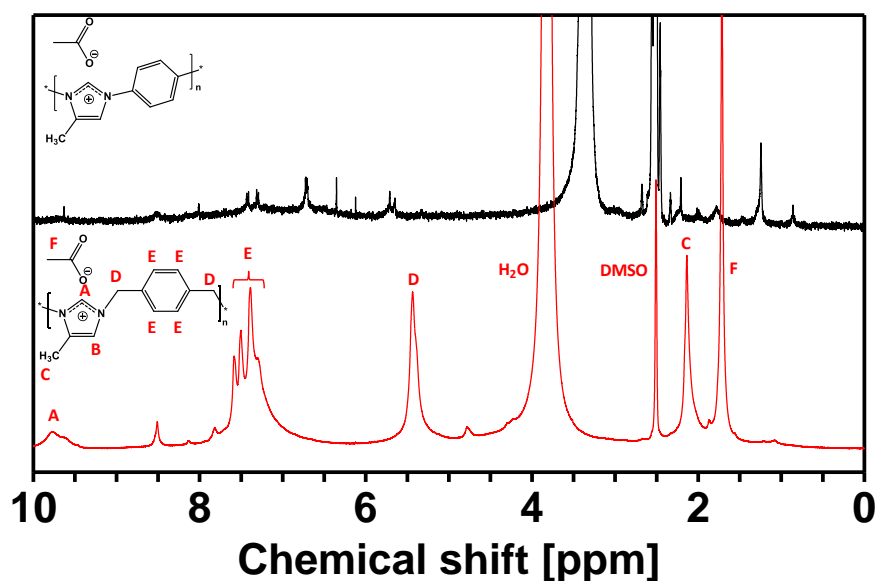
Figure 57. ^{1}H-NMR spectra of PILPh+Ac- and PILC2Ph+Ac- recorded in DMSO.

Imidazolium polymers whose structure was previously confirmed by NMR spectroscopy were characterized using GPC. Prior to the measurements, all the polymers were purified by dialysis (3.5 kDa tubing, dialysis against MiliQ® water) and the characterization was performed in the eluent composed of acetate buffer / MeOH mixture (numbear and weight average molar mass of the polymers were calculated against pullulan standards). When 1,4-daminobutane was used as the polymer precursor, the obtained product displayed a M_n of 34 kg/mol, having monomodal molar mass distribution ($Đ$ = 1.6, Figure 58). The utilization of longer diamines yielded polymers having slightly higher values of M_n (e.g. 45 kg/mol for PILC8+Ac-, 42 kg/mol for PILC10+Ac-, 44 kg/mol for PILC12+Ac-). $Đ$ values of these polymers varied in the range from 1.6 to 2.0 which can be considered as typical results

for polycondensation processes. Imidazolium polymer having phenylene group in its structure (obtained from the reaction with *p*-xylylenediamine) has M_n of 29 kg/mol and $Đ$ = 1.7. Therefore it can be concluded that the developed synthetic method is a facile way to obtain various imidazolium polymers having satisfactory molar masses. Among the performed reactions, only a slight effect of the choice of diamine compound on the molecular weight of the product was observed. In general, the dialyzed imidazolium polymers show monomonal molar masses distribution, having typically M_n in the range from 30 to 45 kg/mol and $Đ$ values slightly below 2. However, the above-mentioned results were calculated using pullalan standards which do not fully mimic the solution behavior of PILs. Thus, the obtained values are only apparent molar masses and they may substantially differ from the absolute molar masses of imidazolium polymers.
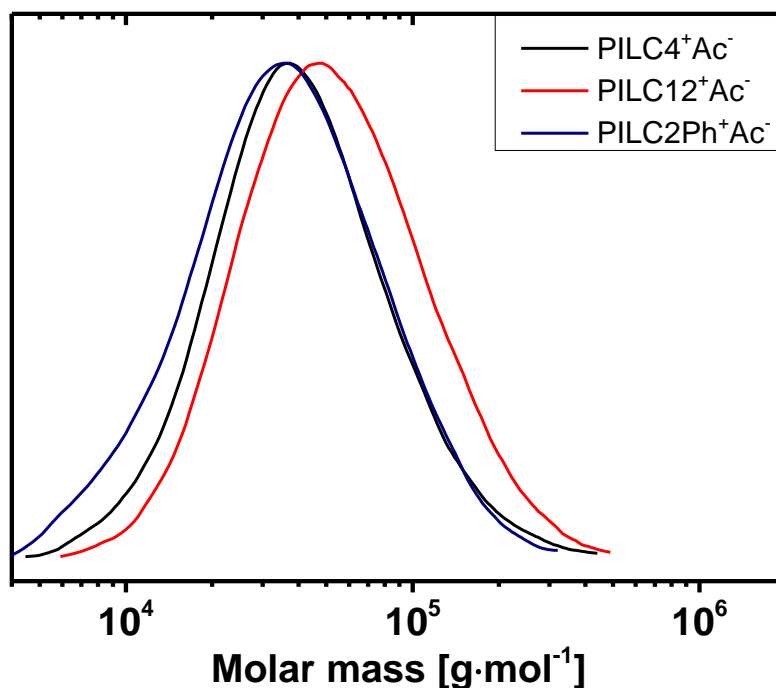

Figure 58. Molar mass distribution of the selected PILs (smoothing function was applied to to the plotted data).

It has been reported that main chain imidazolium PILs having alkyl spacers and TFSI⁻ counteranions possess superior thermal stability.[141] TGA measurements revealed that herein

synthesized PILs having alkyl spacers and Ac^- counteranion decompose at relatively lower temperatures. For instance, $PILC5^+Ac^-$ decomposes at 260 °C (the temperature of 10 % of weight loss). Nonetheless, exchanging counterion to $TFSI^-$ leads to the polymers having a superior thermal stability. $PILC5^+TFSI^-$ is thermally stable up to 440 °C (Figure 59), among the most stable PILs reported in literature. PILs bearing Ac^- anions and *p*-phenylene or *p*-xylylene spacers between imidazolioum-moieties decompose relatively early, at 255 °C and 210 °C, respectively. Nevertheless, at 1000 °C their TGA traces display high residues content ($PILPh^+Ac^-$, - 38 %, $PILC2Ph^+Ac^-$, - 32 %, Figure 60) indicating that these PILs can be potentially used as precursors for carbon materials. In order to increase the carbonization yield in the TGA measurement even more, counterions of such polymers were exchanged to $TFSI^-$ and $N(CN)_2^-$. $PILC2Ph^+N(CN)_2^-$ and $PILPh^+TFSI^-$ display similar thermal properties. They decompose at 320 °C and leave more that 40 % of solid residues at 1000 °C. However, both of them are significantly outperformed by $PILPh^+N(CN)_2^-$, which in addition to the high decomposition temperature (385 °C) leaves 65 % of the carbonized material at 1000 °C. Such high carbonization yield could derive from the material properties of $PILPh^+N(CN)_2^-$ or be an artifact due to the contamination of the sample. The presence of inorganic impurities such as sodium salts (which are reactants used in the PILs anion exchange) could distort the obtained results, artificially increasing the carbonization yield. For this reason, the residues obtained from TGA were characterized by elemental analysis. However, the obtained results revealed that such carbon material constitutes of 87 % of carbon, 10.6 % of nitrogen and 1.5 % of hydrogen, thus is free of the relevant amounts of inorganic impurities.

The above-mentioned values were compared with the results reported for nitrogen-doped carbons synthesized from ILs and PILs. ILs and PILs are not volatile, but at elevated temperatures they often decompose creating well volatile products. Due to such reason, very often during heating up to 1000 °C under atmosphere of an inert gas they decompose

completely or leave small amount of residual mass (less than 30 %),[142] despite one 1,3_bis(cyanomethyl)imidazolium IL gave carbonization yield as high as 53 % (at 800 °C).[143] Specifically, when PILs were applied as precursors for carbon materials, the typical values of carbonization yields obtained at 1000 °C amount to 20 %.[144] This comparison highlights the importance of the results obtained as a part of this PhD work. However, further studies must be performed to investigate and tune the graphitization degree as well as porosity of carbon materials obtained from $PILPh^+X^-$, which may impact the properties of the final materials, such as its conductivity, oxidation stability, and catalytic activity.[142]
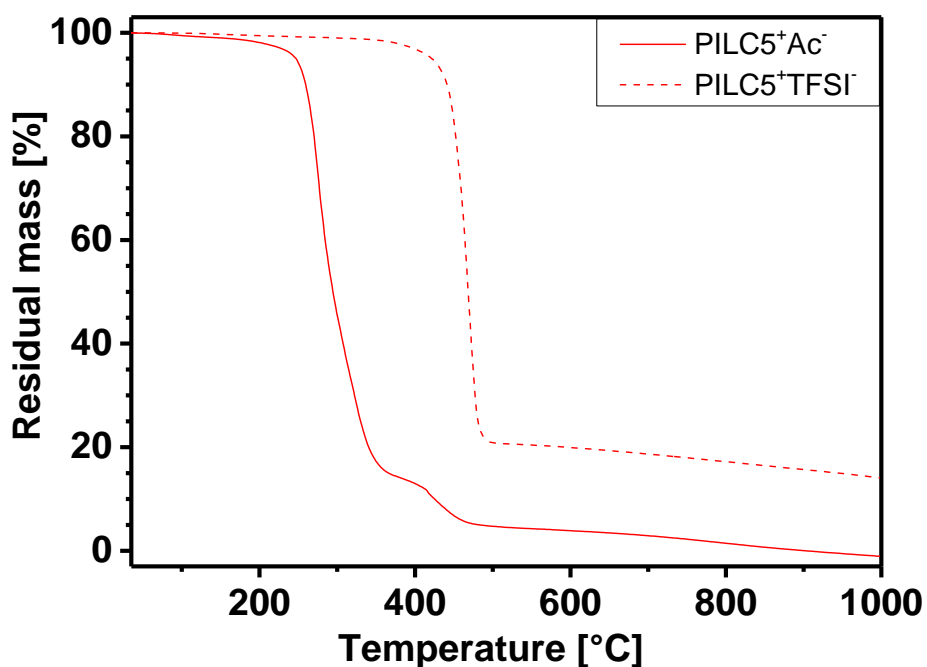
Figure 59. TGA thermograms recorded for PILs having alkyl spacers.
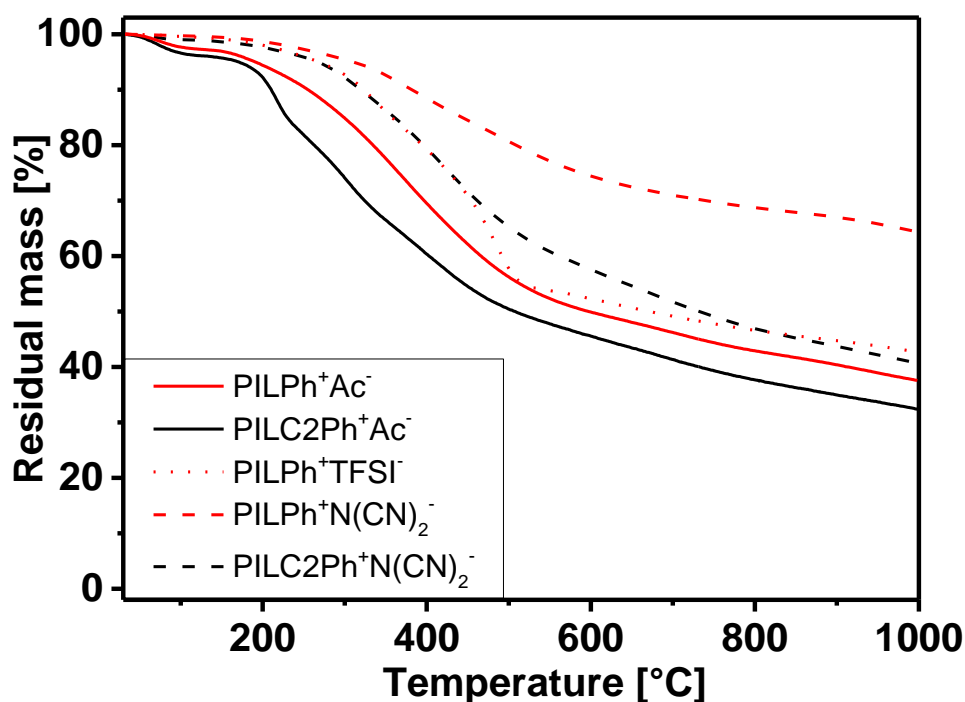
Figure 60. TGA thermograms of PILs having *p*-phenylene or *p*-xylylene linkers.

4.3 Conclusion

To sum up, in the first section of this chapter, a new synthetic method for polyester-type PILs which are partially derived from bio-mass was established. Several PILs bearing different counterions were successfully synthesized. It was presented that such PILs are interesting candidates for CO_2 capture materials. In the latter section, a one-step synthetic route towards main-chain imidazolium-type PILs was developed. Interestingly, this method requires neither sophisticated reaction conditions nor elevated temperatures. Moreover, it utilizes mostly or exclusively simple compounds which can be accessed from bio-resources. Finally, the novel PILs can serve as good precursors for nitrogen-doped carbon materials since they display very high carbonization yields in the TGA measurements.

5. SUMMARY AND OUTLOOK

The research described in this PhD work succeeded in developing new chemical structures of PILs and establishing novel synthetic pathways towards such polymers and their hybrid composites. Various PILs were efficiently applied as stabilizers, phase transfer agents, binders, and CO_2 capture materials.

In chapter 2, the main objective of using a common imidazolium-type PIL as stabilizer for CNFs was to enable processing of CNFs in organic media to unleash their full potential. Since a direct mixing of a cationic PIL and anionic CNFs yielded only the precipitation of a non-dispersible polylelectrolyte complex, the *in situ* polymerization of ILMs in water in the presence of CNTs was applied for the electrostatic grafting of PILs onto CNFs. As a result, a well dispersed PIL-CNF hybrid material which preserved fibrillar, bundle-free morphology was obtained. Such hybrid merged advantages of both its components: superior mechanical strength of CNFs and versatile solution properties of PILs. The omnidispersible CNFs@PILs were easily transferred from water to organic solvents by simple anion exchange and further incorporated into porous polyelectrolyte membranes. Eventually, the reinforced membranes containing only 5 % of hybrids possess around 30 % higher tensile strength and Young's modulus than its hybrid-free counterpart, outperforming also analogous polyelectrolyte porous membranes described in the literature.

Chapter 3 describes the synthesis of two series of PILs which bear in their structure thiazolium cations as functional, ionic moieties. In the first part, thiazolium-type monomer was synthesized from 4-methylthiazole by its quaternization with 4-chloromethylostyrene. The subsequent polymerization of this ionic monomer yielded a hydrophilic polymer having tunable thermal and solution properties. To vary such features of thiazolium PILs, their Cl⁻ counterions

were replaced with TFSI⁻, TFO⁻, BF₄⁻, and PF₆⁻. Decomposition temperature of the polymers strongly depends on the employed anion and increases in the order of Cl⁻ > PF₆⁻, TFO⁻ > TFSI⁻ > BF₄⁻ varying in the range from 200 °C to 295 °C. Moreover, the products exhibited versatile, anion-reliant solubility in water and organic solvents, *i.e.* MeOH, acetone, DMF, and DMSO. As an exemplary application, the thiazolium-polymers served as precursors for sulfur-nitrogen doped carbons and as stabilization and phase transfer agents for CNTs in aqueous and organic media. In the 2nd part of Chapter 3, the structure of thiazolium-containing monomers and polymers was simplified in order to increase the concentration of IL species in bulk PILs. For this reason 4-methyl-5-vinyl thiazole was utilized as a monomer precursor and underwent quaternization with methyl iodide. Counteranions of MVT⁺I⁻ were exchanged to PF₆⁻, BF₄⁻, and TFSI⁻ to generate ILMs of various types. Consequently, each of these monomers was independently polymerized in solution and/or bulk. This synthetic pathway has an advantage over the previous approach, since it yielded PILs and ionic polymers of the high purity, free of non-exchanged counterion contaminants. TGA measurements revealed that structural modification of the polymeric backbone led to PILs whose thermal stability increased up to 385 °C. Among these PILs, P(MVT⁺TFSI⁻) was applied as a binder for electrodes in lithium-ion batteries. Such electrodes showed an excellent stability up to 400 cycles at 5C charge/discharge test and high specific capacity of 140 mAh/g at 1 C test, outperforming for more than 15 % specific capacities measured for electrodes containing commercially used PVDF binder. The studies conducted in this thesis can be regarded as initial research on thiazolium polymers and likely to attract more scientific interest.

In Chapter 4, substrates originating from biomass were successfully harnessed to synthesize main-chain imidazolium-type PILs. In the initial section, a polyester-type imidazolium PILs was formed from bio-derived compounds, such as 1,3-propanediol and a room temperature IL, which partially derives from pyruvaldehyde, glycine, and formaldehyde.

Further anion exchange reactions led to the polymers having adjustable solution and thermal properties. These PILs were tested for CO_2 sorption, reaching capacity up to 0.32 mmol CO_2/g. In the latter section, the new synthetic method towards PILs utilizing diamine compounds for a modified Debus-Radziszewski method was developed. The advantage of this route was that polymers with high molar masses were accessible by one-step synthesis performed in water, at ambient temperature, and without the necessity of using oxygen-free conditions. Moreover, such PILs derived partly or exclusively from simple molecules which stem from bio-resources. The structures of PILs with different charge density and chemical composition of spacers between imidazolium rings were synthesized and characterized. Interestingly, in the case of PILs possessing phenylene linkers, the exchange of counterions from acetate to $TFSI^-$ and $N(CN)_2^-$ yielded products of significantly increased thermal stability and carbonization yield (reaching over 60 %), respectively. Thus, such polymers can be recognized as promising precursors of N-doped carbon materials. The presented here synthetic route serves as a powerful tool giving an easy access to various structures of PILs. Exemplarily, it can be exploited for the synthesis of various functional PILs having for instance pH responsive or fluorescent properties, which depend on the proper selection of diamine. Certain features of PILs can be also altered by the proper choice of carbonyl compounds. In addition, a reaction with multivalent amines for the one-step synthesis of nanogels will be performed in the follow up studies.

A. LIST OF ABBREVIATIONS

^{13}C-NMR	^{13}C nuclear magnetic resonance
^{1}H-^{13}C HMBC	Proton-carbon heteronuclear multiple bond correlation
^{1}H-^{13}C HSQC	Proton-carbon heteronuclear single quantum coherence spectroscopy
^{1}H-NMR	Proton nuclear magnetic resonance
AFM	Atomic force microscopy
ATR-FTIR	Attenuated total reflection Fourier transform infrared spectroscopy
BF_4^-	Tetrafluoroborate
$CHCl_3$	Chloroform
CNF	Cellulose nanofiber
CNF@PIL-X	PIL grafted onto CNFs hybrid material (X – counterion)
CNT	Carbon nanotube
CRP	Controlled radical polymerization
$Đ$	Dispersity index
DLS	Dynamic light scattering
DMF	Dimethylformamide
DMSO	Dimethylsulfoxide
EtAC	Ethyl acetate
EtOH	Ethanol
EVIm$^+$Br$^-$	1-ethyl-3-vinylimidazolium bromide
GPC	Gel permeation chromatography
hν	High vacuum
IL	Ionic liquid
ILM	Ionic liquid monomer
ImDE$^+$TFO$^-$	1,3-bis(2-ethoxy-2-oxoethyl)-5-methylimidazolium trifluoromethanesulfonate

MeOH	Methanol
M_n	Number average molar mass
MVBT$^+$X$^-$	4-Methyl-3-(4-vinylbenzyl)thiazol-3-ium X$^-$ (X$^-$ - counterion)
MVT$^+$X$^-$	3,4-Dimethyl-5-vinylthiazolium X$^-$ (X$^-$ - counterion)
MWCNT	Multiwalled carbon nanotube
N(CN)$_2$	Dicyanamide
P(MVBT$^+$X$^-$)	Poly[4-methyl-3-(4-vinylbenzyl)thiazolium) chloride] (X$^-$ - counterion)
P(MVT$^+$X$^-$)	Poly(3,4-dimethyl-5-vinylthiazolium X$^-$) (X$^-$ - counterion)
PAA	Poly(acrylic acid)
PCMVImPF$_6$	Poly(3-cyanomethyl-1-vinylimidazolium hexafluorophosphate)
PF$_6^-$	Hexafluorophosphate
PIL	Poly(ionic liquid), Polymerized ionic liquid
PVDF	Poly(vinylidene fluoride)
SEM	Scanning electron micrograph
STP	Standard temperature and pressure
SWCNT	Single walled carbon nanotube
TEMPO	2,2,6,6-tetramethylpiperidine-1-oxyl
TFO$^-$	Triflurosulfonate
TFSI$^-$	Bis(trifluoromethane sulfonate)imide
T_g	Glass transition temperature
TGA	Thermogravimetric analysis
THF	Tetrahydrofuran
TnBABr	Tetra-n-butylammonium bromide
VA86	2,2'-azobis[2-methyl-N-(2-hydroxyethyl) propionamide]

B. INSTRUMENTATION AND CHARACTERIZATION METHODS

Atomic Force Micrographs were taken using Nanoscope MultiMode 8 atomic force microscope (Bruker, Santa Barbara, CA) equipped with an E-scanner operating in tapping mode using a Tap150 cantilever (Bruker, Camarillo, CA). Freshly cleaved mica was used as substrate. In the case of CNF@PIL-Br hybrids, the substrate was immersed in 0.02% sample solution for 10 sec, then rinsed with water, and blown dry with a flow of filtered nitrogen gas. For the CNF, mica was first immersed into 0.01 g/L polyethylenimine for 1 sec, followed by rinsing with water. Afterwards such pre-treated substrate was immersed in CNF (0.02 % w/w) for 60 seconds, rinsed with water and blown dry with a flow of filtered nitrogen gas. All measurements were performed in air at room temperature.

Attenuated Total Reflection Fourier-transform infrared spectroscopy (ATR-FTIR) was performed at room temperature with a BioRad 6000 FT-IR spectrometer equipped with a Single Reflection Diamond ATR.

Differential scanning calorimetry (DSC) measurements were done under nitrogen flow using Perkin-Elmer DSC-1 instrument.

Dispersibility tests were performed by mixing 20 mg of CNFs or CNF@PIL hybrids with 10 mL of different solvents followed by sonication for 30 sec using an ultrasonic finger at 50% of full amplitude.

Electrochemical analysis: The electrodes were prepared by spreading slurry of acetylene black, binder and lithium iron phosphate ($LiFePO_4$) in N-methyl-2-pyrrolidone on an aluminum

foil current collector. The ratio was kept constant in all 80% $LiFePO_4$, 10% acetylene black, and 10% binder material. The electrodes were dried at 80 °C for 3 h followed by drying at 120 °C for 24 h. The loading of mixture was controlled at ~2.5mg. The electrodes were assembled in two-electrode Swagelok-type cells. Assembling process was performed inside glovebox under atmosphere of argon. Lithium foil was used as a counter electrode and glass fiber membrane was employed as a separator. As the electrolyte solution, 1 M lithium hexafluorophosphate in mixture of ethylene carbonate and dimethyl carbonate (1:1 volume ratio) was used. The cells were cycled in potential window between 2 and 4 V vs Li/Li^+ using multichannel potentiostatic / galvanostatic system (Bio-Logic). The C-rate was calculated on the basis of $LiFePO_4$ assuming a theoretical specific capacity of 170 mAh/g.

Elemental analysis was accomplished as a combustion analysis using a Vario Micro device.

Gel permeation chromatography (GPC) was performed using:

Chapter 2: TSK Gel Guard (50 x 7.5mm) + 6000 + 5000 + 4000 + 3000 (300x7.5mm, 10µm) column with 0.2M Na_2SO_4 + 1% acetic acid solution in water (flow rate 1.00 mL/min, Pullulan PSS Polymer Standard Service 0.342kD – 710kD, equipped with UV-Detector Spectra System UV 2000 and double detector WGE SEC-3010).

Chapter 3 and chapter 4.1 Gel permeation chromatography was performed using NOVEMA-column with mixture of 80 % of acetate buffer and 20 % of methanol (flow rate 1.00 mL·min^{-1}, PEO standards using RI detector - Optilab-DSP-Interferometric Refractometer (Wyatt-Technology)

Chapter 4.2 Gel permeation chromatography was performed using NOVEMA Max linear XL-column with mixture of 80 % of acetate buffer and 20 % of methanol (flow rate 1.00 mL min-1, Pullalan standards using RI detector - RI -101 Refractometer (Shodex)

Grafting density was calculated for CNF@PIL-Br hybrids. The determined C/N ratio of CNF@PIL-Br hybrid was 4.23. It was confirmed that CNFs do not contain nitrogen (<0.05 wt%). For the calculation of the amount of grafted polymer, C/N for the hybrid material was compared with the theoretical C/N value for pure PIL-Br polymer. The calculated weight ratio of grafted PIL-Br to CNFs was 2.45:1. The calculations were performed as follows: Firstly, surface area of CNFs in the sample of CNF@PIL-Br hybrid material (of weight m; $m = m_{CNF} + m_{PIL}$; according to elemental analysis $m_{PIL} = 2.45 \cdot m_{CNF}$) was calculated according to the following equation:

$$A = \frac{2\, m_{CNF}}{\rho \cdot r}$$

Where A is the surface area of CNFs, m_{CNF} - the weight of the CNFs in the sample of hybrid material, ρ the density of nanocellulose (1.45 g·cm^{-3}), and r is the radius of CNFs (5 nm, the alue obtained from AFM image - Figure 4)

Then grafting density (σ) was calculated according to the following equation:
$$\sigma = \frac{2.45 \cdot m_{CNF} \cdot N_A}{A \cdot M_n} = 0.15\ [chains \cdot nm^{-2}]$$

Where $2.45 \cdot m_{CNF}$ is the weight of PIL-Br in the sample of CNF@PIL-Br hybrid material, N_A is the Avogadro number and M_n the number average molar mass of PIL-Br.[81]

Nuclear Magnetic Spectroscopy (NMR): **Carbon nuclear magnetic resonance (^{13}C-NMR)** spectra were recorded at room temperature using a Bruker DPX-400 spectrometer operating at 400.1 MHz. **Proton nuclear magnetic resonance (^{1}H-NMR)** spectra were recorded at room

temperature using a Bruker DPX-400 spectrometer operating at 400.1 MHz. **Heteronuclear multiple bond correlation (^{1}H-^{13}C HMBC)** NMR spectra were recorded at room temperature on a VARIAN 400-MR (400 MHz) spectrometer.

Scanning electron microscopy (SEM) was performed on a GEMINI LEO 1550 microscope at 3 kV acceleration voltage.

Solubility tests were performed by mixing 10 mg of samples with different solvents (1 wt%) in 5 mL vials. After 24 hours of shaking vials, the presence of solid inside vials was checked.

Sonication Branson Digital Sonifier model W450D was used for the ultrasound treatment. A microtip (1/8′′ in diameter) was immersed in the dispersion and the sonifier was run at different amplitudes. Dispersions were cooled in an ice batch during the whole process.

Tensile tests were performed using a custom-made instrument equipped with a video extensometer. For this purpose membrane strips (2 mm wide, 60-140 µm thick and around 2.5 cm long) were glued onto metal plates (distance between metal plates was in the range 1.3-1.5 cm), which were fixed on the tensile tester by a pin and hole assembly to allow for sample alignment in the strain direction during the tensile test. Samples were kept in the wet state during whole process of sample preparation as well as during stress/strain measurement.

Thermogravimetric analysis (TGA) experiments were performed under nitrogen flow at a heating rate of 10 K min^{-1} using a Netzsch TG209-F1 apparatus.

Transmission electron microscopy (TEM) measurements were performed on a Zeiss EM 912 Omega microscope operating at 120 kV. TEM samples were prepared by dropping 5 µL of a diluted stabilized CNTs suspension on a 200 mesh carbon-coated copper TEM grid.

C. MATERIALS

Acids: Trifluoromethanesulfonic acid (98 +%, Alfa Aesar), acetic acid (≥ 99%, Sigma).

Diamines: Ethylenediamine (99 %, Alfa Aesar), 1,4-diaminobutane (99 %, Aldrich), 1,5-diaminopentane (98 %, Acros Organics), 1,6-diaminohexane, (98 +%, Alfa Aesar), 1,8-diaminooctane (98 %, Aldrich), 1,10-diamidodecane (97 %, Aldrich), 1,12-diaminododecane (98 %, Aldrich), *p*-phenylenediamine (≥ 99 %, Aldrich), *p*-xylylenediamine (99 %, Aldrich).

Halogenated alkyls: Bromoethane (Aldrich 98 %), 1-bromobutane (99 %, Sigma-Aldrich), 4-vinylbenzyl chloride (90%, Acros), methyl iodide (99 %, Alfa Aesar).

Monomer precursors: 1-vinylimidazole (Aldrich 99 %) 4-Methylthiazole, (99 %),4-Methyl-5-vinylthiazole (≥ 97 %, Sigma Aldrich).

Polymerization initiators: 2,2′-Azobis(2-methylpropionitrile) (Sigma Aldrich, 98 %) was recrystallized from methanol. 2,2'-azobis[2-methyl-N-(2-hydroxyethyl)propionamide] (Wake Chemicals) was used without further purification.

Salts: Lithium bis(trifluoromethylsulfonyl) imide (99 %, Io-li-tec), Potassium hexafluorophosphate (99 %, Alfa Aesar), Tetra-n-butylammonium bromide (98 +%, Alfa Aesar) sodium trifluoromethanesulfonate (98 %, Alfa Aesar), sodium tetrafluoroborate (98 %, Sigma Aldrich), silver tetrafluoroborate (98 %, Aldrich), sodium dicyianamide (≥ 97 %, Aldrich), Lithium Iron Phosphate (MES)

Other reagents: formaldehyde (37 % aqueous solution, Applichem), glycine (> 99 %, Merck), 1,3-Propanediol (98 %, Aldrich), pyruvaldehyde (40 % aqueous solution, Sigma), poly(acrylic acid) (PAA, solid powder, M_w = 1800 g/mol, Sigma-Aldrich) Inhibitor 2,6-ditertbutylo 4-methyl phenol (99.0 %; Aldrich), Catalysts Tin (II) 2-ethylhexanoate (95 %, Aldrich), Single-walled carbon nanotubes (Sigma-Aldrich), multi-walled carbon nanotubes (Baytubes® C150P) were used as received.

TEMPO oxidized cellulose nanofibers were obtained from a defibrillation process of soft wood pulp.[145] In brief, an aqueous suspension of pulp from Norwegian spruce was subjected to an enzymatic pre-treatment to liberate wood fibers followed by a TEMPO-mediated oxidation step to render carboxylated fibers (600 mmol/g charge). Subsequent subjection of the fibers to mechanical disintegration using a high-pressure microfluidizer equipped with a 100 μm chamber (Microfluidizer M-110EH, Microfluidics Corp., USA) provides fully defibrillated cellulose nanofibers. This mechanical treatment renders a highly viscous CNF dispersion with a concentration of about 1 wt%. The CNFs are long and flexible fibers with a thickness of 5 nm and 1-2 μm in length (Figure 4 A).[81]

1-Cyanomethyl-3-vinylimidazolium bromide (CMVImBr), and 3-ethyl-1-vinylimidazolium bromide was synthesized according to the method described in the literature.[54, 146] Poly(3-cyanomethyl-1-vinylimidazolium hexafluorophosphate (PCMVImPF$_6$) was prepared by anion exchange of PCMVImBr with KPF$_6$ salt in aqueous solution.

Green muscovite mica obtained from AXIM Enterprises (New York, US) was used in the AFM studies. Polyethylenimine with a molar mass of about 60 000 g/mol (supplied by Arcos organics, US) was used as received.

All used solvents were of analytic grade.

D. EXPERIMENTAL

D.1 Chapter 2

In situ stabilization of CNFs and the anion exchange

CNF dispersion (10 g, 1 wt%) was diluted with MiliQ® water (40 mL) and sonicated using an ultrasonic horn (10 min. of active sonication at 10% of full amplitude, 3 sec on/3 sec off cycles, followed by 10 minutes of active sonication at 50% of full amplitude, 3 sec on/3 sec off cycles). Subsequently, additional amount of MiliQ® water (120 mL) was added and the dispersion was sonicated for 10 min (at 50 % of full amplitude, 3 sec on/3 sec off cycles). During the sonication processes the sample was immersed in an ice bath. 1-Ethyl-3-vinylimidazolium bromide monomer solution (4.0 g, 19.70 mmol in 20 mL of MiliQ® water) and VA86 initiator solution (80 mg, 0.277 mmol in 10 mL of MiliQ® water) were added dropwise to vigorously stirred CNFs dispersion, followed by charging into a 250 mL Schlenk flask and 5 cycles of degassing – filling with argon. The polymerization reaction was performed under argon at 85 °C for 20 h. The crude product was purified from free polymer by the ultrafiltration method (filters with 50 nm pores). For the anion exchange, one batch of the stabilized CNF dispersion (100 mL of suspension) was dispersed using an ultrasonic horn device (10 minutes of active working at 50% of amplitude, 3 sec on/3 sec off cycles) and solutions of KPF_6 (400 mg, 2.17 mmol in in 50 mL of MiliQ® water) or LiTFSI (624 mg, 2.17 mmol in 50 mL of MiliQ® water) was added dropwise into vigorously stirred suspension of CNFs. After one hour of stirring of such mixtures, products were purified by ultrafiltration (filters with 50 nm pores).

Membranes preparation

PCMVImPF$_6$ (1.0 g) was dissolved in DMSO (9.0 g). Poly(acrylic acid) (PAA) (2.58g, M_w: 1800 g/mol) was dissolved in DMSO (10.0 g). PAA solution (1.258 g of the sulution) was added to PCMVImPF$_6$ solution (10.0 g) and stirred for 1 h. Then 1.5 g of such mixture was cast onto a clean glass plate and dried in air at 80 °C for 3h, followed by immersing in 0.2 wt% aqueous ammonia (pH=10.8, 20 °C, 2 h). After 2 h, a flexible, yellowish freestanding membrane was detached from the glass surface and washed with demineralized water.

Reinforced membranes were prepared in an analogous way to the above-mentioned, but in the first step PCMVImPF$_6$ (1.0 g) was dissolved in DMSO followed by the addition of 63 mg of CNF@PIL-PF$_6$ hybrid dispersed in a stock solution in DMSO (the concentration of CNF@PIL-PF$_6$ hybrid in the stock solution was determined by TGA measurement) and tuning the overall amount of DMSO to 9.0 g. Then 1.258 g of PAA solution was added to the mixture followed by the sonication using ultrasonic horn device (10 minutes of active working, 50 % of full amplitude in 3 sec on/3 sec off cycles). During the sonication process the sample was immersed in an ice bath.[81]

Characterization of free-standing polymer

For the characterization of free-standing polymer, the filtrate eluting during the ultrafiltration process was concentrated under the reduced pressure and dried for 24 h at 40 °C. Subsequently, M_n and Đ of the free PIL chains were determined by GPC (calculated against pullalan standards) to be 35 kg/mol and 1.5, respectively.

D.2 Chapter 3.1

Monomers Synthesis

4-methyl-3-(4-vinylbenzyl)thiazol-3-ium chloride (MVBT$^+$Cl$^-$): 4-methylthiazole (20.0 g; 0.20 mol), 2,6-ditertbutylo4-methyl phenol (0.300 g, 1.36 mmol) and EtAc (100 mL) were loaded into a 250 mL round bottom flask. 4-Chloromethyl styrene (102.6 g; 0.61 mol) was added to the flask under vigorous stirring and stirred at 70 °C for 20 days. Every 5 days, the precipitate was collected by filtration, washed several times with ethyl acetate and dried under high vacuum at 40 °C for 24 h (21.45 g, yield 42%). ^{1}H-NMR (400.1 MHz, D$_2$O): 7.87 (s, 1H, CH), 7.6 (d, 2H; ArH), 7.3 (d, 2H; ArH), 6.8 (q, 1H; CH), 5.9 (d, 1H; CH$_2$), 5.64 (s, 2H; CH$_2$), 5.4 (d, 1H; CH$_2$), 2.50 (s, 3H; CH$_3$); the peak of the acidic proton of imidazolium ring is absent due to a fast proton exchange in D$_2$O. However, its existence was confirmed by ^{1}H NMR analysis in DMSO-d$_6$.

4-methyl-3-(4-vinylbenzyl)thiazol-3-ium bis(trifluoromethylsulfonyl) imide (MVBT$^+$TFSI$^-$): MVBT$^+$Cl$^-$ (1.50 g, 5.96 mmol) was dissolved in MiliQ® water (10 mL). LiTFSI (1.82 g, 6.34 mmol) was dissolved in MiliQ® water (40 mL) and added dropwise to the monomer solution under vigorous stirring. Phase separation was observed. After 24 h the upper phase was decanted. The bottom part was washed 3 times with MiliQ® water, dissolved in methanol (50 mL), and re-precipitated from MiliQ® water. The product was collected and dried under high vacuum at 40 °C for 48 h (2.10 g, yield 71%). ^{1}H-NMR (400 MHz, DMSO-d_6): 10.14 (s, 1H, CH), 8.05 (s, 1H, CH), 7.5 (d, 2H; ArH), 7.3 (d, 2H; ArH), 6.8 (q, 1H; CH), 5.9 (d, 1H; CH$_2$), 5.7 (s, 2H; CH$_2$), 5.3 (d, 1H; CH$_2$), 2.4 (s, 3H; CH$_3$)

4-methyl-3-(4-vinylbenzyl)thiazol-3-ium hexafluorophosphate (MVBT$^+$PF$_6^-$): was synthesized according to the analogous procedure that the one established for MVBT$^+$TFSI$^-$ except that acetone was used instead of methanol for dissolving the crude product. (2.15 g, yield 76%). ^{1}H NMR (400 MHz, DMSO-d_6): 10.14 (s, 1H, CH), 8.05 (s, 1H, CH), 7.6 (d, 2H; ArH), 7.3 (d, 2H; ArH), 6.8 (q, 1H; CH), 5.9 (d, 1H; CH$_2$),), 5.7 (s, 2H; CH$_2$), 5.3 (d, 1H; CH$_2$), 2.4 (s, 3H; CH$_3$)

Synthesis of 4-methyl-3-(4-vinylbenzyl)thiazol-3-ium tetrafluoroborate (MVBT$^+$BF$_4^-$): MVBT$^+$Cl$^-$ (1.5g, 6.0 mmol), NaBF$_4$ (0.73 g, 6.5 mmol) and acetonitrile (100 mL) were charged into a beaker and stirred at room temperature for 72 h. Afterwards, solid particles were centrifuged out. The supernatant was collected and solvent was removed under reduced pressure. The product was dried under high vacuum at 40 °C for 48 h (1,63 g of MVBT$^+$BF$_4^-$, yield 90 %). ^{1}H NMR (400 MHz, DMSO-d6, δ): 10.13 (s, 1H, CH), 8.05 (s, 1H, CH), 7.6 (d, 2H; ArH), 7.3 (d, 2H; ArH), 6.8 (q, 1H; CH), 5.9 (d, 1H; CH$_2$),), 5.74 (s, 2H; CH$_2$), 5.3 (d, 1H; CH$_2$), 2.44 (s, 3H; CH$_3$)

4-methyl-3-(4-vinylbenzyl)thiazol-3-ium trifluoromethanesulfonate (MVBT$^+$TFO$^-$): MVBT$^+$Cl$^-$ (1.00 g, 4,0 mmol), sodium trifluoromethanesulfonate (NaTFO; 0.70 g, 4.0 mmol) and acetonitrile (100 mL) were loaded into a beaker and stirred at room temperature for 72 h. Afterwards, the solid particles were centrifuged out and the supernatant was collected. Acetonitrile was removed using under reduced pressure, using rotary evaporator. The product was dried under high vacuum at 40 °C for 48 h. (1,44 g of MVBT$^+$TFO$^-$, yield 99 %). ^{1}H-NMR (400 MHz, DMSO-d_6, δ): 10.14 (s, 1H, CH), 8,05 (s, 1H, CH), 7.6 (d, 2H; ArH), 7.3 (d, 2H; ArH), 6.8 (q, 1H; CH), 5.9 (d, 1H; CH$_2$), 5.74 (s, 2H; CH$_2$), 5.3 (d, 1H; CH$_2$), 2.44 (s, 3H; CH$_3$)

Polymer synthesis

P(MVBT$^+$Cl$^-$): MVBT$^+$Cl$^-$ (7.6 g, 30.1 mmol) and 2,2'-azobis[2-methyl-N-(2-hydroxyethyl)propionamide] (0.23 g, 0.79 mmol) were charged into a 100 mL Schlenk flask and dissolved in MiliQ® water (40 mL). The mixture underwent 3 cycles of freeze-pump-thaw procedure. Polymerization was performed under atmosphere of an inert gas at 90 °C for 48 h. Crude product was purified by dialysis against MiliQ® water and lyophilized (6.35 g, yield 84 %).

P(MVBT$^+$TFSI$^-$): P(MVBT$^+$Cl$^-$) (1.00 g) was dissolved in MiliQ® water (30 mL). LiTFSI (1.25 g, 4.35 mmol) solution in MiliQ® water (20 mL) was added dropwise under vigorous stirring. White precipitate was observed. After 24 h precipitate was filtered off on a Büchner funnel, washed several times with MiliQ® water and dried at 40 °C for 48 h (1.63 g, yield 89%).

P(MVBT$^+$PF$_6^-$) was obtained in the analogous procedure to the one established for P(MVBT$^+$TFSI$^-$), but KPF$_6$ (0.81 g, 4.36 mmol) was used for an anion exchange. Crude product was purified by centrifugation and 5 times of washing with MiliQ® water (1.03 g, yield 72%).

P(MVBT$^+$TFO$^-$): P(MVBT$^+$Cl$^-$) (100 mg), NaTFO (77.0 mg, 0.448 mmol), and acetonitrile (20.0 mL) were stirred in a beaker at room temperature for 24 h. Then, solid particles were centrifuged out. The supernatant was collected and acetonitrile was removed under reduced pressure. The crude product was washed with MiliQ® water and dried under high vacuum at 40°C for 48 h (109.1 mg, yield 75%).

P(MVBT$^+$Cl$^-$) (100 mg), NaBF$_4$ (77,0 mg, 0,448 mmole) and acetonitrile (20.0 mL) a beaker and stirred at room temperature for 24 h. Afterwards, solid particles were centrifuged out. The supernatant was collected followed by removal of acetonitrile under reduced pressure.

The crude product was washed with water, dried under high vacuum at 40 °C for 48 h [122 mg of P(MVBT$^+$ BF$_4^-$), yield 99 %]

Stabilization of CNTs and carbonization

In the case of stabilization of MWCNTs and SWCNTs, CNTs (1.0 mg), P(MVBT$^+$Cl$^-$) (100 mg), and water (25 mL) were charged into a beaker. Afterwards, the mixture was sonicated using Branson Digital Sonifier model W450D (60 % of amplitude, 10 min. of active sonication, 5 sec. on/15 sec. off). During the sonication process the beaker was cooled in an ice bath. The sonication of such mixture yielded stable for weeks, black dispersion. For anion exchange, MWCNTs/P(MVBT$^+$Cl$^-$) dispersion (15 mL) was transferred to 25 mL vial and the solution of KPF$_6$ (80 mg, 0.43 mmol KPF$_6$ in 10 mL of MiliQ® water) was added dropwise. After 24 hours, black precipitate was separated by centrifugation, washed 5 times with water, and re-dispersed in acetone.

Carbonization of P(MVBT$^+$Cl$^-$)

100 mg of P(MVBT$^+$Cl$^-$) was charged into a crucible placed in the oven and flushed with nitrogen for 30 min. Afterwards, the sample was heated to a final temperature at a heating rate of 3 K min^{-1} and carbonized for 1 hour (the whole carbonization process was performed under nitrogen).

D.3 Chapter 3.2

Monomers synthesis:

3,4-Dimethyl-5-vinylthiazol-3-ium iodide (MVT⁺I⁻): Methyl iodide (0.31 mol, 19.5 mL) was added dropwise under vigorous stirring to the mixture of 4-methyl-5-vinylthiazole (20.0 g, 0.155 mol) and 2,6-ditertbutylo-4-methylphenol (100 mg, 0.45 mmol) into 250 mL round bottom flask. The flask was closed with a stopper and thermostated at 40 °C for 20 h. The solid product was dissolved in DMSO (200 mL) and subsequently precipitated from 4.0 L of 1:1 volume mixture of diethyl ether and THF. The precipitate was filtered on a Büchner funnel, washed with 1:1 volume mixture of diethyl ether and THF, and dried overnight at 40 °C, at high vacuum (37.6 g of MVT⁺I⁻, 88% yield). ^{1}H-NMR (400 MHz, DMF-d_7) δ 10.38 (s, 1H), 7.19 (dd, J = 17.2, 11.1 Hz, 1H), 6.02 (d, J = 17.2 Hz, 1H), 5.66 (d, J = 11.1 Hz, 1H), 4.36 (s, 3H), 2.69 (s, 3H); ^{13}C-NMR (101 MHz, DMF-d_7) δ 158.38, 144.50, 135.92, 125.98, 121.95, 41.81, 12.50.

3,4-Dimethyl-5-vinylthiazol-3-ium bis(trifluoromethylsulfonyl) imide (MVT⁺TFSI⁻): LiTFSI solution (52.11 g, 180 mmol in 500 mL of MiliQ® water was added dropwise to the solution of MVT⁺I⁻ (40.0 g, 150 mmol in 1L of MiliQ® water) followed by stirring for 2 h. The precipitate was separated on by vacuum filtration on a Büchner funnel and washed with MiliQ® water. The product was dried overnight at 40 °C degree at high vacuum (36.96 g 3,4-dimethyl-5-vinylthiazol-3-ium bis(trifluoromethylsulfonyl) imide, 59 % yield). ^{1}H-NMR (400 MHz, DMF-d_7) δ 10.28 (s, 1H), 7.17 (dd, J = 17.2, 11.1 Hz, 1H), 6.03 (d, J = 17.3 Hz, 1H), 5.69 (d, J = 11.1 Hz, 1H), 4.33 (s, 3H), 2.68 (s, 3H); ^{13}C-NMR (101 MHz, DMF-d_7) δ 158.29, 144.43, 136.07, 125.98, 122.78, 121.96, 119.59, 116.39, 41.40, 12.04.

3,4-Dimethyl-5-vinylthiazol-3-ium hexafluorophosphate (MVT$^+$PF$_6^-$): KPF$_6$ solution (44,5 mmol, 8.35 g in 100 mL of MiliQ® water) was added dropwise, under vigorous stirring to the solution MVT$^+$I$^-$ (8.0 g, 30.0 mmol in 100 mL of MiliQ® water). After stirring for 30 min, the brown precipitate was centrifuged out and washed twice with water. The product was dried overnight at 40 °C, at high vacuum (4.36 g of MVT$^+$PF$_6^-$, 51 % yield). ^{1}H-NMR (400 MHz, DMF-d_7) δ 10.24 (s, 1H), 7.16 (dd, J = 17.2, 11.1 Hz, 1H), 6.03 (d, J = 17.3 Hz, 1H), 5.69 (d, J = 11.1 Hz, 1H), 4.32 (s, 3H), 2.74 (s, 3H); ^{13}C NMR (101 MHz, DMF-d_7) δ 158.00, 144.29, 135.93, 125.69, 121.88, 41.27, 11.89.

3,4-Dimethyl-5-vinylthiazol-3-ium tetrafluoroborate (MVT$^+$BF$_4^-$): MVT$^+$I$^-$ (4.0 g, 15.0 mmol) was dissolved in the mixture of 30.0 g of MiliQ water ad 90.0 g of acetone. AgBF$_4$ (2.95 g 15.0 mmol) was dissolved in the mixture of 10.0 g of MiliQ water and 30.0 g of acetone, following by adding dropwise, under vigorous stirring to the MVT$^+$I$^-$ solution. After 30 min, the yellow precipitate was centrifuged out. The supernatant was collected and dried by evaporation of acetone under reduced pressure followed by lyophilization. (3.20 g of MVT$^+$BF$_4^-$, 94 % yield). ^{1}H NMR (400 MHz, DMF-d7) δ 10.23 (s, 1H), 7.17 (dd, J = 17.3, 11.1 Hz, 1H), 6.03 (d, J = 17.3 Hz, 1H), 5.68 (d, J = 11.1 Hz, 1H), 4.32 (d, J = 0.8 Hz, 3H), 2.67 (s, 3H), ^{13}C NMR (101 MHz, DMF) δ 158.07, 144.40, 135.94, 125.81, 121.90, 41.32, 11.95.

Polymers synthesis:

Poly(3,4-dimethyl-5-vinylthiazol-3-ium iodide) [P(MVT$^+$I$^-$)]: MVT$^+$I$^-$ (4.0 g, 15.0 mmol), 2,2'-azobis[2-methyl-N-(2-hydroxyethyl)propionamide] (0.10 g, 0.35 mmol) and 8.0 mL of MiliQ® water were loaded into a 50 mL Schlenk flask and stirred. The flask was 5 times degassed / filled with argon and reaction was carried out under argon at 90 °C for 20 h. The mixture was diluted with 5.0 mL of MiliQ® water and precipitated from 300 mL of

acetone. The product was collected by filtration and dried overnight at 80 °C, at high vacuum [2,9 g of P(MVT⁺I⁻), 73 % yield].

Poly(3,4-dimethyl-5-vinylthiazol-3-ium bis(trifluoromethylsulfonyl) imide) [P(MVT⁺TFSI⁻)]: MVT⁺TFSI⁻ (2.0 g, 4.8 mmol) and AIBN (40 mg, 0.24 mmol) were loaded into a 50 mL Schlenk flask together with the stirring bar. The flask was 5 times degassed / filled with argon and bulk polymerization was carried out under argon at 120 °C for 6 h. The crude product was dissolved in 5.0 mL of acetone followed by precipitation from 100 mL of chloroform. The product was collected by filtration and dried overnight at 100 °C, at high vacuum [1.8 g of poly(3,4-dimethyl-5-vinylthiazol-3-ium bis(trifluoromethylsulfonyl) imide), 90 % yield).

Poly(3,4-dimethyl-5-vinylthiazol-3-ium hexafluorophosphate) [P(MVT⁺PF₆⁻)]: a) bulk polymerization: MVT⁺PF₆⁻ (0.50 g, 1.75 mmol) was loaded into a 50 mL Schlenk flask together with the stirring bar. The flask was 5 times degassed / filled with argon and bulk polymerization was carried out under argon at 170°C for 8 h. The crude product was dissolved in 3.0 mL of DMF followed by precipitation from 50 mL of THF. The product was collected by centrifugation and dried overnight at 80 °C, at high vacuum [0.45 g of P(MVT⁺PF₆⁻), 90 % yield); b) polymerization in solution: MVT⁺PF₆⁻ (1.0 g, 3.5 mmol), AIBN (20 mg, 0.12 mmol) were charged into 10 mL Schlenk flask and dissolved in DMF (1.0 g). The mixture was 5 times degassed / filled with argon and polymerization was conducted for 24 h at 90 °C. The crude product was dissolved in 4.0 mL of DMF and precipitated from 100 mL of THF. The precipitate was collected by centrifugation, washed with THF and dried overnight at 80 °C (940 mg of P(MVT⁺PF₆⁻), 94 % yield).

Poly(3,4-dimethyl-5-vinylthiazol-3-ium tetrafluoroborate) [P(MVT$^+$BF$_4^-$)]: a) bulk polymerization: MVT$^+$BF$_4^-$ (1.0 g, 4.4 mmol) was loaded into a 50 mL Schlenk flask together with the stirring bar. The flask was 5 times degassed / filled with argon and bulk polymerization was carried out under argon at 170 °C for 8 h. The crude product was dissolved in 10 mL of DMF followed by precipitation from 100 mL of acetone. The product was collected by centrifugation and dried overnight at 80 °C, at high vacuum [0.83 g of P(MVT$^+$BF$_4^-$)], 83 % yield); b) polymerization in solution: MVT$^+$BF$_4^-$ (1.0 g, 4.4 mmol), AIBN (20 mg, 0.12 mmol) were charged into 10 mL Schlenk flask and dissolved in DMF (2.0 g). The mixture was 5 times degassed / filled with argon and polymerization was conducted for 24 h at 90 °C. The crude product was dissolved in 3.0 mL of DMF and precipitated from 100 mL of acetone. The precipitate was collected by centrifugation and dried overnight at 80 °C (810 mg of P(MVT$^+$BF$_4^-$), 81 % yield).

D.4 Chapter 4.1

1,3-bis(carboxymethyl)-5-methylimidazolium acetate was synthesized by Sarah Kirchhecker according to the published method.[117] In a typical reaction, pyruvaldehyde (0.05 mol), glycine (0.1 mol) and formaldehyde (0.05 mol) were dissolved in water (100 mL) in a round bottom flask. Acetic acid (0.3 mol) was added and the reaction was stirred for 1 h at room temperature. The reaction mixture was then freeze-dried. The residue was washed with acetic acid and dried under high vacuum at 40 °C for 24 hours (6.83 g of 1,3-bis(carboxymethyl)-5-methylimidazolium acetate, 74 % yield).

1,3-bis(2-ethoxy-2-oxoethyl)-5-methylimidazolium trifluoromethanesulfonate was synthesized by Sarah Kirchhecker according to the following procedure: 1,3-bis(carboxymethyl)-5-methylimidazolium acetate (4.0 g, 0.02 mol),

trifluoromethanesulfonic acid (1.95 mL, 0.022 mol) and ethanol (200 mL) were charged under argon into 250 mL round bottom flask equipped with a Soxhlet apparatus containing 3Å molecular sieves, and a condenser. The reaction was carried out for 12 h at 120 °C. Conversion to 1,3-bis(2-ethoxy-2-oxoethyl)-5-methylimidazolium trifluoromethanesulfonate (calculated from ^{1}H-NMR spectra) was 97 %. After the reaction, ethanol was removed under reduced pressure. The product was stored under high vacuum at 40 °C.

Polymer TFO (PImDE$^+$TFO$^-$): Before polymerization, the purification step was performed for 1,3-bis(2-ethoxy-2-oxoethyl)-5-methylimidazolium trifluoromethanesulfonate in order to remove an excess of triflic acid. In a typical purification process, 1,3-bis(2-ethoxy-2-oxoethyl)-5-methylimidazolium trifluoromethanesulfonate (3.0 g) was dissolved in 3.0 g of THF followed by precipitation from diethyl ether (150 mL). Above mentioned sequence was repeated 2 times. Afterwards crude product was dried under high vacuum at 40 °C for 20 h (2.55 g of 1,3-bis(2-ethoxy-2-oxoethyl)-5-methylimidazolium trifluoromethanesulfonate was obtained). Subsequently, 1,3-bis(2-ethoxy-2-oxoethyl)-5-methylimidazolium trifluoromethanesulfonate (623 mg, 1.154 mmol) and 1,3-propanediol (353 mg, 4.634 mmol) were charged into a 100 mL Schlenk flask. A reflux condenser was closed from the top with a rubber balloon and attached to the flask. The set-up was 5 times evacuated-filled with argon. Afterwards Sn(Oct)$_2$ (10 µL, 31 µmol) was added under argon and set-up was placed into an oil bath, thermostated at 160 °C. After three hours reflux condenser was replaced with a stopper and high vacuum was slowly applied. Reaction mixture was heated up to 215 °C within 30 min and then stirred at 215 °C under high vacuum (hv) for 4 h. Afterwards, the mixture was cooled down to room temperature and crude product was dissolved DMF (5.0 mL) followed by precipitation from THF (100 mL). Separated product was dried under high vacuum, at 60 °C for 20 h (251 mg of PImDE TFO was obtained, 42 % yield).

Polymer Br (PImDE$^+$Br$^-$): The purified according to the above-mentioned procedure 1,3-bis(2-ethoxy-2-oxoethyl)-5-methylimidazolium trifluoromethanesulfonate (2.36 g, 5.85 mmol) and 1,3-propanediol (1.33 g, 17.48 mmol) were charged into 100 mL Schlenk flask. A reflux condenser was closed from the top with rubber balloon and attached to the flask. The set-up was 5 times evacuated-filled with argon. Afterwards Sn(Oct)$_2$ (38 µL, 117 µmol) was added under argon and set-up was placed into an oil bath, thermostated at 160 °C. After three hours reflux condenser was replaced with a stopper and high vacuum was applied. Reaction mixture was heated up to 215 °C within 30 minutes and then stirred at 215 °C under hv for 4 h. TnBABr (1.60 g, 4.96 mmol) was dissolved in the mixture of 40 mL of acetone and 2 mL of water. Product of the reaction was dissolved in 40 mL of acetone and added dropwise, under vigorous stirring to the solution of TnBABr. Mixture was stirred for 30 min and then the precipitate was separated *via* centrifugation. To purify the product from the excess of salt, it was dissolved in dimethylformamide (5.0 mL) followed by precipitation from the mixture of acetone and water (60 mL of acetone and 2.0 mL of water). Separated product was dried under high vacuum, at 60 °C for 20 h (0.98 g of PImDE$^+$Br$^-$, 52 % yield).

PImDE$^+$TFSI$^-$: For the anion exchange, PImDE$^+$Br$^-$ (91.8 mg, 0.29 mmol) was dissolved in 4.0 mL of MiliQ® water. LiTFSI (100 mg, 0.35 mmol) was dissolved in 2.0 mL of MiliQ® water and added dropwise under vigorous stirring to the polymer solution. After 30 min of stirring, the liquid was decanted, followed by rinsing of a crude product with MiliQ® water. In order to remove excess of LiTFSI salt, the product was dissolved in 500 mg of acetone and precipitated from 10 mL of MiliQ® water. The collected product was dried overnight under high vacuum, at 80 °C (116 mg of PImDE$^+$TFSI$^-$, 78 % yield).

PImDE$^+$PF$_6^-$: For the anion exchange, PImDE$^+$Br$^-$ (283 mg, 0.89 mmol) was dissolved in 15.0 mL of water. KPF$_6$ (183 mg, 0.98 mmol) was dissolved in 40.0 mL of water and added

dropwise under vigorous stirring to the polymer solution. After 30 min of stirring, the precipitate was separated *via* centrifugation. The product was dissolved in 500 mg of acetone and precipitated from 20.0 mL of water in order to remove traces of salt. The collected product was dried overnight under high vacuum, at 80 °C (262 mg of $PImDE^+PF_6^-$, 77 % yield).

D.5 Chapter 4.2

In the typical reaction, MiliQ® water (3.7 mL) and glacial acetic acid (3.3 mL, 57 mmol) were added under vigorous stirring to 1.0 g (9.4 mmol) of cadaverine. Such mixture was then injected to the mixture of methylglyoxal (1.46 mL, 9.0 mmol) and formaldehyde (0.71 mL, 9.0 mmol). The solution was stirred for 24 h, diluted with MiliQ® water and dialyzed against MiliQ® water using 3.5 kD tubing.

In the case of other diamines (except *p*-phenylenediamine) the synthetic procedure was analogous. 1.0 g of diamine was mixed with water (the overall amount of water, also being a part of aldehydes solutions, was tuned to 5.0 mL) and 6.0 molar excess of acetic acid (in regard to diamine) was used for the reaction. Such mixture was then added to 1.2 molar excess (regarding diamine) of formaldehyde and pyruvaldehyde. The solutions were stirred for 24 h, diluted with MiliQ® water and dialyzed against MiliQ® water using 3.5 kDa tubing.

The reaction with *p*-phenylenediamine was analogous to the above mentioned, but overall amount of water was tuned to 40 mL (from which 10 mL were added to the mixture of aldehydes). The reaction time was 15 min.

For the anion exchange to TFSI, 1.2 molar excess of LiTFSI solution (calculated to the theoretical amount of imidazolium rings at 100 % of conversion) in MiliQ® water (20 mL) was

added to the dialyzed solution of polymers. After 30 min. the precipitate was centrifuged out and 3 times washed with water/centrifuged. Anion exchange to $N(CN)_2$ was performed in an analogous method to the above-mentioned, but 5.0 molar excess of $NaN(CN)_2$ dissolved in 100 mL of water was used for the reactions.

E. LIST OF PUBLICATIONS

1. K. Grygiel, B. Wicklein, Q. Zhao, M. Eder, T. Pettersson, L. Bergstrom, M. Antonietti, and J. Yuan, Omnidispersible poly (ionic liquid)-functionalized cellulose nanofibrils: surface grafting and polymer membrane reinforcement, *Chemical Communications* (Cambridge, U. K.), 2014, 50, 12486-12489.

2. K. Grygiel, L. Chabanne, Y. Men, and J. Yuan, Thiazolium-Containing Poly(ionic liquid)s and Ionic Polymers, *Macromolecular Symposia*, 2014, 342, 67-77.

3. S. Prescher, S. Ghasimi, P. Höhne, K. Grygiel, K. Landfester, K. A. I. Zhang, and J. Yuan, Polyfluorene polyelectrolyte nanoparticles: synthesis of innovative stabilizers for heterophase polymerization, *Macromolecular Rapid Communications*, 2014, 35, 1925-1930.

4. P. Haro Dominguez, K. Grygiel, and J. Weber, Nanostructured poly(benzimidazole) membranes by N-alkylation, *eXPRESS Polymer Letters*, 2014, 8, 1, 30-38

F. DECLARATION OF INDEPENDENT WORK

I hereby declare that I have made this work by myself using only the referenced materials and sources.

Hiermit erkläre ich, dass ich die vorliegende Arbeit selbstständig angefertigt und keine

anderen als die angegebenen Hilfsmittel und Quellen verwendet habe.

Potsdam, den 02.03.2015

Konrad Grygiel

G. ACKNOWLEDGEMENT

H. REFERENCES

1. J. C. Salamone, S. C. Israel, P. Taylor and B. Snider, *Polymer*, 1973, **14**, 639-644.

2. H. Ohno and K. Ito, *Chem. Lett.*, 1998, 751-752.

3. M. Yoshizawa and H. Ohno, *Chem. Lett.*, 1999, **28**, 889-890

4. M. Hirao, K. Ito and H. Ohno, *Electrochim. Acta*, 2000, **45**, 1291-1294.

5. M. Yoshizawa, W. Ogihara and H. Ohno, *Polym. Adv. Technol.*, 2002, **13**, 589-594.

6. H. Ohno, M. Yoshizawa and W. Ogihara, *Electrochim. Acta*, 2004, **50**, 255-261.

7. S. Washiro, M. Yoshizawa, H. Nakajima and H. Ohno, *Polymer*, 2004, **45**, 1577-1582.

8. M. Yoshio, T. Mukai, H. Ohno and T. Kato, *J. Am. Chem. Soc.*, 2004, **126**, 994-995.

9. W. Ogihara, N. Suzuki, N. Nakamura and H. Ohno, *Polym. J.*, 2006, **38**, 117-121.

10. W. Ogihara, S. Washiro, H. Nakajima and H. Ohno, *Electrochim. Acta*, 2006, **51**, 2614-2619.

11. M. Yoshio, T. Kagata, K. Hoshino, T. Mukai, H. Ohno and T. Kato, *J. Am. Chem. Soc.*, 2006, **128**, 5570-5577.

12. H. Ohno, *Macromol. Symp.*, 2007, **249-250**, 551-556.

13. O. Mel'nik, A. Shaplov, E. Lozinskaya, N. Popova, M. Makarov, I. Odinets, K. Lysenko, G. Timofeeva, I. Malyshkina and Y. Vygodskii, *Polymer Science Series B*, 2010, **52**, 316-326.

14. C. Detrembleur, A. Debuigne, M. Hurtgen, C. Jérôme, J. Pinaud, M. v. Fèvre, P. Coupillaud, J. Vignolle and D. Taton, *Macromolecules*, 2011, **44**, 6397-6404.

15. R. Marcilla, J. Alberto Blazquez, J. Rodriguez, J. A. Pomposo and D. Mecerreyes, *Journal of Polymer Science Part A: Polymer Chemistry*, 2004, **42**, 208-212.

16. O. Green, S. Grubjesic, S. Lee and M. A. Firestone, *Polym. Rev. (Philadelphia, PA, U. S.)*, 2009, **49**, 339-360.

17. Q. Zhao, T.-P. Fellinger, M. Antonietti and J. Yuan, *Macromol. Rapid Commun.*, 2012, **33**, 1149-1153.

18. Q. Zhao, P. Zhang, M. Antonietti and J. Yuan, *J. Am. Chem. Soc.*, 2012, **134**, 11852-11855.

19. F. D. Francesco, N. Calisi, M. Creatini, B. Melai, P. Salvo and C. Chiappe, *Green Chem.*, 2011, **13**, 1712-1717.

20. M. D. Green, D. Wang, S. T. Hemp, J.-H. Choi, K. I. Winey, J. R. Heflin and T. E. Long, *Polymer*, 2012, **53**, 3677-3686.

21. J. Yuan, S. Soll, M. Drechsler, A. H. E. Müller and M. Antonietti, *J. Am. Chem. Soc.*, 2011, **133**, 17556-17559.

22. R. Marcilla, E. Ochoteco, C. Pozo-Gonzalo, H. Grande, J. A. Pomposo and D. Mecerreyes, *Macromol. Rapid Commun.*, 2005, **26**, 1122-1126.

23. Y. Ye and Y. A. Elabd, *Macromolecules*, 2011, **44**, 8494-8503.

24. R. L. Weber, Y. Ye, A. L. Schmitt, S. M. Banik, Y. A. Elabd and M. K. Mahanthappa, *Macromolecules*, 2011, **44**, 5727-5735.

25. D. England, N. Tambe and J. Texter, *ACS Macro Lett.*, 2012, **1**, 310-314.

26. Q. Zhao, S. Soll, M. Antonietti and J. Yuan, *Polymer Chemistry*, 2013, **4**, 2432-2435.

27. A. Wilke, J. Yuan, M. Antonietti and J. Weber, *ACS Macro Lett.*, 2012, 1028-1031.

28. S. Supasitmongkol and P. Styring, *Energy & Environmental Science*, 2010, **3**, 1961-1972.

29. P. G. Mineo, L. Livoti, M. Giannetto, A. Gulino, S. Lo Schiavo and P. Cardiano, *J. Mater. Chem.*, 2009, **19**, 8861-8870.

30. M. Watanabe, S.-i. Yamada and N. Ogata, *Electrochim. Acta*, 1995, **40**, 2285-2288.

31. J. Yuan, A. G. Marquez, J. Reinacher, C. Giordano, J. Janek and M. Antonietti, *Polym. Chem.*, 2011, **2**, 1654-1657.

32. W. S. Ogihara W., Nakajima H., Ohno H, *Electrochimica Acta*, 2006, **51**, 6.

33. A.-L. Pont, R. Marcilla, I. De Meatza, H. Grande and D. Mecerreyes, *J. Power Sources*, 2009, **188**, 558-563.

34. P. Dimitrov-Raytchev, S. Beghdadi, A. Serghei and E. Drockenmuller, *Journal of Polymer Science Part A: Polymer Chemistry*, 2013, **51**, 34-38.

35. D. Mecerreyes, *Prog. Polym. Sci.*, 2011, **36**, 1629-1648.

36. D. Mecerreyes, *Prog. Polym. Sci.*, 2011, **36**, 1629-1648.

37. M. Hirao, K. Ito and H. Ohno, *Electrochim. Acta*, 2000, **45**, 1291-1294.

38. D. Batra, S. Seifert, L. M. Varela, A. C. Y. Liu and M. A. Firestone, *Adv. Funct. Mater.*, 2007, **17**, 1279-1287.

39. T. Mizumo, T. Watanabe, N. Matsumi and H. Ohno, *Polym. Adv. Technol.*, 2008, **19**, 1445-1450.

40. Y. S. Vygodskii, A. S. Shaplov, E. I. Lozinskaya, K. A. Lyssenko, D. G. Golovanov, I. A. Malyshkina, N. D. Gavrilova and M. R. Buchmeiser, *Macromol. Chem. Phys.*, 2008, **209**, 40-51.

41. K. Vijayakrishna, S. K. Jewrajka, A. Ruiz, R. Marcilla, J. A. Pomposo, D. Mecerreyes, D. Taton and Y. Gnanou, *Macromolecules*, 2008, **41**, 6299-6308.

42. J. Yuan, H. Schlaad, C. Giordano and M. Antonietti, *Eur. Polym. J.*, 2011, **47**, 772-781.

43. X. He, W. Yang and X. Pei, *Macromolecules*, 2008, **41**, 4615-4621.

44. J. Texter, V. A. Vasantha, R. Crombez, R. Maniglia, L. Slater and T. Mourey, *Macromol. Rapid Commun.*, 2012, **33**, 69-74.

45. P. Coupillaud, M. Fèvre, A.-L. Wirotius, K. Aissou, G. Fleury, A. Debuigne, C. Detrembleur, D. Mecerreyes, J. Vignolle and D. Taton, *Macromol. Rapid Commun.*, 2014, **35**, 422-430.

46. D. Cordella, A. Kermagoret, A. Debuigne, R. Riva, I. German, M. Isik, C. Jérôme, D. Mecerreyes, D. Taton and C. Detrembleur, *ACS Macro Letters*, 2014, **3**, 1276-1280.

47. F. Zhao, Y. Meng and J. L. Anderson, *Journal of Chromatography A*, 2008, **1208**, 1-9.

48. Q. Zhao, M. Yin, A. P. Zhang, S. Prescher, M. Antonietti and J. Yuan, *J. Am. Chem. Soc.*, 2013, **135**, 5549-5552.

49. Q. Zhao, J. W. C. Dunlop, X. Qiu, F. Huang, Z. Zhang, J. Heyda, J. Dzubiella, M. Antonietti and J. Yuan, *Nat Commun*, 2014, **5**.

50. M. Ambrogi, Y. Men, F. Polzer and J. Yuan, *RSC Advances*, 2014, **4**, 37714-37720.

51. J. Pinaud, J. Vignolle, Y. Gnanou and D. Taton, *Macromolecules*, 2011, **44**, 1900-1908.

52. D. Kuzmicz, P. Coupillaud, Y. Men, J. Vignolle, G. Vendraminetto, M. Ambrogi, D. Taton and J. Yuan, *Polymer*, 2014, **55**, 3423-3430.

53. R. Marcilla, M. L. Curri, P. D. Cozzoli, M. T. Martínez, I. Loinaz, H. Grande, J. A. Pomposo and D. Mecerreyes, *Small*, 2006, **2**, 507-512.

54. S. Soll, M. Antonietti and J. Yuan, *ACS Macro Lett.*, 2012, **1**, 84-87.

55. D. Batra, S. Seifert, L. Varela, A. Liu and M. Firestone, *Adv. Funct. Mater.*, 2007, **17**, 1279-1287.

56. J. von Zamory, M. Bedu, S. Fantini, S. Passerini and E. Paillard, *J. Power Sources*, 2013, **240**, 745-752.

57. Y. Men, X.-H. Li, M. Antonietti and J. Yuan, *Polym. Chem.*, 2012, **3**, 871-873.

58. Y. Men, X.-H. Li, M. Antonietti and J. Yuan, *Polymer Chemistry*, 2012, **3**, 871-873.

59. Y. Men, H. Schlaad and J. Yuan, *ACS Macro Letters*, 2013, **2**, 456-459.

60. J. Tang, Y. Shen, M. Radosz and W. Sun, *Ind. Eng. Chem. Res.*, 2009, **48**, 9113-9118.

61. J. Tang, M. Radosz and Y. Shen, *Macromolecules*, 2007, **41**, 493-496.

62.   M. Isik, R. Gracia, L. C. Kollnus, L. C. Tomé, I. M. Marrucho and D. Mecerreyes, *ACS Macro Letters*, 2013, **2**, 975-979.

63.   S. Xiao, X. Lu and Q. Lu, *Macromolecules*, 2007, **40**, 7944-7950.

64.   S. Sharma, G. Chauhan, R. Gupta and J. H. Ahn, *J. Mater. Sci.: Mater. Med.*, 2010, **21**, 717-724.

65.   S. Prescher, F. Polzer, Y. Yang, M. Siebenbürger, M. Ballauff and J. Yuan, *J. Am. Chem. Soc.*, 2013, **136**, 12-15.

66.   M. Dobbelin, V. Jovanovski, I. Llarena, L. J. Claros Marfil, G. Cabanero, J. Rodriguez and D. Mecerreyes, *Polymer Chemistry*, 2011, **2**, 1275-1278.

67.   R. J. Moon, A. Martini, J. Nairn, J. Simonsen and J. Youngblood, *Chem. Soc. Rev.*, 2011, **40**, 3941-3994.

68.   D. Klemm, F. Kramer, S. Moritz, T. Lindström, M. Ankerfors, D. Gray and A. Dorris, *Angewandte Chemie International Edition*, 2011, **50**, 5438-5466.

69.   H. Sehaqui, Q. Zhou, O. Ikkala and L. A. Berglund, *Biomacromolecules*, 2011, **12**, 3638-3644.

70.   N. Lin, G. Chen, J. Huang, A. Dufresne and P. R. Chang, *J. Appl. Polym. Sci.*, 2009, **113**, 3417-3425.

71.   H. Lönnberg, K. Larsson, T. Lindström, A. Hult and E. Malmström, *ACS Appl. Mater. Interfaces*, 2011, **3**, 1426-1433.

72.   K. Littunen, U. Hippi, L.-S. Johansson, M. Österberg, T. Tammelin, J. Laine and J. Seppälä, *Carbohydr. Polym.*, 2011, **84**, 1039-1047.

73.   E. Karabulut, T. Pettersson, M. Ankerfors and L. Wågberg, *ACS Nano*, 2012, **6**, 4731-4739.

74.   J. M. Felix and P. Gatenholm, *J. Appl. Polym. Sci.*, 1991, **42**, 609-620.

75.   L. Heux, G. Chauve and C. Bonini, *Langmuir*, 2000, **16**, 8210-8212.

76. C. Aulin, A. Shchukarev, J. Lindqvist, E. Malmström, L. Wågberg and T. Lindström, *J. Colloid Interface Sci.*, 2008, **317**, 556-567.

77. D.-Y. Kim, Y. Nishiyama and S. Kuga, *Cellulose*, 2002, **9**, 361-367.

78. G. Siqueira, J. Bras and A. Dufresne, *Langmuir*, 2009, **26**, 402-411.

79. I. Filpponen, E. Kontturi, S. Nummelin, H. Rosilo, E. Kolehmainen, O. Ikkala and J. Laine, *Biomacromolecules*, 2012, **13**, 736-742.

80. K. Missoum, M. Belgacem and J. Bras, *Materials*, 2013, **6**, 1745-1766.

81. K. Grygiel, B. Wicklein, Q. Zhao, M. Eder, T. Pettersson, L. Bergstrom, M. Antonietti and J. Yuan, *Chem. Commun. (Cambridge, U. K.)*, 2014, **50**, 12486-12489.

82. R. P. Swatloski, S. K. Spear, J. D. Holbrey and R. D. Rogers, *J. Am. Chem. Soc.*, 2002, **124**, 4974-4975.

83. N. E. Heimer, R. E. Del Sesto, Z. Meng, J. S. Wilkes and W. R. Carper, *J. Mol. Liq.*, 2006, **124**, 84-95.

84. X. Wang, D. Fang, K. Yoon, B. S. Hsiao and B. Chu, *J. Membr. Sci.*, 2006, **278**, 261-268.

85. J. Liu, X. Lu, C. Wu and C. Zhao, *J. Polym. Res.*, 2013, **20**, 1-10.

86. P. Sukitpaneenit and T.-S. Chung, *Environ. Sci. Technol.*, 2012, **46**, 7358-7365.

87. G. D. Vilakati, E. M. V. Hoek and B. B. Mamba, *J. Appl. Polym. Sci.*, 2014, n/a-n/a.

88. R. F. Shamoun, A. Reisch and J. B. Schlenoff, *Adv. Funct. Mater.*, 2012, **22**, 1923-1931.

89. P. Maheswari and D. Mohan, *High Perform. Polym.*, 2013, **25**, 641-651.

90. C. Zorzi Bueno and Â. Maria Moraes, *J. Appl. Polym. Sci.*, 2011, **122**, 624-631.

91. D. Enders, O. Niemeier and A. Henseler, *Chem. Rev. (Washington, DC, U. S.)*, 2007, **107**, 5606-5655.

92. C. J., L.-C. F. and D. L., *The Journal of Organic Chemistry*, 1988, **53**, 4.

93.   A. G. M. Barrett, A. C. Love and L. Tedeschi, *Org. Lett.*, 2004, **6**, 3377-3380.

94.   S. A. Dharaskar, K. L. Wasewar, M. N. Varma, D. Z. Shende and C. K. Yoo, *Ind. Eng. Chem. Res.*, 2014, **53**, 19845-19854.

95.   P. C. Hillesheim, S. M. Mahurin, P. F. Fulvio, J. S. Yeary, Y. Oyola, D.-e. Jiang and S. Dai, *Ind. Eng. Chem. Res.*, 2012, **51**, 11530-11537.

96.   Q. Cao and J. A. Rogers, *Adv. Mater. (Weinheim, Ger.)*, 2009, **21**, 29-53.

97.   W. Peng, C. Xing, H. Nancy, T. Un Chong, B. Ola, Z. Alex and R. B. Carolyn *Angew. Chem.*, 2008, **120**, 5100-5103.

98.   V. C. Tung, J. Kim, L. J. Cote and J. Huang, *J. Am. Chem. Soc.*, 2011, **133**, 9262-9265.

99.   S. Meuer, L. Braun and R. Zentel, *Macromol. Chem. Phys.*, 2009, **210**, 1528-1535.

100.   M. Zheng, A. Jagota, E. D. Semke, B. A. Diner, R. S. McLean, S. R. Lustig, R. E. Richardson and N. G. Tassi, *Nat. Mater.*, 2003, **2**, 338-342.

101.   D. Wang, W.-X. Ji, Z.-C. Li and L. Chen, *J. Am. Chem. Soc.*, 2006, **128**, 6556-6557.

102.   M. Antonietti, Y. Shen, T. Nakanishi, M. Manuelian, R. Campbell, L. Gwee, Y. A. Elabd, N. Tambe, R. Crombez and J. Texter, *ACS Appl. Mater. Inter.*, 2010, **2**, 649-653.

103.   J. D. Burgess, *Metal ions in solution / by John Burgess*, Ellis Horwood ; distributed by Halsted Press, Chichester : New York, 1978.

104.   T. Buffeteau, J. Grondin and J.-C. Lassègues, *Appl. Spectrosc.*, 2010, **64**, 112-119.

105.   J. H. Davis Jr and K. J. Forrester, *Tetrahedron Lett.*, 1999, **40**, 1621-1622.

106.   R. C. Thompson, C. J. Moore, F. S. vom Saal and S. H. Swan, *Plastics, the environment and human health: current consensus and future trends*, 2009.

107.   D. P. Ho, H. H. Ngo and W. Guo, *Bioresour. Technol.*, 2014, **169**, 742-749.

108. A. Srivastava and R. Prasad, *Renewable and Sustainable Energy Reviews*, 2000, **4**, 111-133.

109. R. Auras, B. Harte and S. Selke, *Macromol. Biosci.*, 2004, **4**, 835-864.

110. M. Rose and R. Palkovits, *Macromol. Rapid Commun.*, 2011, **32**, 1299-1311.

111. Y. Ikada and H. Tsuji, *Macromol. Rapid Commun.*, 2000, **21**, 117-132.

112. S. T. Handy, M. Okello and G. Dickenson, *Org. Lett.*, 2003, **5**, 2513-2515.

113. R. Sasi, T. P. Rao and S. J. Devaki, *ACS Appl. Mater. Interfaces*, 2014, **6**, 4126-4133.

114. C. Mukesh, D. Mondal, M. Sharma and K. Prasad, *Chem. Commun. (Cambridge, U. K.)*, 2013, **49**, 6849-6851.

115. m. isik, H. Sardon, M. Saenz and D. Mecerreyes, *RSC Advances*, 2014.

116. M. Moreno, M. Ali Aboudzadeh, M. J. Barandiaran and D. Mecerreyes, *Journal of Polymer Science Part A: Polymer Chemistry*, 2012, **50**, 1049-1053.

117. D. Esposito, S. Kirchhecker and M. Antonietti, *Chemistry – A European Journal*, 2013, **19**, 15097-15100.

118. S. Kirchhecker, M. Antonietti and D. Esposito, *Green Chem.*, 2014, **16**, 3705-3709.

119. R. M. Painter, D. M. Pearson and R. M. Waymouth, *Angewandte Chemie International Edition*, 2010, **49**, 9456-9459.

120. C. B. Rasrendra, B. A. Fachri, I. G. B. N. Makertihartha, S. Adisasmito and H. J. Heeres, *ChemSusChem*, 2011, **4**, 768-777.

121. D. Esposito and M. Antonietti, *ChemSusChem*, 2013, **6**, 989-992.

122. A. V. B. Bridgwater, D. G. B, *Developments in Thermochemical Biomass Conversion Vol. 2.*, Springer.

123. G. Reuss, W. Disteldorf, A. O. Gamer and A. Hilt, in *Ullmann's Encyclopedia of Industrial Chemistry*, Wiley-VCH Verlag GmbH & Co. KGaA, 2000.

124. Y. Zhang, J. Xiao and L. Shen, *Ind. Eng. Chem. Res.*, 2009, **48**, 5351-5359.

125.   J. Jules and W. Anna, *Trends in new crops and new uses.*, ASHS Press, Alexandria, 2002.

126.   A. Margeot, B. Hahn-Hagerdal, M. Edlund, R. Slade and F. Monot, *Curr. Opin. Biotechnol.*, 2009, **20**, 372-380.

127.   H. Biebl, K. Menzel, A. P. Zeng and W. D. Deckwer, *Appl. Microbiol. Biotechnol.*, 1999, **52**, 289-297.

128.   , US 7919658 B2, 2004.

129.   I. M. Hodge, *Macromolecules*, 1983, **16**, 898-902.

130.   O. Höfft, S. Bahr and V. Kempter, *Langmuir*, 2008, **24**, 11562-11566.

131.   M. Yamaguchi and A. Ohira, *The Journal of Physical Chemistry A*, 2012, **116**, 10850-10863.

132.   E. L. Varetti, *Spectrochimica Acta Part A: Molecular Spectroscopy*, 1988, **44**, 733-738.

133.   A. B. Horn and K. Jessica Sully, *Phys. Chem. Chem. Phys.*, 1999, **1**, 3801-3806.

134.   J. Kiefer, J. Fries and A. Leipertz, *Appl. Spectrosc.*, 2007, **61**, 1306-1311.

135.   I. Rey, P. Johansson, J. Lindgren, J. C. Lassègues, J. Grondin and L. Servant, *The Journal of Physical Chemistry A*, 1998, **102**, 3249-3258.

136.   S. Soll, Q. Zhao, J. Weber and J. Yuan, *Chem. Mater.*, 2013, **25**, 3003-3010.

137.   S. G. Kazarian, M. F. Vincent, F. V. Bright, C. L. Liotta and C. A. Eckert, *J. Am. Chem. Soc.*, 1996, **118**, 1729-1736.

138.   Y.-B. Xiong, H. Wang, Y.-J. Wang and R.-M. Wang, *Polym. Adv. Technol.*, 2012, **23**, 835-840.

139.   J. K. Fink, Scrivener Publishing LLC, Salem, 2011.

140.   K.-S. Krannig, D. Esposito and M. Antonietti, *Macromolecules*, 2014, **47**, 2350-2353.

141. Y.-N. Hsieh, C.-H. Kuei, Y.-K. Chou, C.-C. Liu, K.-L. Leu, T.-H. Yang, M.-Y. Wang and W.-Y. Ho, *Tetrahedron Lett.*, 2010, **51**, 3666-3669.

142. J. P. Paraknowitsch, J. Zhang, D. Su, A. Thomas and M. Antonietti, *Adv. Mater. (Weinheim, Ger.)*, 2010, **22**, 87-92.

143. T.-P. Fellinger, A. Thomas, J. Yuan and M. Antonietti, *Adv. Mater. (Weinheim, Ger.)*, 2013, **25**, 5838-5855.

144. Q. Zhao, T.-P. Fellinger, M. Antonietti and J. Yuan, *Journal of Materials Chemistry A*, 2013, **1**, 5113-5120.

145. L. Wågberg, G. Decher, M. Norgren, T. Lindström, M. Ankerfors and K. Axnäs, *Langmuir*, 2008, **24**, 784-795.

146. J. Yuan, C. Giordano and M. Antonietti, *Chem. Mater.*, 2010, **22**, 5003-5012.